Nevio Benvenuto | Giovanni Cherubini | Stefano Tomasin

2nd Edition

Algorithms for Communications Systems and their Applications

WILEY

Algorithms for Communications Systems and their Applications

Algorithms for Communications Systems and their Applications

Second Edition

Nevio Benvenuto
University of Padua
Italy

Giovanni Cherubini
IBM Research Zurich
Switzerland

Stefano Tomasin
University of Padua
Italy

WILEY

This edition first published 2021

Registered Offices
John Wiley & Sons, Inc., 111 River Street, Hoboken, NJ 07030, USA
John Wiley & Sons Ltd, The Atrium, Southern Gate, Chichester, West Sussex, PO19 8SQ, UK

Editorial Office
The Atrium, Southern Gate, Chichester, West Sussex, PO19 8SQ, UK

For details of our global editorial offices, customer services, and more information about Wiley products visit us at www.wiley.com.

Wiley also publishes its books in a variety of electronic formats and by print-on-demand. Some content that appears in standard print versions of this book may not be available in other formats.

Library of Congress Cataloging-in-Publication Data

Names: Benvenuto, Nevio, author. | Cherubini, Giovanni, 1957- author. |
Tomasin, Stefano, 1975- author.
Title: Algorithms for communications systems and their applications / Nevio
Benvenuto, University of Padua, Italy, Giovanni Cherubini,
IBM Research Zurich, Switzerland, Stefano Tomasin, University of Padua,
Italy.
Description: Second edition. | Hoboken, NJ, USA : Wiley, 2021. | Includes
bibliographical references and index.
Identifiers: LCCN 2020004346 (print) | LCCN 2020004347 (ebook) | ISBN
9781119567967 (cloth) | ISBN 9781119567974 (adobe pdf) | ISBN
9781119567981 (epub)
Subjects: LCSH: Signal processing–Mathematics. | Telecommunication
systems–Mathematics. | Algorithms.
Classification: LCC TK5102.9 .B46 2020 (print) | LCC TK5102.9 (ebook) |
DDC 621.382/2–dc23
LC record available at https://lccn.loc.gov/2020004346
LC ebook record available at https://lccn.loc.gov/2020004347

Cover Design: Wiley
Cover Image: © betibup33/Shutterstock

Set in 9.5/12.5pt STIXGeneral by SPi Global, Chennai, India

10 9 8 7 6 5 4 3 2 1

To Adriana, to Antonio, Claudia, and Mariuccia, and in memory of Alberto

Contents

Preface *xxv*
Acknowledgements *xxvii*

1 Elements of signal theory *1*
1.1 Continuous-time linear systems *1*
1.2 Discrete-time linear systems *2*
Discrete Fourier transform *7*
The DFT operator *7*
Circular and linear convolution via DFT *8*
Convolution by the overlap-save method *10*
IIR and FIR filters *11*
1.3 Signal bandwidth *14*
The sampling theorem *17*
Heaviside conditions for the absence of signal distortion *17*
1.4 Passband signals and systems *18*
Complex representation *18*
Relation between a signal and its complex representation *21*
Baseband equivalent of a transformation *26*
Envelope and instantaneous phase and frequency *28*
1.5 Second-order analysis of random processes *29*
1.5.1 Correlation *29*
Properties of the autocorrelation function *30*
1.5.2 Power spectral density *30*
Spectral lines in the PSD *30*
Cross power spectral density *31*
Properties of the PSD *32*
PSD through filtering *32*
1.5.3 PSD of discrete-time random processes *32*
Spectral lines in the PSD *33*
PSD through filtering *34*
Minimum-phase spectral factorization *35*
1.5.4 PSD of passband processes *36*
PSD of in-phase and quadrature components *36*
Cyclostationary processes *38*
1.6 The autocorrelation matrix *43*

1.7 Examples of random processes *46*
1.8 Matched filter *52*
White noise case *53*
1.9 Ergodic random processes *55*
1.9.1 Mean value estimators *57*
Rectangular window *58*
Exponential filter *59*
General window *59*
1.9.2 Correlation estimators *60*
Unbiased estimate *60*
Biased estimate *60*
1.9.3 Power spectral density estimators *61*
Periodogram or instantaneous spectrum *61*
Welch periodogram *62*
Blackman and Tukey correlogram *63*
Windowing and window closing *63*
1.10 Parametric models of random processes *65*
ARMA *65*
MA *67*
AR *67*
Spectral factorization of AR models *69*
Whitening filter *70*
Relation between ARMA, MA, and AR models *70*
1.10.1 Autocorrelation of AR processes *72*
1.10.2 Spectral estimation of an AR process *74*
Some useful relations *75*
AR model of sinusoidal processes *77*
1.11 Guide to the bibliography *78*
Bibliography *78*
Appendix 1.A Multirate systems *79*
1.A.1 Fundamentals *79*
1.A.2 Decimation *81*
1.A.3 Interpolation *83*
1.A.4 Decimator filter *84*
1.A.5 Interpolator filter *86*
1.A.6 Rate conversion *88*
1.A.7 Time interpolation *90*
Linear interpolation *90*
Quadratic interpolation *91*
1.A.8 The noble identities *91*
1.A.9 The polyphase representation *92*
Efficient implementations *93*
Appendix 1.B Generation of a complex Gaussian noise *98*
Appendix 1.C Pseudo-noise sequences *99*
Maximal-length *99*
CAZAC *101*
Gold *102*

2 The Wiener filter *105*
2.1 The Wiener filter *105*
Matrix formulation *106*
Optimum filter design *107*
The principle of orthogonality *109*
Expression of the minimum mean-square error *110*
Characterization of the cost function surface *110*
The Wiener filter in the z-domain *111*
2.2 Linear prediction *114*
Forward linear predictor *115*
Optimum predictor coefficients *115*
Forward prediction error filter *116*
Relation between linear prediction and AR models *117*
First- and second-order solutions *117*
2.3 The least squares method *118*
Data windowing *119*
Matrix formulation *119*
Correlation matrix *120*
Determination of the optimum filter coefficients *120*
2.3.1 The principle of orthogonality *121*
Minimum cost function *121*
The normal equation using the data matrix *122*
Geometric interpretation: the projection operator *122*
2.3.2 Solutions to the LS problem *123*
Singular value decomposition *124*
Minimum norm solution *125*
2.4 The estimation problem *126*
Estimation of a random variable *126*
MMSE estimation *127*
Extension to multiple observations *128*
Linear MMSE estimation of a random variable *129*
Linear MMSE estimation of a random vector *129*
2.4.1 The Cramér–Rao lower bound *131*
Extension to vector parameter *132*
2.5 Examples of application *134*
2.5.1 Identification of a linear discrete-time system *134*
2.5.2 Identification of a continuous-time system *135*
2.5.3 Cancellation of an interfering signal *138*
2.5.4 Cancellation of a sinusoidal interferer with known frequency *139*
2.5.5 Echo cancellation in digital subscriber loops *140*
2.5.6 Cancellation of a periodic interferer *141*
Bibliography *142*
Appendix 2.A The Levinson–Durbin algorithm *142*
Lattice filters *144*
The Delsarte–Genin algorithm *145*

3 Adaptive transversal filters *147*
3.1 The MSE design criterion *148*
3.1.1 The steepest descent or gradient algorithm *148*
Stability *149*
Conditions for convergence *150*
Adaptation gain *151*
Transient behaviour of the MSE *152*
3.1.2 The least mean square algorithm *153*
Implementation *154*
Computational complexity *155*
Conditions for convergence *155*
3.1.3 Convergence analysis of the LMS algorithm *156*
Convergence of the mean *157*
Convergence in the mean-square sense: real scalar case *157*
Convergence in the mean-square sense: general case *159*
Fundamental results *161*
Observations *162*
Final remarks *163*
3.1.4 Other versions of the LMS algorithm *163*
Leaky LMS *164*
Sign algorithm *164*
Normalized LMS *164*
Variable adaptation gain *165*
3.1.5 Example of application: the predictor *166*
3.2 The recursive least squares algorithm *171*
Normal equation *172*
Derivation *173*
Initialization *174*
Recursive form of the minimum cost function *175*
Convergence *176*
Computational complexity *176*
Example of application: the predictor *177*
3.3 Fast recursive algorithms *177*
3.3.1 Comparison of the various algorithms *177*
3.4 Examples of application *178*
3.4.1 Identification of a linear discrete-time system *178*
Finite alphabet case *179*
3.4.2 Cancellation of a sinusoidal interferer with known frequency *181*
Bibliography *181*

4 Transmission channels *183*
4.1 Radio channel *183*
4.1.1 Propagation and used frequencies in radio transmission *183*
Basic propagation mechanisms *184*
Frequency ranges *184*
4.1.2 Analog front-end architectures *185*
Radiation masks *185*
Conventional superheterodyne receiver *186*

Alternative architectures *187*
Direct conversion receiver *187*
Single conversion to low-IF *188*
Double conversion and wideband IF *188*
4.1.3 General channel model *189*
High power amplifier *189*
Transmission medium *191*
Additive noise *191*
Phase noise *191*
4.1.4 Narrowband radio channel model *193*
Equivalent circuit at the receiver *195*
Multipath *196*
Path loss as a function of distance *197*
4.1.5 Fading effects in propagation models *200*
Macroscopic fading or shadowing *200*
Microscopic fading *201*
4.1.6 Doppler shift *202*
4.1.7 Wideband channel model *204*
Multipath channel parameters *205*
Statistical description of fading channels *206*
4.1.8 Channel statistics *208*
Power delay profile *208*
Coherence bandwidth *209*
Doppler spectrum *210*
Coherence time *211*
Doppler spectrum models *211*
Power angular spectrum *211*
Coherence distance *212*
On fading *212*
4.1.9 Discrete-time model for fading channels *213*
Generation of a process with a pre-assigned spectrum *214*
4.1.10 Discrete-space model of shadowing *216*
4.1.11 Multiantenna systems *218*
Line of sight *218*
Discrete-time model *219*
Small number of scatterers *220*
Large number of scatterers *220*
Blockage effect *222*
4.2 Telephone channel *222*
4.2.1 Distortion *222*
4.2.2 Noise sources *222*
Quantization noise: *222*
Thermal noise: *224*
4.2.3 Echo *224*
Bibliography *225*
Appendix 4.A Discrete-time NB model for mmWave channels *226*
4.A.1 Angular domain representation *226*

5	**Vector quantization**	*229*
5.1	Basic concept	*229*
5.2	Characterization of VQ	*230*
	Parameters determining VQ performance	*231*
	Comparison between VQ and scalar quantization	*232*
5.3	Optimum quantization	*233*
	Generalized Lloyd algorithm	*233*
5.4	The Linde, Buzo, and Gray algorithm	*235*
	Choice of the initial codebook	*236*
	Splitting procedure	*236*
	Selection of the training sequence	*238*
5.4.1	k-means clustering	*239*
5.5	Variants of VQ	*239*
	Tree search VQ	*239*
	Multistage VQ	*240*
	Product code VQ	*240*
5.6	VQ of channel state information	*242*
	MISO channel quantization	*242*
	Channel feedback with feedforward information	*244*
5.7	Principal component analysis	*244*
5.7.1	PCA and k-means clustering	*246*
	Bibliography	*248*
6	**Digital transmission model and channel capacity**	*249*
6.1	Digital transmission model	*249*
6.2	Detection	*253*
6.2.1	Optimum detection	*253*
	ML	*254*
	MAP	*254*
6.2.2	Soft detection	*256*
	LLRs associated to bits of BMAP	*256*
	Simplified expressions	*258*
6.2.3	Receiver strategies	*260*
6.3	Relevant parameters of the digital transmission model	*260*
	Relations among parameters	*261*
6.4	Error probability	*262*
6.5	Capacity	*265*
6.5.1	Discrete-time AWGN channel	*266*
6.5.2	SISO narrowband AWGN channel	*266*
	Channel gain	*267*
6.5.3	SISO dispersive AGN channel	*267*
6.5.4	MIMO discrete-time NB AWGN channel	*269*
	Continuous-time model	*270*
	MIMO dispersive channel	*270*
6.6	Achievable rates of modulations in AWGN channels	*270*
6.6.1	Rate as a function of the SNR per dimension	*271*
6.6.2	Coding strategies depending on the signal-to-noise ratio	*272*
	Coding gain	*274*

6.6.3 Achievable rate of an AWGN channel using PAM *275*
Bibliography *276*
Appendix 6.A Gray labelling *277*
Appendix 6.B The Gaussian distribution and Marcum functions *278*
6.B.1 The Q function *278*
6.B.2 Marcum function *279*

7 Single-carrier modulation *281*
7.1 Signals and systems *281*
7.1.1 Baseband digital transmission (PAM) *281*
Modulator *281*
Transmission channel *283*
Receiver *283*
Power spectral density *284*
7.1.2 Passband digital transmission (QAM) *285*
Modulator *285*
Power spectral density *286*
Three equivalent representations of the modulator *287*
Coherent receiver *288*
7.1.3 Baseband equivalent model of a QAM system *288*
Signal analysis *288*
7.1.4 Characterization of system elements *291*
Transmitter *291*
Transmission channel *291*
Receiver *293*
7.2 Intersymbol interference *294*
Discrete-time equivalent system *294*
Nyquist pulses *295*
Eye diagram *298*
7.3 Performance analysis *302*
Signal-to-noise ratio *302*
Symbol error probability in the absence of ISI *303*
Matched filter receiver *303*
7.4 Channel equalization *304*
7.4.1 Zero-forcing equalizer *304*
7.4.2 Linear equalizer *305*
Optimum receiver in the presence of noise and ISI *305*
Alternative derivation of the IIR equalizer *306*
Signal-to-noise ratio at detector *310*
7.4.3 LE with a finite number of coefficients *310*
Adaptive LE *311*
Fractionally spaced equalizer *313*
7.4.4 Decision feedback equalizer *315*
Design of a DFE with a finite number of coefficients *318*
Design of a fractionally spaced DFE *320*
Signal-to-noise ratio at the decision point *322*
Remarks *322*
7.4.5 Frequency domain equalization *323*

	DFE with data frame using a unique word	*323*
7.4.6	LE-ZF	*326*
7.4.7	DFE-ZF with IIR filters	*327*
	DFE-ZF as noise predictor	*331*
	DFE as ISI and noise predictor	*331*
7.4.8	Benchmark performance of LE-ZF and DFE-ZF	*333*
	Comparison	*333*
	Performance for two channel models	*334*
7.4.9	Passband equalizers	*335*
	Passband receiver structure	*335*
	Optimization of equalizer coefficients and carrier phase offset	*337*
	Adaptive method	*338*
7.5	Optimum methods for data detection	*340*
	Maximum a posteriori probability (MAP) criterion	*341*
7.5.1	Maximum-likelihood sequence detection	*341*
	Lower bound to error probability using MLSD	*342*
	The Viterbi algorithm	*343*
	Computational complexity of the VA	*346*
7.5.2	Maximum a posteriori probability detector	*347*
	Statistical description of a sequential machine	*347*
	The forward–backward algorithm	*348*
	Scaling	*351*
	The log likelihood function and the Max-Log-MAP criterion	*352*
	LLRs associated to bits of BMAP	*353*
	Relation between Max-Log–MAP and Log–MAP	*354*
7.5.3	Optimum receivers	*354*
7.5.4	The Ungerboeck's formulation of MLSD	*356*
7.5.5	Error probability achieved by MLSD	*358*
	Computation of the minimum distance	*361*
7.5.6	The reduced-state sequence detection	*365*
	Trellis diagram	*365*
	The RSSE algorithm	*367*
	Further simplification: DFSE	*369*
7.6	Numerical results obtained by simulations	*370*
	QPSK over a minimum-phase channel	*370*
	QPSK over a non-minimum phase channel	*370*
	8-PSK over a minimum phase channel	*372*
	8-PSK over a non-minimum phase channel	*372*
7.7	Precoding for dispersive channels	*373*
7.7.1	Tomlinson–Harashima precoding	*374*
7.7.2	Flexible precoding	*376*
7.8	Channel estimation	*378*
7.8.1	The correlation method	*378*
7.8.2	The LS method	*379*
	Formulation using the data matrix	*380*
7.8.3	Signal-to-estimation error ratio	*380*
	Computation of the signal-to-estimation error ratio	*381*
	On the selection of the channel length	*384*

7.8.4 Channel estimation for multirate systems *384*
7.8.5 The LMMSE method *385*
7.9 Faster-than-Nyquist Signalling *386*
Bibliography *387*
Appendix 7.A Simulation of a QAM system *389*
Appendix 7.B Description of a finite-state machine *393*
Appendix 7.C Line codes for PAM systems *394*
7.C.1 Line codes *394*
Non-return-to-zero format *395*
Return-to-zero format *396*
Biphase format *397*
Delay modulation or Miller code *398*
Block line codes *398*
Alternate mark inversion *398*
7.C.2 Partial response systems *399*
The choice of the PR polynomial *401*
Symbol detection and error probability *404*
Precoding *406*
Error probability with precoding *407*
Alternative interpretation of PR systems *408*
7.D Implementation of a QAM transmitter *410*

8 Multicarrier modulation *413*
8.1 MC systems *413*
8.2 Orthogonality conditions *414*
Time domain *415*
Frequency domain *415*
z-Transform domain *415*
8.3 Efficient implementation of MC systems *416*
MC implementation employing matched filters *416*
Orthogonality conditions in terms of the polyphase components *418*
MC implementation employing a prototype filter *419*
8.4 Non-critically sampled filter banks *422*
8.5 Examples of MC systems *426*
OFDM or DMT *426*
Filtered multitone *427*
8.6 Analog signal processing requirements in MC systems *429*
8.6.1 Analog filter requirements *429*
Interpolator filter and virtual subchannels *429*
Modulator filter *430*
8.6.2 Power amplifier requirements *431*
8.7 Equalization *432*
8.7.1 OFDM equalization *432*
8.7.2 FMT equalization *434*
Per-subchannel fractionally spaced equalization *434*
Per-subchannel T-spaced equalization *435*
Alternative per-subchannel T-spaced equalization *436*
8.8 Orthogonal time frequency space modulation *437*

OTFS equalization 437
8.9 Channel estimation in OFDM 437
Instantaneous estimate or LS method 438
LMMSE 440
The LS estimate with truncated impulse response 440
8.9.1 Channel estimate and pilot symbols 441
8.10 Multiuser access schemes 442
8.10.1 OFDMA 442
8.10.2 SC-FDMA or DFT-spread OFDM 443
8.11 Comparison between MC and SC systems 444
8.12 Other MC waveforms 445
Bibliography 446

9 Transmission over multiple input multiple output channels 447
9.1 The MIMO NB channel 447
Spatial multiplexing and spatial diversity 451
Interference in MIMO channels 452
9.2 CSI only at the receiver 452
9.2.1 SIMO combiner 452
Equalization and diversity 455
9.2.2 MIMO combiner 455
Zero-forcing 456
MMSE 456
9.2.3 MIMO non-linear detection and decoding 457
V-BLAST system 457
Spatial modulation 458
9.2.4 Space-time coding 459
The Alamouti code 459
The Golden code 461
9.2.5 MIMO channel estimation 461
The least squares method 462
The LMMSE method 463
9.3 CSI only at the transmitter 463
9.3.1 MISO linear precoding 463
MISO antenna selection 464
9.3.2 MIMO linear precoding 465
ZF precoding 465
9.3.3 MIMO non-linear precoding 466
Dirty paper coding 467
TH precoding 468
9.3.4 Channel estimation for CSIT 469
9.4 CSI at both the transmitter and the receiver 469
9.5 Hybrid beamforming 470
Hybrid beamforming and angular domain representation 472
9.6 Multiuser MIMO: broadcast channel 472
CSI only at the receivers 473
CSI only at the transmitter 473
9.6.1 CSI at both the transmitter and the receivers 473
Block diagonalization 473

User selection *474*
Joint spatial division and multiplexing *475*
9.6.2 Broadcast channel estimation *476*
9.7 Multiuser MIMO: multiple-access channel *476*
CSI only at the transmitters *477*
CSI only at the receiver *477*
9.7.1 CSI at both the transmitters and the receiver *477*
Block diagonalization *477*
9.7.2 Multiple-access channel estimation *478*
9.8 Massive MIMO *478*
9.8.1 Channel hardening *478*
9.8.2 Multiuser channel orthogonality *479*
Bibliography *479*

10 Spread-spectrum systems *483*
10.1 Spread-spectrum techniques *483*
10.1.1 Direct sequence systems *483*
Classification of CDMA systems *490*
Synchronization *490*
10.1.2 Frequency hopping systems *491*
Classification of FH systems *491*
10.2 Applications of spread-spectrum systems *493*
10.2.1 Anti-jamming *494*
10.2.2 Multiple access *496*
10.2.3 Interference rejection *496*
10.3 Chip matched filter and rake receiver *496*
Number of resolvable rays in a multipath channel *497*
Chip matched filter *498*
10.4 Interference *500*
Detection strategies for multiple-access systems *502*
10.5 Single-user detection *502*
Chip equalizer *502*
Symbol equalizer *503*
10.6 Multiuser detection *504*
10.6.1 Block equalizer *504*
10.6.2 Interference cancellation detector *506*
Successive interference cancellation *506*
Parallel interference cancellation *507*
10.6.3 ML multiuser detector *508*
Correlation matrix *508*
Whitening filter *508*
10.7 Multicarrier CDMA systems *509*
Bibliography *510*
Appendix 10.A Walsh Codes *511*

11 Channel codes *515*
11.1 System model *516*
11.2 Block codes *517*
11.2.1 Theory of binary codes with group structure *518*

Properties *518*
Parity check matrix *520*
Code generator matrix *522*
Decoding of binary parity check codes *523*
Cosets *523*
Two conceptually simple decoding methods *524*
Syndrome decoding *525*
11.2.2 Fundamentals of algebra *527*
modulo-q arithmetic *528*
Polynomials with coefficients from a field *530*
Modular arithmetic for polynomials *531*
Devices to sum and multiply elements in a finite field *534*
Remarks on finite fields *535*
Roots of a polynomial *538*
Minimum function *541*
Methods to determine the minimum function *542*
Properties of the minimum function *544*
11.2.3 Cyclic codes *545*
The algebra of cyclic codes *545*
Properties of cyclic codes *546*
Encoding by a shift register of length r *551*
Encoding by a shift register of length k *552*
Hard decoding of cyclic codes *552*
Hamming codes *554*
Burst error detection *556*
11.2.4 Simplex cyclic codes *556*
Property *557*
Relation to PN sequences *558*
11.2.5 BCH codes *558*
An alternative method to specify the code polynomials *558*
Bose-Chaudhuri–Hocquenhem codes *560*
Binary BCH codes *562*
Reed–Solomon codes *564*
Decoding of BCH codes *566*
Efficient decoding of BCH codes *568*
11.2.6 Performance of block codes *575*
11.3 Convolutional codes *576*
11.3.1 General description of convolutional codes *579*
Parity check matrix *581*
Generator matrix *581*
Transfer function *582*
Catastrophic error propagation *585*
11.3.2 Decoding of convolutional codes *586*
Interleaving *587*
Two decoding models *587*
Decoding by the Viterbi algorithm *588*
Decoding by the forward-backward algorithm *589*
Sequential decoding *590*
11.3.3 Performance of convolutional codes *592*

11.4 Puncturing *593*
11.5 Concatenated codes *593*
The soft-output Viterbi algorithm *593*
11.6 Turbo codes *597*
Encoding *597*
The basic principle of iterative decoding *600*
FBA revisited *601*
Iterative decoding *608*
Performance evaluation *610*
11.7 Iterative detection and decoding *611*
11.8 Low-density parity check codes *614*
11.8.1 Representation of LDPC codes *614*
Matrix representation *614*
Graphical representation *615*
11.8.2 Encoding *616*
Encoding procedure *616*
11.8.3 Decoding *617*
Hard decision decoder *617*
The sum-product algorithm decoder *619*
The LR-SPA decoder *622*
The LLR-SPA or log-domain SPA decoder *623*
The min-sum decoder *625*
Other decoding algorithms *625*
11.8.4 Example of application *625*
Performance and coding gain *625*
11.8.5 Comparison with turbo codes *627*
11.9 Polar codes *627*
11.9.1 Encoding *628*
Internal CRC *630*
LLRs associated to code bits *631*
11.9.2 Tanner graph *631*
11.9.3 Decoding algorithms *633*
Successive cancellation decoding – the principle *634*
Successive cancellation decoding – the algorithm *635*
Successive cancellation list decoding *638*
Other decoding algorithms *639*
11.9.4 Frozen set design *640*
Genie-aided SC decoding *640*
Design based on density evolution *641*
Channel polarization *643*
11.9.5 Puncturing and shortening *644*
Puncturing *644*
Shortening *645*
Frozen set design *647*
11.9.6 Performance *647*
11.10 Milestones in channel coding *648*
Bibliography *649*
Appendix 11.A Non-binary parity check codes *652*
Linear codes *653*

Parity check matrix *654*
Code generator matrix *655*
Decoding of non-binary parity check codes *656*
Coset *656*
Two conceptually simple decoding methods *656*
Syndrome decoding *657*

12 Trellis coded modulation *659*
12.1 Linear TCM for one- and two-dimensional signal sets *660*
12.1.1 Fundamental elements *660*
Basic TCM scheme *661*
Example *662*
12.1.2 Set partitioning *664*
12.1.3 Lattices *666*
12.1.4 Assignment of symbols to the transitions in the trellis *671*
12.1.5 General structure of the encoder/bit-mapper *675*
Computation of d_{free} *677*
12.2 Multidimensional TCM *679*
Encoding *680*
Decoding *682*
12.3 Rotationally invariant TCM schemes *684*
Bibliography *685*

13 Techniques to achieve capacity *687*
13.1 Capacity achieving solutions for multicarrier systems *687*
13.1.1 Achievable bit rate of OFDM *687*
13.1.2 Waterfilling solution *688*
Iterative solution *689*
13.1.3 Achievable rate under practical constraints *689*
Effective SNR and system margin in MC systems *690*
Uniform power allocation and minimum rate per subchannel *690*
13.1.4 The bit and power loading problem revisited *691*
Problem formulation *692*
Some simplifying assumptions *692*
On loading algorithms *693*
The Hughes-Hartogs algorithm *694*
The Krongold–Ramchandran–Jones algorithm *694*
The Chow–Cioffi–Bingham algorithm *696*
Comparison *698*
13.2 Capacity achieving solutions for single carrier systems *698*
Achieving capacity *702*
Bibliography *703*

14 Synchronization *705*
14.1 The problem of synchronization for QAM systems *705*
14.2 The phase-locked loop *707*
14.2.1 PLL baseband model *708*
Linear approximation *709*

14.2.2 Analysis of the PLL in the presence of additive noise *711*
Noise analysis using the linearity assumption *711*
14.2.3 Analysis of a second-order PLL *713*
14.3 Costas loop *716*
14.3.1 PAM signals *716*
14.3.2 QAM signals *719*
14.4 The optimum receiver *720*
Timing recovery *721*
Carrier phase recovery *725*
14.5 Algorithms for timing and carrier phase recovery *725*
14.5.1 ML criterion *726*
Assumption of slow time varying channel *726*
14.5.2 Taxonomy of algorithms using the ML criterion *726*
Feedback estimators *727*
Early-late estimators *728*
14.5.3 Timing estimators *729*
Non-data aided *729*
NDA synchronization via spectral estimation *732*
Data aided and data directed *733*
Data and phase directed with feedback: differentiator scheme *735*
Data and phase directed with feedback: Mueller and Muller scheme *735*
Non-data aided with feedback *738*
14.5.4 Phasor estimators *738*
Data and timing directed *738*
Non-data aided for M-PSK signals *738*
Data and timing directed with feedback *739*
14.6 Algorithms for carrier frequency recovery *740*
14.6.1 Frequency offset estimators *741*
Non-data aided *741*
Non-data aided and timing independent with feedback *742*
Non-data aided and timing directed with feedback *743*
14.6.2 Estimators operating at the modulation rate *743*
Data aided and data directed *744*
Non-data aided for M-PSK *744*
14.7 Second-order digital PLL *744*
14.8 Synchronization in spread-spectrum systems *745*
14.8.1 The transmission system *745*
Transmitter *745*
Optimum receiver *745*
14.8.2 Timing estimators with feedback *746*
Non-data aided: non-coherent DLL *747*
Non-data aided modified code tracking loop *747*
Data and phase directed: coherent DLL *747*
14.9 Synchronization in OFDM *751*
14.9.1 Frame synchronization *751*
Effects of STO *751*
Schmidl and Cox algorithm *752*
14.9.2 Carrier frequency synchronization *754*

Estimator performance *755*
Other synchronization solutions *755*
14.10 Synchronization in SC-FDMA *756*
Bibliography *756*

15 Self-training equalization *759*
15.1 Problem definition and fundamentals *759*
Minimization of a special function *762*
15.2 Three algorithms for PAM systems *765*
The Sato algorithm *765*
Benveniste–Goursat algorithm *766*
Stop-and-go algorithm *766*
Remarks *767*
15.3 The contour algorithm for PAM systems *767*
Simplified realization of the contour algorithm *769*
15.4 Self-training equalization for partial response systems *770*
The Sato algorithm *770*
The contour algorithm *772*
15.5 Self-training equalization for QAM systems *773*
The Sato algorithm *773*
15.5.1 Constant-modulus algorithm *775*
The contour algorithm *776*
Joint contour algorithm and carrier phase tracking *777*
15.6 Examples of applications *779*
Bibliography *783*
Appendix 15.A On the convergence of the contour algorithm *784*

16 Low-complexity demodulators *787*
16.1 Phase-shift keying *787*
16.1.1 Differential PSK *787*
Error probability of M-DPSK *789*
16.1.2 Differential encoding and coherent demodulation *791*
Differentially encoded BPSK *791*
Multilevel case *791*
16.2 (D)PSK non-coherent receivers *793*
16.2.1 Baseband differential detector *793*
16.2.2 IF-band (1 bit) differential detector *794*
Signal at detection point *796*
16.2.3 FM discriminator with integrate and dump filter *797*
16.3 Optimum receivers for signals with random phase *798*
ML criterion *799*
Implementation of a non-coherent ML receiver *800*
Error probability for a non-coherent binary FSK system *804*
Performance comparison of binary systems *806*
16.4 Frequency-based modulations *807*
16.4.1 Frequency shift keying *807*
Coherent demodulator *808*
Non-coherent demodulator *808*

Limiter–discriminator FM demodulator *809*
16.4.2 Minimum-shift keying *810*
Power spectral density of CPFSK *812*
Performance *814*
MSK with differential precoding *815*
16.4.3 Remarks on spectral containment *816*
16.5 Gaussian MSK *816*
16.5.1 Implementation of a GMSK scheme *819*
Configuration I *821*
Configuration II *821*
Configuration III *822*
16.5.2 Linear approximation of a GMSK signal *824*
Performance of GMSK *824*
Performance in the presence of multipath *829*
Bibliography *830*
Appendix 16.A Continuous phase modulation *831*
Alternative definition of CPM *831*
Advantages of CPM *832*

17 Applications of interference cancellation *833*
17.1 Echo and near-end crosstalk cancellation for PAM systems *834*
Crosstalk cancellation and full-duplex transmission *835*
Polyphase structure of the canceller *836*
Canceller at symbol rate *836*
Adaptive canceller *837*
Canceller structure with distributed arithmetic *838*
17.2 Echo cancellation for QAM systems *842*
17.3 Echo cancellation for OFDM systems *844*
17.4 Multiuser detection for VDSL *846*
17.4.1 Upstream power back-off *850*
17.4.2 Comparison of PBO methods *851*
Bibliography *855*

18 Examples of communication systems *857*
18.1 The 5G cellular system *857*
18.1.1 Cells in a wireless system *857*
18.1.2 The release 15 of the 3GPP standard *858*
18.1.3 Radio access network *859*
Time-frequency plan *859*
NR data transmission chain *861*
OFDM numerology *861*
Channel estimation *862*
18.1.4 Downlink *862*
Synchronization *863*
Initial access or beam sweeping *864*
Channel estimation *865*
Channel state information reporting *865*
18.1.5 Uplink *865*

Transform precoding numerology 866
Channel estimation 866
Synchronization 866
Timing advance 867
18.1.6 Network slicing 867
18.2 GSM 868
Radio subsystem 870
18.3 Wireless local area networks 872
Medium access control protocols 872
18.4 DECT 873
18.5 Bluetooth 875
18.6 Transmission over unshielded twisted pairs 875
18.6.1 Transmission over UTP in the customer service area 876
18.6.2 High-speed transmission over UTP in local area networks 880
18.7 Hybrid fibre/coaxial cable networks 881
Ranging and power adjustment in OFDMA systems 885
Ranging and power adjustment for uplink transmission 886
Bibliography 889
Appendix 18.A Duplexing 890
Three methods 890
Appendix 18.B Deterministic access methods 890

19 High-speed communications over twisted-pair cables *893*
19.1 Quaternary partial response class-IV system 893
Analog filter design 893
Received signal and adaptive gain control 894
Near-end crosstalk cancellation 895
Decorrelation filter 895
Adaptive equalizer 895
Compensation of the timing phase drift 896
Adaptive equalizer coefficient adaptation 896
Convergence behaviour of the various algorithms 897
19.1.1 VLSI implementation 897
Adaptive digital NEXT canceller 897
Adaptive digital equalizer 900
Timing control 904
Viterbi detector 906
19.2 Dual-duplex system 906
Dual-duplex transmission 906
Physical layer control 908
Coding and decoding 909
19.2.1 Signal processing functions 912
The 100BASE-T2 transmitter 912
The 100BASE-T2 receiver 913
Computational complexity of digital receive filters 914
Bibliography 915
Appendix 19.A Interference suppression 915

Index *917*

Preface

The motivation for writing this book is twofold. On the one hand, we provide a teaching tool for advanced courses in communications systems. On the other hand, we present a collection of fundamental algorithms and structures useful as an in-depth reference for researchers and engineers. The contents reflect our experience in teaching university courses on algorithms for telecommunications, as well as our professional experience acquired in industrial research laboratories.

The text illustrates the steps required for solving problems posed by the design of systems for reliable communications over wired or wireless channels. In particular, we have focused on fundamental developments in the field in order to provide the reader with the necessary insight to design practical systems.

The second edition of this book has been enriched by new solutions in fields of application and standards that have emerged since the first edition of 2002. To name one, the adoption of multiple antennas in wireless communication systems has received a tremendous impulse in recent years, and an entire chapter is now dedicated to this topic. About error correction, *polar* codes have been invented and are considered for future standards. Therefore, they also have been included in this new book edition. On the standards side, cellular networks have evolved significantly, thus we decided to dedicate a large part of a chapter to the new fifth-generation (5G) of cellular networks, which is being finalized at the time of writing. Moreover, a number of transmission techniques that have been designed and studied for application to 5G systems, with special regard to multi-carrier transmission, have been treated in this book. Lastly, many parts have been extensively integrated with new material, rewritten, and improved, with the purpose of illustrating to the reader their connection with current research trends, such as advances in machine learning.

Acknowledgements

We gratefully acknowledge all who have made the realization of this book possible. In particular, the editing of the various chapters would never have been completed without the contributions of numerous students in our courses on Algorithms for Telecommunications. Although space limitations preclude mentioning them all by name, we nevertheless express our sincere gratitude. We also thank Christian Bolis and Chiara Paci for their support in developing the software for the book, Charlotte Bolliger and Lilli M. Pavka for their assistance in administering the project, and Urs Bitterli and Darja Kropaci for their help with the graphics editing. For text processing, also for the Italian version, the contribution of Barbara Sicoli and Edoardo Casarin was indispensable; our thanks also go to Jane Frankenfield Zanin for her help in translating the text into English. We are pleased to thank the following colleagues for their invaluable assistance throughout the revision of the book: Antonio Assalini, Leonardo Bazzaco, Paola Bisaglia, Matthieu Bloch, Alberto Bononi, Alessandro Brighente, Giancarlo Calvagno, Giulio Colavolpe, Roberto Corvaja, Elena Costa, Daniele Forner, Andrea Galtarossa, Antonio Mian, Carlo Monti, Ezio Obetti, Riccardo Rahely, Roberto Rinaldo, Antonio Salloum, Fortunato Santucci, Andrea Scaggiante, Giovanna Sostrato, and Luciano Tomba. We gratefully acknowledge our colleague and mentor Jack Wolf for letting us include his lecture notes in the chapter on channel codes. We also acknowledge the important contribution of Ingmar Land on writing the section on polar codes. An acknowledgement goes also to our colleagues Werner Bux and Evangelos Eleftheriou of the IBM Zurich Research Laboratory, and Silvano Pupolin of the University of Padova, for their continuing support. Finally, special thanks go to Hideki Ochiai of Yokohama National University and Jinhong Yuan of University of New South Wales for hosting Nevio Benvenuto in the Fall 2018 and Spring 2019, respectively: both colleagues provided an ideal setting for developing the new book edition.

To make the reading of the adopted symbols easier, the Greek alphabet is reported below.

The Greek alphabet					
α	A	alpha	ν	N	nu
β	B	beta	ξ	Ξ	xi
γ	Γ	gamma	o	O	omicron
δ	Δ	delta	π	Π	pi
ϵ, ε	E	epsilon	ρ, ϱ	P	rho
ζ	Z	zeta	σ, ς	$\sum$	sigma
η	H	eta	τ	T	tau
θ, ϑ	Θ	theta	υ	Y	upsilon
ι	I	iota	ϕ, φ	Φ	phi
κ	K	kappa	χ	X	chi
λ	Λ	lambda	ψ	Ψ	psi
μ	M	mu	ω	Ω	omega

Chapter 1

Elements of signal theory

In this chapter, we recall some concepts on signal theory and random processes. For an in-depth study, we recommend the companion book [1]. First, we introduce various forms of the Fourier transform. Next, we provide the complex representation of passband signals and their baseband equivalent. We will conclude with the study of random processes, with emphasis on the statistical estimation of first- and second-order ergodic processes, i.e. periodogram, correlogram, auto-regressive (AR), moving-average (MA), and auto-regressive moving average (ARMA) models.

1.1 Continuous-time linear systems

A time-invariant continuous-time continuous-amplitude linear system, also called analog filter, is represented in Figure 1.1, where x and y are the input and output signals, respectively, and h denotes the filter impulse response.

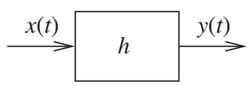

Figure 1.1 Analog filter as a time-invariant linear system with continuous domain.

The output at a certain instant $t \in \mathbb{R}$, where $\mathbb{R}$ denotes the set of real numbers, is given by the convolution integral

$$y(t) = \int_{-\infty}^{\infty} h(t-\tau)\, x(\tau)\, d\tau = \int_{-\infty}^{\infty} h(\tau)\, x(t-\tau)\, d\tau \tag{1.1}$$

denoted in short

$$y(t) = x * h(t) \tag{1.2}$$

We also introduce the Fourier transform of the signal $x(t)$, $t \in \mathbb{R}$,

$$\mathcal{X}(f) = \mathcal{F}[x(t)] = \int_{-\infty}^{+\infty} x(t)\, e^{-j2\pi ft}\, dt \qquad f \in \mathbb{R} \tag{1.3}$$

where $j = \sqrt{-1}$. The inverse Fourier transform is given by

$$x(t) = \int_{-\infty}^{\infty} \mathcal{X}(f)\, e^{j2\pi ft}\, df \tag{1.4}$$

Algorithms for Communications Systems and their Applications, Second Edition.
Nevio Benvenuto, Giovanni Cherubini, and Stefano Tomasin.

In the frequency domain, (1.2) becomes

$$\mathcal{Y}(f) = \mathcal{X}(f)\ \mathcal{H}(f), \qquad f \in \mathbb{R} \tag{1.5}$$

where $\mathcal{H}$ is the filter frequency response. The magnitude of the frequency response, $|\mathcal{H}(f)|$, is usually called *magnitude response* or *amplitude response*.

General properties of the Fourier transform are given in Table 1.1,[1] where we use two important functions

$$\text{step function:} \quad 1(t) = \begin{cases} 1 & t > 0 \\ 0 & t < 0 \end{cases} \tag{1.6}$$

$$\text{sign function:} \quad \text{sgn}(t) = \begin{cases} 1 & t > 0 \\ -1 & t < 0 \end{cases} \tag{1.7}$$

Moreover, we denote by $\delta(t)$ the *Dirac impulse* or delta function,

$$\delta(t) = \frac{d1(t)}{dt} \tag{1.8}$$

where the derivative is taken in the generalized sense.

Definition 1.1
We introduce two functions that will be extensively used:

$$\text{rect}(f) = \begin{cases} 1 & |f| < \frac{1}{2} \\ 0 & \text{elsewhere} \end{cases} \tag{1.9}$$

$$\text{sinc}(t) = \frac{\sin(\pi t)}{\pi t} \tag{1.10}$$

The following relation holds

$$\mathcal{F}[\text{sinc}(Ft)] = \frac{1}{F}\text{rect}\left(\frac{f}{F}\right) \tag{1.11}$$

as illustrated in Figure 1.2. □

Further examples of signals and relative Fourier transforms are given in Table 1.2.

We reserve the notation $H(s)$ to indicate the Laplace transform of $h(t)$, $t \in \mathbb{R}$:

$$H(s) = \int_{-\infty}^{+\infty} h(t)e^{-st}dt \tag{1.12}$$

with s complex variable; $H(s)$ is also called the *transfer function* of the filter. A class of functions $H(s)$ often used in practice is characterized by the ratio of two polynomials in s, each with a finite number of coefficients.

It is easy to observe that if the curve $s = j2\pi f$ in the s-plane belongs to the convergence region of the integral in (1.12), then $\mathcal{H}(f)$ is related to $H(s)$ by

$$\mathcal{H}(f) = H(s)|_{s=j2\pi f} \tag{1.13}$$

1.2 Discrete-time linear systems

A discrete-time time-invariant linear system, with sampling period T_c, is shown in Figure 1.3, where $x(k)$ and $y(k)$ are, respectively, the input and output signals at the time instant kT_c, $k \in \mathbb{Z}$, where $\mathbb{Z}$ denotes

[1] x^* denotes the complex conjugate of x, while $Re(x)$ and $Im(x)$ denote, respectively, the real and imaginary part of x.

Table 1.1: Some general properties of the Fourier transform.

property	*signal*	*Fourier transform*
	$x(t)$	$\mathcal{X}(f)$
linearity	$a\ x(t) + b\ y(t)$	$a\ \mathcal{X}(f) + b\ \mathcal{Y}(f)$
duality	$\mathcal{X}(t)$	$x(-f)$
time inverse	$x(-t)$	$\mathcal{X}(-f)$
complex conjugate	$x^*(t)$	$\mathcal{X}^*(-f)$
real part	$Re[x(t)] = \dfrac{x(t) + x^*(t)}{2}$	$\dfrac{1}{2}\ [\mathcal{X}(f) + \mathcal{X}^*(-f)]$
imaginary part	$Im[x(t)] = \dfrac{x(t) - x^*(t)}{2j}$	$\dfrac{1}{2j}\ [\mathcal{X}(f) - \mathcal{X}^*(-f)]$
time scaling	$x(at),\ a \neq 0$	$\dfrac{1}{\lvert a\rvert}\ \mathcal{X}\left(\dfrac{f}{a}\right)$
time shift	$x(t - t_0)$	$e^{-j2\pi f t_0}\ \mathcal{X}(f)$
frequency shift	$x(t)\ e^{j2\pi f_0 t}$	$\mathcal{X}(f - f_0)$
modulation	$x(t)\cos(2\pi f_0 t + \varphi)$	$\dfrac{1}{2}\ [e^{j\varphi}\mathcal{X}(f - f_0) + e^{-j\varphi}\mathcal{X}(f + f_0)]$
	$x(t)\sin(2\pi f_0 t + \varphi)$	$\dfrac{1}{2j}\ [e^{j\varphi}\mathcal{X}(f - f_0) - e^{-j\varphi}\mathcal{X}(f + f_0)]$
	$Re[x(t)\ e^{j(2\pi f_0 t + \varphi)}]$	$\dfrac{1}{2}[e^{j\varphi}\mathcal{X}(f - f_0) + e^{-j\varphi}\mathcal{X}^*(-f - f_0)]$
differentiation	$\dfrac{d}{dt}\ x(t)$	$j2\pi f\ \mathcal{X}(f)$
integration	$\displaystyle\int_{-\infty}^{t} x(\tau)\ d\tau = 1 * x(t)$	$\dfrac{1}{j2\pi f}\ \mathcal{X}(f) + \dfrac{\mathcal{X}(0)}{2}\ \delta(f)$
convolution	$x * y(t)$	$\mathcal{X}(f)\ \mathcal{Y}(f)$
correlation	$[x(\tau) * y^*(-\tau)](t)$	$\mathcal{X}(f)\ \mathcal{Y}^*(f)$
product	$x(t)\ y(t)$	$\mathcal{X} * \mathcal{Y}(f)$
real signal	$x(t) = x^*(t)$	$\mathcal{X}(f) = \mathcal{X}^*(-f)$, $\mathcal{X}$ Hermitian,
		$Re[\mathcal{X}(f)]$ even, $Im[\mathcal{X}(f)]$ odd,
		$\lvert\mathcal{X}(f)\rvert^2$ even
imaginary signal	$x(t) = -x^*(t)$	$\mathcal{X}(f) = -\mathcal{X}^*(-f)$
real and even signal	$x(t) = x^*(t) = x(-t)$	$\mathcal{X}(f) = \mathcal{X}^*(f) = \mathcal{X}(-f)$,
		$\mathcal{X}$ real and even
real and odd signal	$x(t) = x^*(t) = -x(-t)$	$\mathcal{X}(f) = -\mathcal{X}^*(f) = -\mathcal{X}(-f)$,
		$\mathcal{X}$ imaginary and odd
Parseval theorem	$\displaystyle E_x = \int_{-\infty}^{+\infty} \lvert x(t)\rvert^2\ dt = \int_{-\infty}^{+\infty} \lvert\mathcal{X}(f)\rvert^2\ df = E_{\mathcal{X}}$	
Poisson sum formula	$\displaystyle\sum_{k=-\infty}^{+\infty} x(kT_c) = \frac{1}{T_c} \sum_{\ell=-\infty}^{+\infty} \mathcal{X}\left(\frac{\ell}{T_c}\right)$	

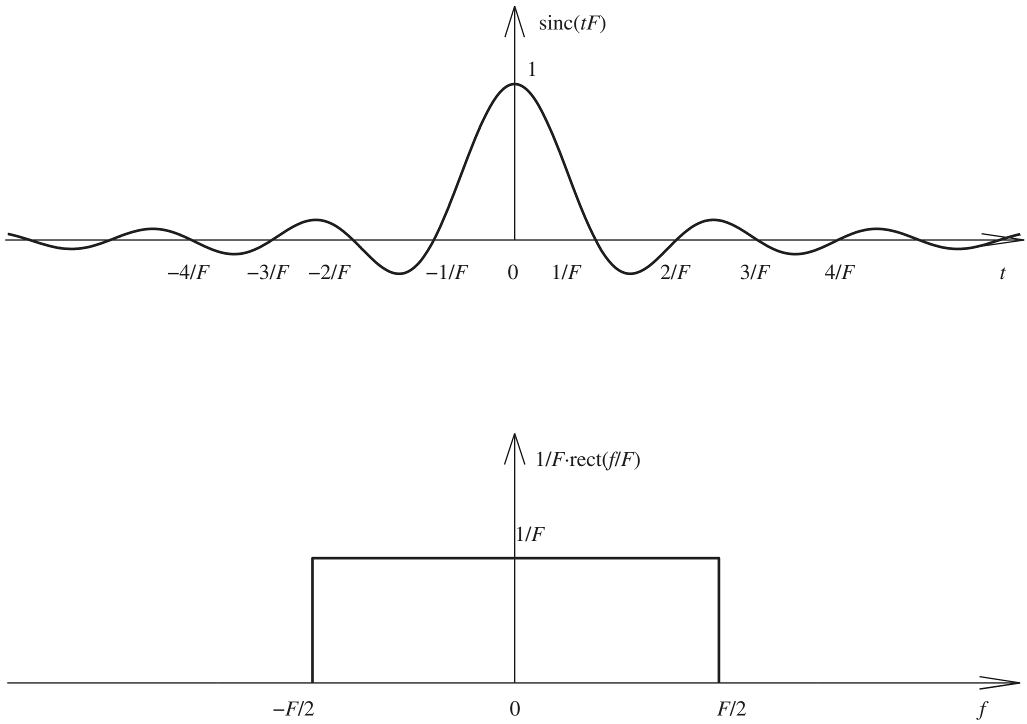

Figure 1.2 Example of signal and Fourier transform pair.

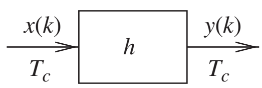

Figure 1.3 Discrete-time linear system (filter).

the set of integers. We denote by $\{x(k)\}$ or $\{x_k\}$ the entire discrete-time signal, also called *sequence*. The impulse response of the system is denoted by $\{h(k)\}$, $k \in \mathbb{Z}$, or more simply by h.

The relation between the input sequence $\{x(k)\}$ and the output sequence $\{y(k)\}$ is given by the convolution operation:

$$y(k) = \sum_{n=-\infty}^{+\infty} h(k-n)x(n) \tag{1.14}$$

denoted as $y(k) = x * h(k)$. In the discrete time, the delta function is simply the *Kronecker impulse*

$$\delta_n = \delta(n) = \begin{cases} 1 & n = 0 \\ 0 & n \neq 0 \end{cases} \tag{1.15}$$

Here are some definitions holding for time-invariant linear systems.

The system is *causal* (anticausal) if $h(k) = 0$, $k < 0$ (if $h(k) = 0$, $k > 0$).

Table 1.2: Examples of Fourier transform signal pairs.

signal	*Fourier transform*
$x(t)$	$\mathcal{X}(f)$
$\delta(t)$	1
1 (constant)	$\delta(f)$
$e^{j2\pi f_0 t}$	$\delta(f-f_0)$
$\cos(2\pi f_0 t)$	$\frac{1}{2}\,[\delta(f-f_0)+\delta(f+f_0)]$
$\sin(2\pi f_0 t)$	$\frac{1}{2j}\,[\delta(f-f_0)-\delta(f+f_0)]$
$1(t)$	$\frac{1}{2}\,\delta(f)+\frac{1}{j2\pi f}$
$\mathrm{sgn}(t)$	$\frac{1}{j\pi f}$
$\mathrm{rect}\left(\frac{t}{T}\right)$	$T\,\mathrm{sinc}(fT)$
$\mathrm{sinc}\left(\frac{t}{T}\right)$	$T\,\mathrm{rect}(fT)$
$\left(1-\frac{\lvert t\rvert}{T}\right)\mathrm{rect}\left(\frac{t}{2T}\right)$	$T\mathrm{sinc}^2(fT)$
$e^{-at}\;1(t),\,a>0$	$\frac{1}{a+j2\pi f}$
$t\,e^{-at}\;1(t),\,a>0$	$\frac{1}{(a+j2\pi f)^2}$
$e^{-a\lvert t\rvert},\,a>0$	$\frac{2a}{a^2+(2\pi f)^2}$
$e^{-at^2},\,a>0$	$\sqrt{\frac{\pi}{a}}e^{-\pi\frac{\pi}{a}f^2}$

The *transfer function* of the filter is defined as the z-transform[2] of the impulse response h, given by

$$H(z)=\sum_{k=-\infty}^{+\infty}h(k)z^{-k} \tag{1.16}$$

Let the *frequency response* of the filter be defined as

$$\mathcal{H}(f)=\mathcal{F}[h(k)]=\sum_{k=-\infty}^{+\infty}h(k)e^{-j2\pi fkT_c}=H(z)_{z=e^{j2\pi fT_c}} \tag{1.17}$$

The inverse Fourier transform of the frequency response yields

$$h(k)=T_c\int_{-\frac{1}{2T_c}}^{+\frac{1}{2T_c}}\mathcal{H}(f)e^{j2\pi fkT_c}df \tag{1.18}$$

We note the property that, for $x(k)=b^k$, where b is a complex constant, the output is given by $y(k)=H(b)\,b^k$. In Table 1.3, some further properties of the z-transform are summarized.

For discrete-time linear systems, in the frequency domain (1.14) becomes

$$\mathcal{Y}(f)=\mathcal{X}(f)\mathcal{H}(f) \tag{1.19}$$

where all functions are periodic of period $1/T_c$.

[2] Sometimes the D transform is used instead of the z-transform, where $D=z^{-1}$, and $H(z)$ is replaced by $h(D)=\sum_{k=-\infty}^{+\infty}h(k)D^k$.

Table 1.3: Properties of the z-transform.

property	*sequence*	*z transform*
	$x(k)$	$X(z)$
linearity	$ax(k) + by(k)$	$aX(z) + bY(z)$
time shift	$x(k-m)$	$z^{-m}X(z)$
complex conjugate	$x^*(k)$	$X^*(z^*)$
time inverse	$x(-k)$	$X\left(\frac{1}{z}\right)$
	$x^*(-k)$	$X^*\left(\frac{1}{z^*}\right)$
z-domain scaling	$a^{-k}x(k)$	$X(az)$
convolution	$x * y(k)$	$X(z)Y(z)$
correlation	$x * (y^*(-m))(k)$	$X(z)Y^*\left(\frac{1}{z^*}\right)$
real sequence	$x(k) = x^*(k)$	$X(z) = X^*(z^*)$

Example 1.2.1
A fundamental example of z-transform is that of the sequence:

$$h(k) = \begin{cases} a^k & k \geq 0 \\ 0 & k < 0 \end{cases}, \qquad |a| < 1 \tag{1.20}$$

Applying the transform (1.16), we find

$$H(z) = \frac{1}{1 - az^{-1}} \tag{1.21}$$

defined for $|az^{-1}| < 1$ or $|z| > |a|$.

Example 1.2.2
Let $q(t)$, $t \in \mathbb{R}$, be a continuous-time signal with Fourier transform $\mathcal{Q}(f)$, $f \in \mathbb{R}$. We now consider the sequence obtained by sampling q, that is

$$h_k = q(kT_c), \qquad k \in \mathbb{Z} \tag{1.22}$$

Using the Poisson formula of Table 1.1, we have that the Fourier transform of the sequence $\{h_k\}$ is related to $\mathcal{Q}(f)$ by

$$\mathcal{H}(f) = \mathcal{F}[h_k] = H\left(e^{j2\pi f T_c}\right) = \frac{1}{T_c} \sum_{\ell=-\infty}^{\infty} \mathcal{Q}\left(f - \ell \frac{1}{T_c}\right) \tag{1.23}$$

Definition 1.2
Let us introduce the useful pulse with parameter N, a positive integer number,

$$\mathrm{sinc}_N(a) = \frac{1}{N} \frac{\sin(\pi a)}{\sin\left(\pi \frac{a}{N}\right)} \tag{1.24}$$

and $\mathrm{sinc}_N(0) = 1$. The pulse is periodic with period N ($2N$) if N is odd (even). For N, very large $\mathrm{sinc}_N(a)$ approximates $\mathrm{sinc}(a)$ in the range $|a| \ll N/2$. □

Example 1.2.3
For the signal

$$h_k = \begin{cases} 1 & k = 0, 1, \dots, N-1 \\ 0 & \text{otherwise} \end{cases} \tag{1.25}$$

with sampling period T_c, it is

$$\mathcal{H}(f) = e^{-j2\pi f \frac{N-1}{2} T_c} N \,\mathrm{sinc}_N(f N T_c) \tag{1.26}$$

Discrete Fourier transform

For a sequence with a finite number of samples, $\{g_k\}$, $k = 0, 1, \dots, N-1$, the Fourier transform becomes

$$\mathcal{G}(f) = \sum_{k=0}^{N-1} g_k e^{-j2\pi f k T_c} \tag{1.27}$$

Evaluating $\mathcal{G}(f)$ at the points $f = m/(NT_c)$, $m = 0, 1, \dots, N-1$, and setting $\mathcal{G}_m = \mathcal{G}(m/(NT_c))$, we obtain:

$$\mathcal{G}_m = \sum_{k=0}^{N-1} g_k W_N^{km}, \qquad W_N = e^{-j\frac{2\pi}{N}} \tag{1.28}$$

The sequence $\{\mathcal{G}_m\}$, $m = 0, 1, \dots, N-1$, is called the discrete Fourier transform (DFT) of $\{g_k\}$, $k = 0, 1, \dots, N-1$. The inverse of (1.28) is given by

$$g_k = \frac{1}{N} \sum_{m=0}^{N-1} \mathcal{G}_m W_N^{-km}, \qquad k = 0, 1, \dots, N-1 \tag{1.29}$$

We note that, besides the factor $1/N$, the expression of the inverse DFT (IDFT) coincides with that of the DFT, provided W_N^{-1} is substituted with W_N.

We also observe that the direct computation of (1.28) requires $N(N-1)$ complex additions and N^2 complex multiplications; however, the algorithm known as fast Fourier transform (FFT) computes the DFT by $N \log_2 N$ complex additions and $\left(\frac{N}{2}\log_2 N - N\right)$ complex multiplications.[3]

A simple implementation is also available when the DFT size is an integer power of some numbers (e.g. 2, 3, and 5). The efficient implementation of a DFT with length power of n (2, 3, and 5) is denoted as radix-n FFT. Moreover, if the DFT size is the product of integer powers of these numbers, the DFT can be implemented as a cascade of FFTs. In particular, by letting $M = 2^{\alpha_2}$, $L = 3^{\alpha_3} \cdot 5^{\alpha_5}$, the DFT of size $N = LM$ can be implemented as the cascade of L M-size DFTs, the multiplication by twiddle factors (operating only on the phase of the signal) and an L-size DFT. Applying again the same approach to the inner M-size DFT, we obtain that the N-size DFT is the cascade of 2^{α_2} FFTs of size $3^{\alpha_3} 5^{\alpha_5}$, each implemented by 3^{α_3} FFTs of size 5^{α_5}.

The DFT operator

The DFT operator can be expressed in matrix form as

$$\boldsymbol{F} = \begin{bmatrix} 1 & 1 & 1 & \dots & 1 \\ 1 & W_N & W_N^2 & \dots & W_N^{(N-1)} \\ 1 & W_N^2 & W_N^4 & \dots & W_N^{2(N-1)} \\ \vdots & \vdots & \vdots & \ddots & \vdots \\ 1 & W_N^{(N-1)} & W_N^{(N-1)2} & \dots & W_N^{(N-1)(N-1)} \end{bmatrix} \tag{1.30}$$

[3] The computational complexity of the FFT is often expressed as $N \log_2 N$.

with elements $[\boldsymbol{F}]_{i,n} = W_N^{in}$, $i, n = 0, 1, \ldots, N-1$. The inverse operator (IDFT) is given by[4]

$$\boldsymbol{F}^{-1} = \frac{1}{N}\boldsymbol{F}^* \tag{1.31}$$

We note that $\boldsymbol{F} = \boldsymbol{F}^T$ and $(1/\sqrt{N})\boldsymbol{F}$ is a unitary matrix.[5]

The following property holds: if $\boldsymbol{C}$ is a right circulant square matrix, i.e. its rows are obtained by successive shifts to the right of the first row, then $\boldsymbol{F}\boldsymbol{C}\boldsymbol{F}^{-1}$ is a diagonal matrix whose elements are given by the DFT of the first row of $\boldsymbol{C}$. This property is exploited in the most common modulation scheme (see Chapter 8).

Introducing the vector formed by the samples of the sequence $\{g_k\}$, $k = 0, 1, \ldots, N-1$,

$$\boldsymbol{g}^T = [g_0, g_1, \ldots, g_{N-1}] \tag{1.32}$$

and the vector of its transform coefficients

$$\boldsymbol{\mathcal{G}}^T = [\mathcal{G}_0, \mathcal{G}_1, \ldots, \mathcal{G}_{N-1}] = \mathrm{DFT}[\boldsymbol{g}] \tag{1.33}$$

from (1.28) we have

$$\boldsymbol{\mathcal{G}} = \boldsymbol{F}\boldsymbol{g} \tag{1.34}$$

Moreover, based on (1.31), we obtain

$$\boldsymbol{g} = \frac{1}{N}\boldsymbol{F}^*\boldsymbol{\mathcal{G}} \tag{1.35}$$

Circular and linear convolution via DFT

Let the two sequences x and h have a finite support of L_x and N samples, respectively, (see Figure 1.4) with $L_x > N$:

$$x(k) = 0 \qquad k < 0 \qquad k > L_x - 1 \tag{1.36}$$

and

$$h(k) = 0 \qquad k < 0 \qquad k > N - 1 \tag{1.37}$$

We define the periodic signals of period L,

$$x_{rep_L}(k) = \sum_{\ell=-\infty}^{+\infty} x(k - \ell L), \qquad h_{rep_L}(k) = \sum_{\ell=-\infty}^{+\infty} h(k - \ell L) \tag{1.38}$$

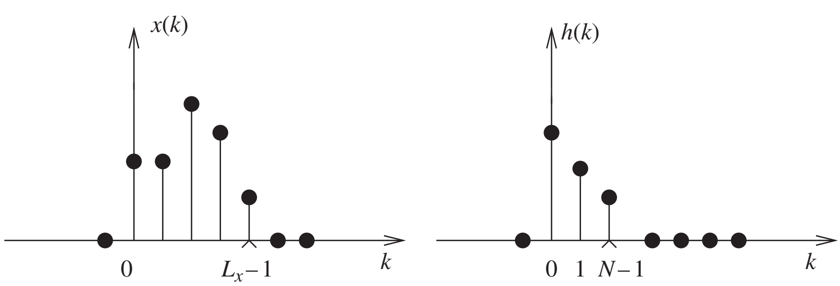

Figure 1.4 Time-limited signals: $\{x(k)\}$, $k = 0, 1, \ldots, L_x - 1$, and $\{h(k)\}$, $k = 0, 1, \ldots, N - 1$.

[4] ^{T} stands for transpose and ^{H} for transpose complex conjugate or Hermitian.

[5] A square matrix $\boldsymbol{A}$ is unitary if $\boldsymbol{A}^H\boldsymbol{A} = \boldsymbol{I}$, where $\boldsymbol{I}$ is the identity matrix, i.e. a matrix for which all elements are zero except the elements on the main diagonal that are all equal to one.

where in order to avoid *time aliasing*, it must be

$$L \geq \max\{L_x, N\} \tag{1.39}$$

Definition 1.3
The *circular convolution* between x and h is a periodic sequence of period L defined as

$$y^{(circ)}(k) = h \overset{L}{\otimes} x(k) = \sum_{i=0}^{L-1} h_{rep_L}(i)\; x_{rep_L}(k-i) \tag{1.40}$$

with *main period* corresponding to $k = 0, 1, \dots, L-1$. □

Then, if we indicate with $\{\mathcal{X}_m\}$, $\{\mathcal{H}_m\}$, and $\{\mathcal{Y}_m^{(circ)}\}$, $m = 0, 1, \dots, L-1$, the L-point DFT of sequences x, h, and $y^{(circ)}$, respectively, we obtain

$$\mathcal{Y}_m^{(circ)} = \mathcal{X}_m \mathcal{H}_m, \qquad m = 0, 1, \dots, L-1 \tag{1.41}$$

In vector notation (1.33), (1.41) becomes[6]

$$\boldsymbol{\mathcal{Y}}^{(circ)} = \left[\mathcal{Y}_0^{(circ)}, \mathcal{Y}_1^{(circ)}, \dots, \mathcal{Y}_{L-1}^{(circ)}\right]^T = \text{diag}\,\{\text{DFT}[\boldsymbol{x}]\}\, \boldsymbol{\mathcal{H}} \tag{1.42}$$

where $\boldsymbol{\mathcal{H}}$ is the column vector given by the L-point DFT of the sequence h, completed with $L - N$ zeros.

We are often interested in the *linear convolution* between x and h given by (1.14):

$$y(k) = x * h(k) = \sum_{i=0}^{N-1} h(i)x(k-i) \tag{1.43}$$

whose support is $k = 0, 1, \dots, L_x + N - 2$.

We give below two relations between the circular convolution $y^{(circ)}$ and the linear convolution y.

Relation 1. For

$$L \geq L_x + N - 1 \tag{1.44}$$

by comparing (1.43) with (1.40), the two convolutions $y^{(circ)}$ and y coincide only for the instants $k = 0, 1, \dots, L-1$, i.e.

$$y(k) = y^{(circ)}(k), \qquad k = 0, 1, \dots, L-1 \tag{1.45}$$

To compute the convolution between the two finite-length sequences x and h, (1.44) and (1.45) require that both sequences be completed with zeros (zero padding) to get a length of $L = L_x + N - 1$ samples. Then, taking the L-point DFT of the two sequences, performing the product (1.41), and taking the inverse transform of the result, one obtains the desired linear convolution.

Relation 2. For $L = L_x > N$, the two convolutions $y^{(circ)}$ and y coincide only for the instants $k = N-1$, $N, \dots, L-1$, i.e.

$$y^{(circ)}(k) = y(k) \qquad \text{only for} \qquad k = N-1, N, \dots, L-1 \tag{1.46}$$

An example of circular convolution is provided in Figure 1.5. Indeed, the result of circular convolution coincides with $\{y(k)\}$, output of the linear convolution, only for a delay k such that it is avoided the product between non-zero samples of the two periodic sequences h_{rep_L} and x_{rep_L}, indicated by • and ∘, respectively. This is achieved only for $k \geq N-1$ and $k \leq L-1$.

[6] The notation diag$\{\boldsymbol{v}\}$ denotes a diagonal matrix whose elements on the diagonal are equal to the elements of the vector $\boldsymbol{v}$.

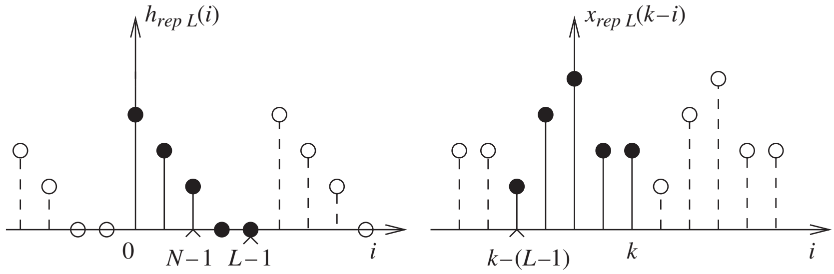

Figure 1.5 Illustration of the *circular convolution* operation between $\{x(k)\}$, $k = 0, 1, \dots, L-1$, and $\{h(k)\}$, $k = 0, 1, \dots, N-1$.

Relation 3. A relevant case wherein the cyclic convolution is equivalent to the linear convolution requires a special structure of the sequence x. Consider $x^{(cp)}$, the extended sequence of x, obtained by partially repeating x with a *cyclic prefix* of N_{cp} samples:

$$x^{(cp)}(k) = \begin{cases} x(k) & k = 0, 1, \dots, L_x - 1 \\ x(L_x + k) & k = -N_{cp}, \dots, -2, -1 \end{cases} \tag{1.47}$$

Let $y^{(cp)}$ be the *linear convolution* between $x^{(cp)}$ and h, with support $\{-N_{cp}, \dots, L_x + N - 2\}$. If $N_{cp} \geq N - 1$, we have

$$y^{(cp)}(k) = y^{(circ)}(k), \qquad k = 0, 1, \dots, L_x - 1 \tag{1.48}$$

Let us define

$$z(k) = \begin{cases} y^{(cp)}(k) & k = 0, 1, \dots, L_x - 1 \\ 0 & \text{elsewhere} \end{cases} \tag{1.49}$$

then from (1.48) and (1.41) the following relation between the corresponding L_x–point DFTs is obtained:

$$\mathcal{Z}_m = \mathcal{X}_m \mathcal{H}_m, \qquad m = 0, 1, \dots, L_x - 1 \tag{1.50}$$

Convolution by the overlap-save method

For a very long sequence x, the application of (1.46) leads to the *overlap-save* method to determine the linear convolution between x and h (with $L = L_x > N$). It is not restrictive to assume that the first $(N-1)$ samples of the sequence $\{x(k)\}$ are zero. If this were not True, it would be sufficient to shift the input by $(N-1)$ samples. A fast procedure to compute the linear convolution $\{y(k)\}$ for instants $k = N-1, N, \dots, L-1$, operates iteratively and processes blocks of L samples, where adjacent blocks are overlapping by $(N-1)$ samples. The procedure operates the following first iteration:[7]

1. *Loading*

$$\boldsymbol{h}'^T = [h(0), h(1), \dots, h(N-1), \overbrace{0, \dots, 0}^{L-N \text{ zeros}}] \tag{1.51}$$

$$\boldsymbol{x}'^T = [x(0), x(1), \dots, x(N-1), x(N), \dots, x(L-1)] \tag{1.52}$$

in which we have assumed $x(k) = 0$, $k = 0, 1, \dots, N-2$.

[7] In this section, the superscript $'$ indicates a vector of L elements.

2. *Transform*

$$\boldsymbol{\mathcal{H}}' = \mathrm{DFT}[\boldsymbol{h}'] \qquad \text{vector} \tag{1.53}$$

$$\boldsymbol{\mathcal{X}}' = \mathrm{diag}\{\mathrm{DFT}[\boldsymbol{x}']\} \quad \text{matrix} \tag{1.54}$$

3. *Matrix product*

$$\boldsymbol{\mathcal{Y}}' = \boldsymbol{\mathcal{X}}'\boldsymbol{\mathcal{H}}' \qquad \text{vector} \tag{1.55}$$

4. *Inverse transform*

$$\boldsymbol{y}'^T = \mathrm{DFT}^{-1}[\boldsymbol{\mathcal{Y}}'^T] = [\overbrace{\sharp, \dots, \sharp}^{N-1 \text{ terms}}, y(N-1), y(N), \dots, y(L-1)] \tag{1.56}$$

where the symbol $\sharp$ denotes a component that is neglected.

The second iteration operates on load

$$\boldsymbol{x}'^T = [x((L-1)-(N-2)), \dots, x(2(L-1)-(N-2))] \tag{1.57}$$

and the desired output samples will be

$$y(k) \qquad k = L, \dots, 2(L-1)-(N-2) \tag{1.58}$$

The third iteration operates on load

$$\boldsymbol{x}'^T = [x(2(L-1)-2(N-2)), \dots, x(3(L-1)-2(N-2))] \tag{1.59}$$

and will yield the desired output samples

$$y(k) \qquad k = 2(L-1)-(N-2)+1, \dots, 3(L-1)-2(N-2) \tag{1.60}$$

The algorithm proceeds iteratively until the entire input sequence is processed.

IIR and FIR filters

An important class of linear systems is identified by the input–output relation

$$\sum_{n=0}^{p} \mathtt{a}_n y(k-n) = \sum_{n=0}^{q} \mathtt{b}_n x(k-n) \tag{1.61}$$

where we will set $\mathtt{a}_0 = 1$ without loss of generality.

If the system is causal, (1.61) becomes

$$y(k) = -\sum_{n=1}^{p} \mathtt{a}_n y(k-n) + \sum_{n=0}^{q} \mathtt{b}_n x(k-n) \qquad k \geq 0 \tag{1.62}$$

and the transfer function for such system is

$$H(z) = \frac{Y(z)}{X(z)} = \frac{\sum_{n=0}^{q} \mathtt{b}_n z^{-n}}{1 + \sum_{n=1}^{p} \mathtt{a}_n z^{-n}} = \frac{\mathtt{b}_0 \prod_{n=1}^{q} (1 - \mathrm{z}_n z^{-1})}{\prod_{n=1}^{p} (1 - \mathrm{p}_n z^{-1})} \tag{1.63}$$

where $\{\mathrm{z}_n\}$ and $\{\mathrm{p}_n\}$ are, respectively, the zeros and poles of $H(z)$. Equation (1.63) generally defines an *infinite impulse response* (IIR) filter. In the case in which $\mathtt{a}_n = 0$, $n = 1, 2, \dots, p$, (1.63) reduces to

$$H(z) = \sum_{n=0}^{q} \mathtt{b}_n z^{-n} \tag{1.64}$$

Table 1.4: Impulse responses of systems having the same magnitude of the frequency response.

	$h(0)$	$h(1)$	$h(2)$	$h(3)$	$h(4)$
h_1 (minimum phase)	$0.9e^{-j1.57}$	0	0	$0.4e^{-j0.31}$	$0.3e^{-j0.63}$
h_2 (maximum phase)	$0.3e^{j0.63}$	$0.4e^{j0.31}$	0	0	$0.9e^{j1.57}$
h_3 (general case)	$0.7e^{-j1.57}$	$0.24e^{j2.34}$	$0.15e^{-j1.66}$	$0.58e^{-j0.51}$	$0.4e^{-j0.63}$

and we obtain a *finite impulse response* (FIR) filter, with $h(n) = \mathtt{b}_n$, $n = 0, 1, \dots, q$. To get the impulse response coefficients, assuming that the z-transform $H(z)$ is known, we can expand $H(z)$ in partial fractions and apply the linear property of the z-transform (see Table 1.3, page 6). If $q < p$, and assuming that all poles are distinct, we obtain

$$H(z) = \sum_{n=1}^{p} \frac{r_n}{1 - \mathrm{p}_n z^{-1}} \Longrightarrow h(k) = \begin{cases} \sum_{n=1}^{p} r_n \mathrm{p}_n^k & k \geq 0 \\ 0 & k < 0 \end{cases} \tag{1.65}$$

where

$$r_n = H(z) \left[1 - \mathrm{p}_n z^{-1}\right]\Big|_{z=\mathrm{p}_n} \tag{1.66}$$

We give now two definitions.

Definition 1.4
A causal system is *stable* (*bounded input-bounded output* stability) if $|\mathrm{p}_n| < 1$, $\forall n$. □

Definition 1.5
The system is *minimum phase* (*maximum phase*) if $|\mathrm{p}_n| < 1$ and $|\mathrm{z}_n| \leq 1$ ($|\mathrm{p}_n| > 1$ and $|\mathrm{z}_n| > 1$), $\forall n$. □

Among all systems having the same magnitude response $|\mathcal{H}(e^{j2\pi f T_c})|$, the minimum (maximum) phase system presents a phase[8] response, $\arg \mathcal{H}(e^{j2\pi f T_c})$, which is below (above) the phase response of all other systems.

Example 1.2.4
It is interesting to determine the phase of a system for a given impulse response. Let us consider the system with transfer function $H_1(z)$ and impulse response $h_1(k)$ shown in Figure 1.6a. After determining the zeros of the transfer function, we factorize $H_1(z)$ as follows:

$$H_1(z) = \mathtt{b}_0 \prod_{n=1}^{4} (1 - \mathrm{z}_n z^{-1}) \tag{1.67}$$

As shown in Figure 1.6a, $H_1(z)$ is minimum phase. We now observe that the magnitude of the frequency response does not change if $1/\mathrm{z}_n^*$ is replaced with z_n in (1.67). If we move all the zeros outside the unit circle, we get a maximum-phase system $H_2(z)$ whose impulse response is shown in Figure 1.6b. A general case, that is a transfer function with some zeros inside and others outside the unit circle, is given in Figure 1.6c. The coefficients of the impulse responses h_1, h_2, and h_3 are given in Table 1.4. The coefficients are normalized so that the three impulse responses have equal energy.

[8] For a complex number c, $\arg c$ denotes the phase of c.

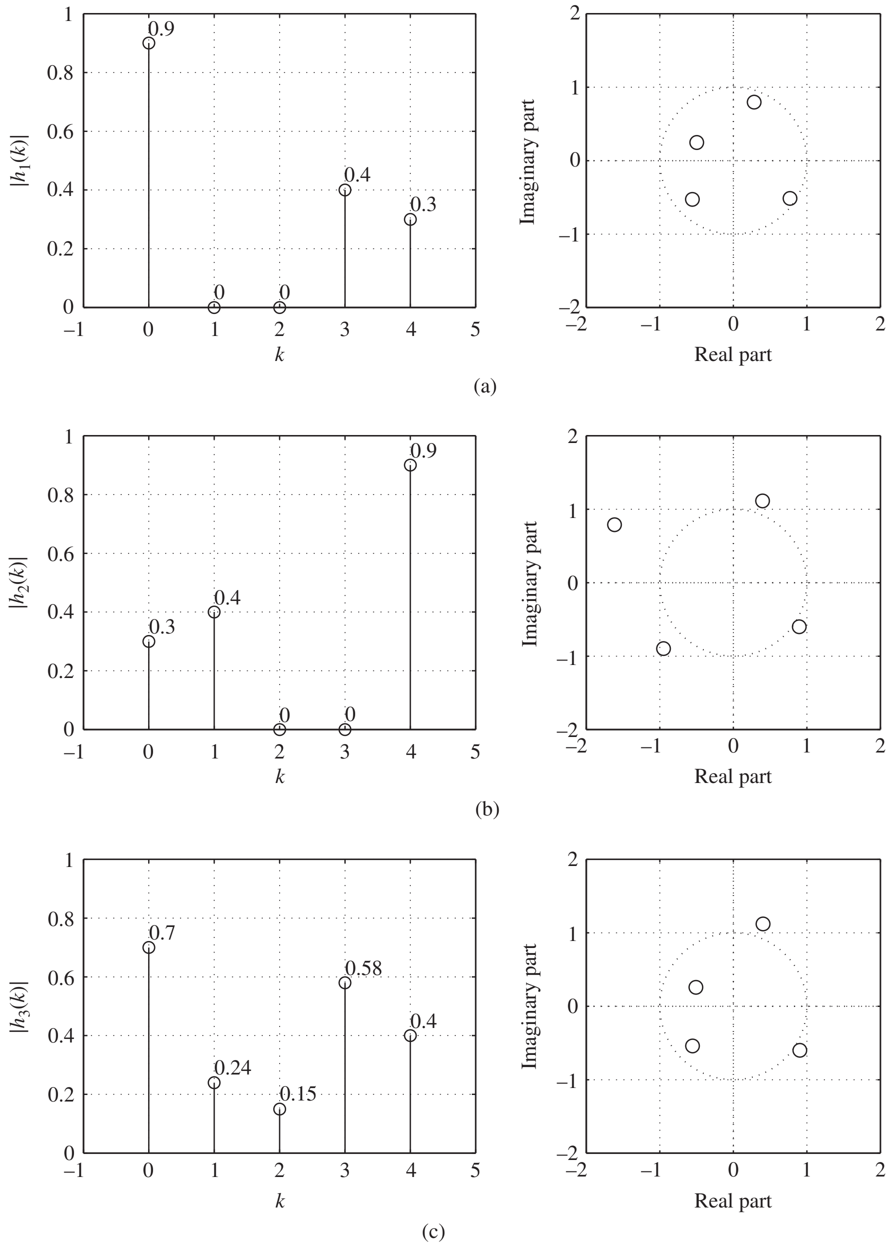

Figure 1.6 Impulse response magnitudes and zero locations for three systems having the same frequency response magnitude. (a) Minimum-phase system, (b) maximum-phase system, and (c) general system.

We define the *partial energy* of a causal impulse response as

$$E(k) = \sum_{i=0}^{k} |h(i)|^2 \tag{1.68}$$

Comparing the partial-energy sequences for the three impulse responses of Figure 1.6, one finds that the minimum (maximum) phase system yields the largest (smallest) $\{E(k)\}$. In other words, the magnitude

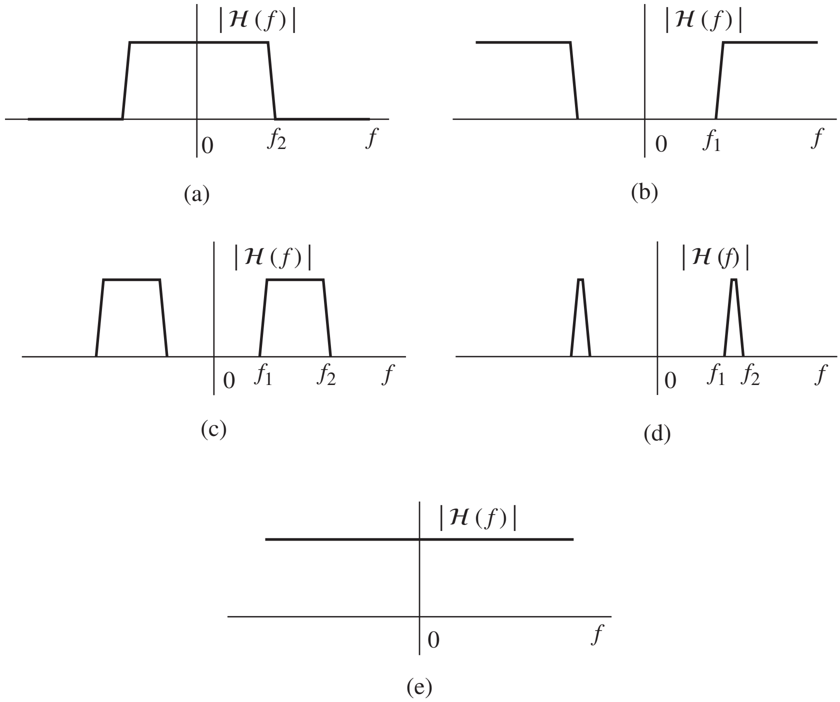

Figure 1.7 Classification of real valued analog filters on the basis of the support of $|\mathcal{H}(f)|$. (a) $f_1 = 0$, $f_2 < \infty$: lowpass filter (LPF). (b) $f_1 > 0$, $f_2 = \infty$: highpass filter (HPF). (c) $f_1 > 0$, $f_2 < \infty$: passband filter (PBF). (d) $B = f_2 - f_1 \ll (f_2 + f_1)/2$: narrowband filter (NBF). (e) $f_1 = 0$, $f_2 = \infty$: allpass filter (APF).

of the frequency responses being equal, a minimum (maximum) phase system concentrates all its energy on the first (last) samples of the impulse response.

Extending our previous considerations also to IIR filters, if h_1 is a causal minimum-phase filter, i.e. $H_1(z) = H_{min}(z)$ is a ratio of polynomials in z^{-1} with poles and zeros inside the unit circle, then $H_{max}(z) = K\, H^*_{min}\left(\frac{1}{z^*}\right)$, where K is a constant, is an anticausal maximum-phase filter, i.e. $H_{max}(z)$ is a ratio of polynomials in z with poles and zeros outside the unit circle.

In the case of a minimum-phase FIR filter with impulse response $h_{min}(n)$, $n = 0, 1, \dots, q$, $H_2(z) = z^{-q}\, H^*_{min}\left(\frac{1}{z^*}\right)$ is a causal maximum-phase filter. Moreover, the relation $\{h_2(n)\} = \{h_1^*(q-n)\}$, $n = 0, 1, \dots, q$, is satisfied. In this text, we use the notation $\{h_2(n)\} = \{h_1^{B*}(n)\}$, where B is the *backward* operator that orders the elements of a sequence from the last to the first.

In Appendix 1.A multirate transformations for systems are described, in which the time domain of the input is different from that of the output. In particular, decimator and interpolator filters are introduced, together with their efficient implementations.

1.3 Signal bandwidth

Definition 1.6

The *support* of a signal $x(\xi)$, $\xi \in \mathbb{R}$, is the set of values $\xi \in \mathbb{R}$ for which $|x(\xi)| \neq 0$. □

Let us consider a filter with impulse response h and frequency response $\mathcal{H}$. If h assumes real values, then $\mathcal{H}$ is Hermitian, $\mathcal{H}(-f) = \mathcal{H}^*(f)$, and $|\mathcal{H}(f)|$ is an even function. Depending on the support

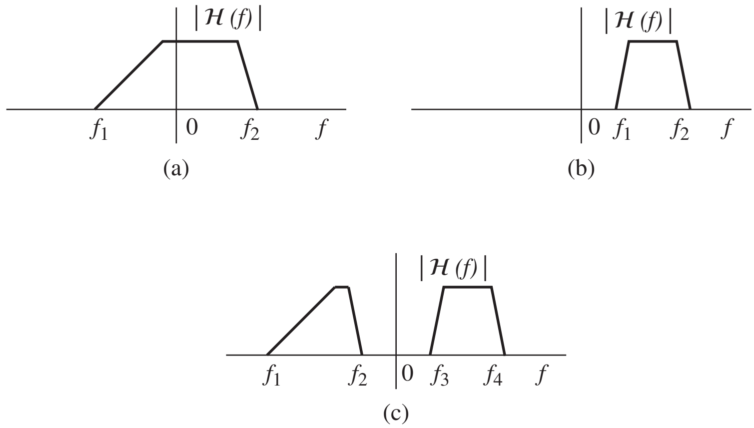

Figure 1.8 Classification of complex-valued analog filters on the basis of support of $|\mathcal{H}(f)|$. (a) $-\infty < f_1 \leq 0$, $0 < f_2 < \infty$: lowpass filter. (b) $f_1 > 0$, $f_2 < \infty$: passband filter. (c) $f_1 > -\infty$, $f_2 < 0$, $f_3 > 0$, $f_4 < \infty$: passband filter.

of $|\mathcal{H}(f)|$, the classification of Figure 1.7 is usually done. If h assumes complex values, the terminology is less standard. We adopt the classification of Figure 1.8, in which the filter is a lowpass filter (LPF) if the support $|\mathcal{H}(f)|$ includes the origin; otherwise, it is a passband filter (PBF).

Analogously, for a signal x, we will use the same denomination and we will say that x is a baseband (BB) or passband (PB) signal depending on whether the support of $|\mathcal{X}(f)|, f \in \mathbb{R}$, includes or not the origin.

Definition 1.7
In general, for a *real-valued signal* x, the set of positive frequencies such that $|\mathcal{X}(f)| \neq 0$ is called *passband* or simply *band* $\mathcal{B}$:

$$\mathcal{B} = \{f \geq 0 : |\mathcal{X}(f)| \neq 0\} \tag{1.69}$$

As $|\mathcal{X}(f)|$ is an even function, we have $|\mathcal{X}(-f)| \neq 0, f \in \mathcal{B}$. We note that $\mathcal{B}$ is equivalent to the support of $\mathcal{X}$ limited to positive frequencies. The bandwidth of x is given by the measure of $\mathcal{B}$:

$$B = \int_{\mathcal{B}} df \tag{1.70}$$

In the case of a *complex-valued signal* x, $\mathcal{B}$ is equivalent to the support of $\mathcal{X}$, and B is thus given by the measure of the entire support. □

Observation 1.1
The signal *bandwidth* may also be given different practical definitions. Let us consider an LPF having frequency response $\mathcal{H}(f)$. The filter gain $\mathcal{H}_0$ is usually defined as $\mathcal{H}_0 = |\mathcal{H}(0)|$; other definitions of gain refer to the average gain of the filter in the passband $\mathcal{B}$, or as $\max_f |\mathcal{H}(f)|$. We give the following four definitions for the bandwidth B of h:

(a) *First zero*:

$$B = \min\{f > 0 : \mathcal{H}(f) = 0\} \tag{1.71}$$

(b) *Based on amplitude*, bandwidth at A dB:

$$B = \max\left\{f > 0 : \frac{|\mathcal{H}(f)|}{\mathcal{H}_0} = 10^{-\frac{A}{20}}\right\} \tag{1.72}$$

Typically, $A = 3, 40$, or 60.

(c) *Based on energy*, bandwidth at $p\%$:

$$\frac{\int_0^B |\mathcal{H}(f)|^2 df}{\int_0^\infty |\mathcal{H}(f)|^2 df} = \frac{p}{100} \tag{1.73}$$

Typically, $p = 90$ or 99.

(d) *Equivalent noise bandwidth*:

$$B = \frac{\int_0^\infty |\mathcal{H}(f)|^2 df}{\mathcal{H}_0^2} \tag{1.74}$$

Figure 1.9 illustrates the various definitions for a particular $|\mathcal{H}(f)|$. For example, with regard to the signals of Figure 1.7, we have that for an LPF $B = f_2$, whereas for a PBF $B = f_2 - f_1$.

For discrete-time filters, for which $\mathcal{H}$ is periodic of period $1/T_c$, the same definitions hold, with the caution of considering the support of $|\mathcal{H}(f)|$ within a period, let us say between $-1/(2T_c)$ and $1/(2T_c)$. In the case of discrete-time highpass filters (HPFs), the passband will extend from a certain frequency f_1 to $1/(2T_c)$.

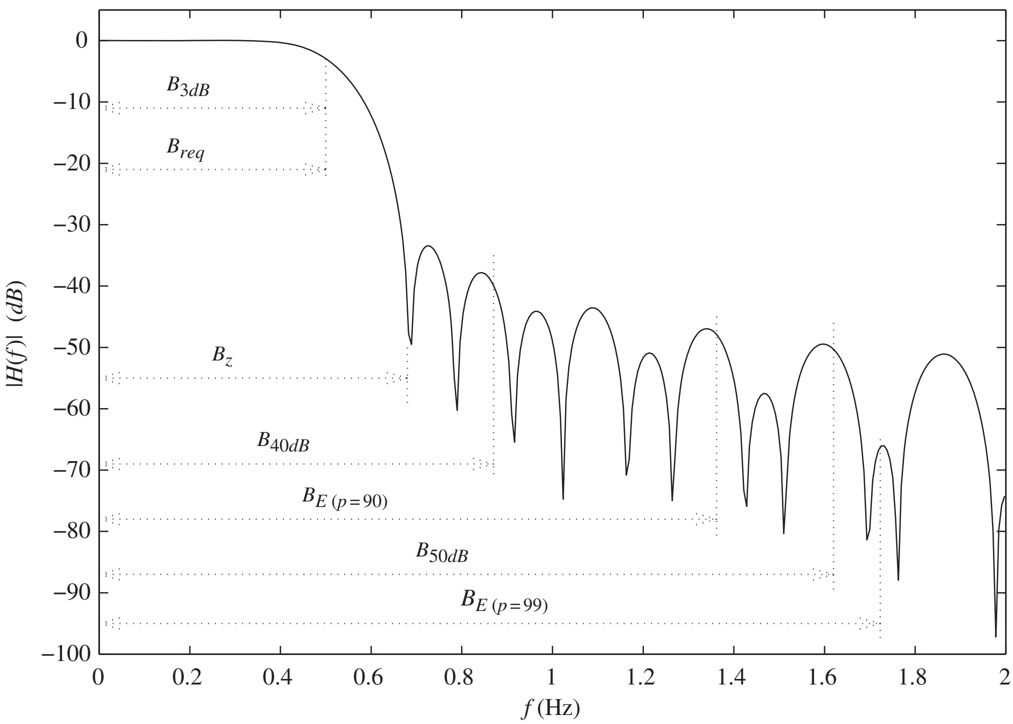

Figure 1.9 The real signal bandwidth following the definitions of (1) bandwidth at first zero: $B_z = 0.652$ Hz; (2) amplitude-based bandwidth: $B_{3\ dB} = 0.5$ Hz, $B_{40\ dB} = 0.87$ Hz, $B_{50\ dB} = 1.62$ Hz; (3) energy-based bandwidth: $B_{E(p=90)} = 1.362$ Hz, $B_{E(p=99)} = 1.723$ Hz; (4) equivalent noise bandwidth: $B_{req} = 0.5$ Hz.

The sampling theorem

As discrete-time signals are often obtained by sampling continuous-time signals, we will state the following fundamental theorem.

Theorem 1.1 (Sampling theorem)
Let $q(t)$, $t \in \mathbb{R}$ be a continuous-time signal, in general complex-valued, whose Fourier transform $\mathcal{Q}(f)$ has support within an interval $\mathcal{B}$ of finite measure B_0. The samples of the signal q, taken with period T_c as represented in Figure 1.10a,

$$h_k = q(kT_c) \tag{1.75}$$

univocally represent the signal $q(t)$, $t \in \mathbb{R}$, under the condition that the *sampling frequency* $1/T_c$ satisfies the relation

$$\frac{1}{T_c} \geq B_0 \tag{1.76}$$

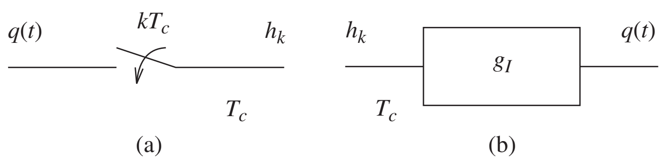

Figure 1.10 Operation of (a) sampling and (b) interpolation.

□

For the proof, which is based on the relation (1.23) between a signal and its samples, we refer the reader to [2].

B_0 is often referred to as the minimum sampling frequency. If $1/T_c < B_0$ the signal cannot be perfectly reconstructed from its samples, originating the so-called *aliasing phenomenon* in the frequency-domain signal representation.

In turn, the signal $q(t)$, $t \in \mathbb{R}$, can be reconstructed from its samples $\{h_k\}$ according to the scheme of Figure 1.10b, where it is employed an interpolation filter having an ideal frequency response given by

$$\mathcal{G}_I(f) = \begin{cases} 1 & f \in \mathcal{B} \\ 0 & \text{elsewhere} \end{cases} \tag{1.77}$$

We note that for *real-valued baseband signals* $B_0 = 2B$. For passband signals, care must be taken in the choice of $B_0 \geq 2B$ to avoid *aliasing* between the positive and negative frequency components of $\mathcal{Q}(f)$.

Heaviside conditions for the absence of signal distortion

Let us consider a filter having frequency response $\mathcal{H}(f)$ (see Figures 1.1 or 1.3) given by

$$\mathcal{H}(f) = \mathcal{H}_0 e^{-j2\pi f t_0}, \qquad f \in \mathcal{B} \tag{1.78}$$

where $\mathcal{H}_0$ and t_0 are two non-negative constants, and $\mathcal{B}$ is the *passband* of the filter input signal x. Then the output is given by

$$\mathcal{Y}(f) = \mathcal{H}(f)\mathcal{X}(f) = \mathcal{H}_0\mathcal{X}(f)\, e^{-j2\pi f t_0} \tag{1.79}$$

or, in the time domain,

$$y(t) = \mathcal{H}_0 x(t - t_0) \tag{1.80}$$

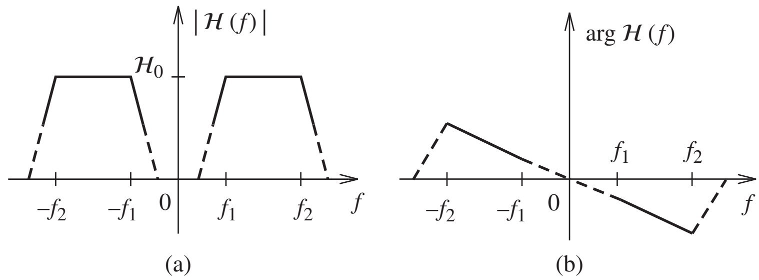

Figure 1.11 Characteristics of a filter satisfying the conditions for the absence of signal distortion in the frequency interval (f_1,f_2). (a) Magnitude and (b) phase.

In other words, for a filter of the type (1.78), the signal at the input is reproduced at the output with a gain factor $\mathcal{H}_0$ and a delay t_0.

A filter of the type (1.78) satisfies the Heaviside conditions for the absence of signal distortion and is characterized by

1. *Constant magnitude*
$$|\mathcal{H}(f)| = \mathcal{H}_0, \qquad f \in \mathcal{B} \tag{1.81}$$
2. *Linear phase*
$$\arg \mathcal{H}(f) = -2\pi f t_0, \qquad f \in \mathcal{B} \tag{1.82}$$
3. *Constant group delay*, also called *envelope delay*
$$\tau(f) = -\frac{1}{2\pi}\frac{d}{df}\arg \mathcal{H}(f) = t_0, \qquad f \in \mathcal{B} \tag{1.83}$$

We underline that it is sufficient that the Heaviside conditions are verified within the support of $\mathcal{X}$; as $|\mathcal{X}(f)| = 0$ outside the support, the filter frequency response may be arbitrary.

We show in Figure 1.11 the frequency response of a PBF, with bandwidth $B = f_2 - f_1$, that satisfies the conditions stated by Heaviside.

1.4 Passband signals and systems

We now provide a compact representation of passband signals and describe their transformation by linear systems.

Complex representation

For a passband signal x, it is convenient to introduce an equivalent representation in terms of a baseband signal $x^{(bb)}$.

Let x be a PB real-valued signal with Fourier transform as illustrated in Figure 1.12. The following two procedures can be adopted to obtain $x^{(bb)}$.

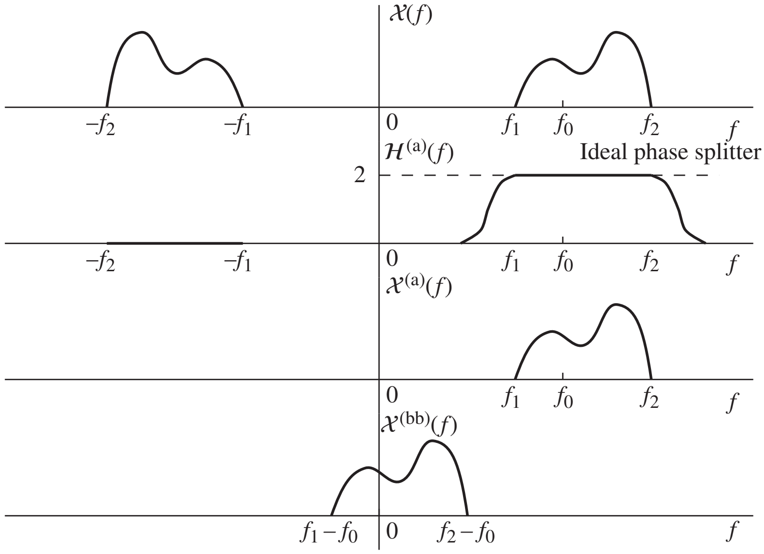

Figure 1.12 Transformations to obtain the baseband equivalent signal $x^{(bb)}$ around the carrier frequency f_0 using a phase splitter.

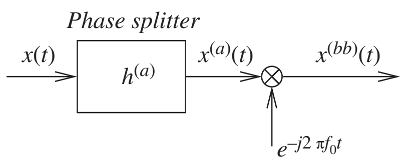

Figure 1.13 Transformations to obtain the baseband equivalent signal $x^{(bb)}$ around the carrier frequency f_0 using a phase splitter.

PB filter. Referring to Figure 1.12 and to the transformations illustrated in Figure 1.13, given x we extract its positive frequency components using an *analytic filter* or *phase splitter*, $h^{(a)}$, having the following ideal frequency response

$$\mathcal{H}^{(a)}(f) = 2 \cdot 1(f) = \begin{cases} 2 & f > 0 \\ 0 & f < 0 \end{cases} \tag{1.84}$$

In practice, it is sufficient that $h^{(a)}$ is a complex PB filter, with $\mathcal{H}^{(a)}(f) \simeq 2$ in the passband that extends from f_1 to f_2, as $\mathcal{X}(f)$, and stopband, in which $|\mathcal{H}^{(a)}(f)| \simeq 0$, that extends from $-f_2$ to $-f_1$. The signal $x^{(a)}$ is called the analytic signal or pre-envelope of x.

It is now convenient to introduce a suitable frequency f_0, called *reference carrier frequency*, which belongs to the passband (f_1, f_2) of x. The filter output, $x^{(a)}$, is frequency shifted by f_0 to obtain a BB signal, $x^{(bb)}$. The signal $x^{(bb)}$ is the *baseband equivalent* of x, also named *complex envelope of x around the carrier frequency f_0*.

Analytically, we have

$$x^{(a)}(t) = x * h^{(a)}(t) \quad \stackrel{\mathcal{F}}{\longleftrightarrow} \quad \mathcal{X}^{(a)}(f) = \mathcal{X}(f)\mathcal{H}^{(a)}(f) \tag{1.85}$$

$$x^{(bb)}(t) = x^{(a)}(t)\, e^{-j2\pi f_0 t} \quad \stackrel{\mathcal{F}}{\longleftrightarrow} \quad \mathcal{X}^{(bb)}(f) = \mathcal{X}^{(a)}(f + f_0) \tag{1.86}$$

and in the frequency domain

$$\mathcal{X}^{(bb)}(f) = \begin{cases} 2\mathcal{X}(f + f_0) & \text{for } f > -f_0 \\ 0 & \text{for } f < -f_0 \end{cases} \tag{1.87}$$

In other words, $x^{(bb)}$ is given by the components of x at positive frequencies, scaled by 2 and frequency shifted by f_0.

BB filter. We obtain the same result using a frequency shift of x followed by a lowpass filter (see Figures 1.14 and 1.15). It is immediate to determine the relation between the frequency responses of the filters of Figures 1.12 and 1.14:

$$\mathcal{H}(f) = \mathcal{H}^{(a)}(f + f_0) \tag{1.88}$$

From (1.88) one can derive the relation between the impulse response of the analytic filter and the impulse response of the lowpass filter:

$$h^{(a)}(t) = h(t)\, e^{j2\pi f_0 t} \tag{1.89}$$

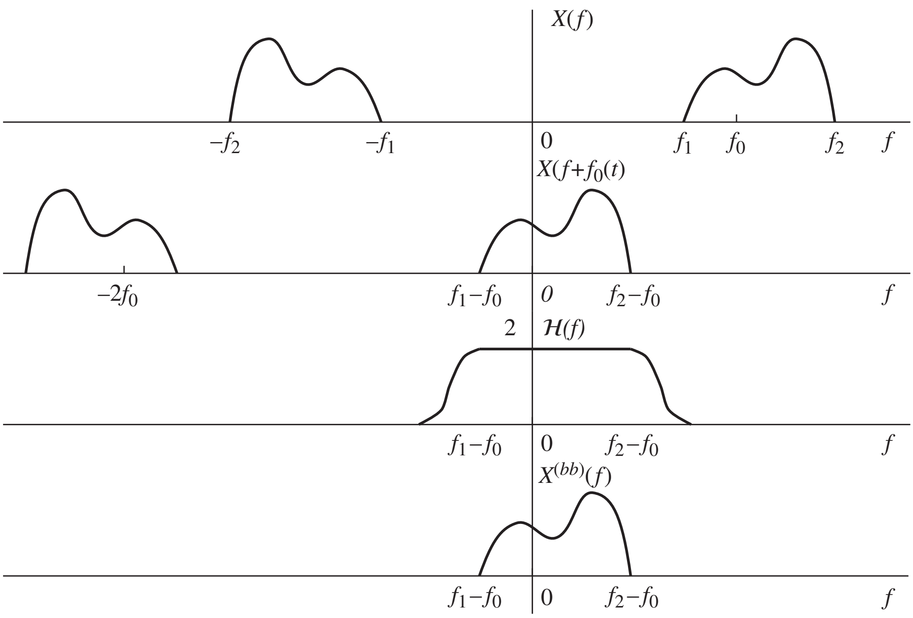

Figure 1.14 Illustration of transformations to obtain the baseband equivalent signal $x^{(bb)}$ around the carrier frequency f_0 using a lowpass filter.

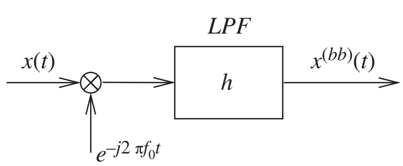

Figure 1.15 Transformations to obtain the baseband equivalent signal $x^{(bb)}$ around the carrier frequency f_0 using a lowpass filter.

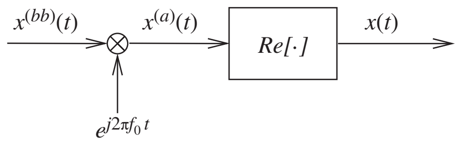

Figure 1.16 Relation between a signal, its complex envelope and the analytic signal.

Relation between a signal and its complex representation

A simple analytical relation exists between a *real signal* x and its complex envelope. In fact, making use of the property $\mathcal{X}(-f) = \mathcal{X}^*(f)$, it follows

$$\mathcal{X}(f) = \mathcal{X}(f)1(f) + \mathcal{X}(f)1(-f) = \mathcal{X}(f)1(f) + \mathcal{X}^*(-f)1(-f) \tag{1.90}$$

or equivalently,

$$x(t) = \frac{x^{(a)}(t) + x^{(a)*}(t)}{2} = Re\,[x^{(a)}(t)] \tag{1.91}$$

Using (1.86) it also follows

$$x(t) = Re\,[x^{(bb)}(t)e^{j2\pi f_0 t}] \tag{1.92}$$

as illustrated in Figure 1.16.

Baseband components of a PB signal. We introduce the notation

$$x^{(bb)}(t) = x_I^{(bb)}(t) + jx_Q^{(bb)}(t) \tag{1.93}$$

where

$$x_I^{(bb)}(t) = Re\,[x^{(bb)}(t)] \tag{1.94}$$

and

$$x_Q^{(bb)}(t) = Im\,[x^{(bb)}(t)] \tag{1.95}$$

are real-valued baseband signals, named *in-phase* and *quadrature components* of x, respectively. Substituting (1.93) in (1.92), we obtain

$$x(t) = x_I^{(bb)}(t)\cos(2\pi f_0 t) - x_Q^{(bb)}(t)\sin(2\pi f_0 t) \tag{1.96}$$

as illustrated in Figure 1.17.

Conversely, given x, one can use the scheme of Figure 1.15 and the relations (1.94) and (1.95) to get the baseband components. If the frequency response $\mathcal{H}(f)$ has Hermitian-symmetric characteristics with respect to the origin, h is real and the scheme of Figure 1.18 holds. The scheme of Figure 1.18 employs instead an ideal Hilbert filter with frequency response given by

$$\mathcal{H}^{(h)}(f) = -j\,\mathrm{sgn}(f) = e^{-j\frac{\pi}{2}\mathrm{sgn}(f)} \tag{1.97}$$

Magnitude and phase of $\mathcal{H}^{(h)}(f)$ are shown in Figure 1.19. We note that $h^{(h)}$ phase-shifts by $-\pi/2$ the positive-frequency components of the input and by $\pi/2$ the negative-frequency components. In practice, these filter specifications are imposed only on the passband of the input signal.[9] To simplify the notation, in block diagrams a Hilbert filter is indicated as $-\pi/2$.

[9] We note that the ideal Hilbert filter in Figure 1.19 has an impulse response given by (see Table 1.2 on page 5):

$$h^{(h)}(t) = \frac{1}{\pi t} \tag{1.98}$$

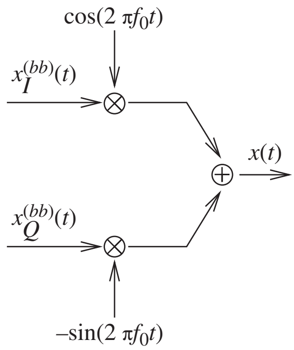

Figure 1.17 Relation between a signal and its baseband components.

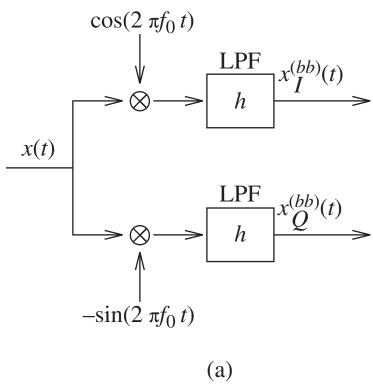

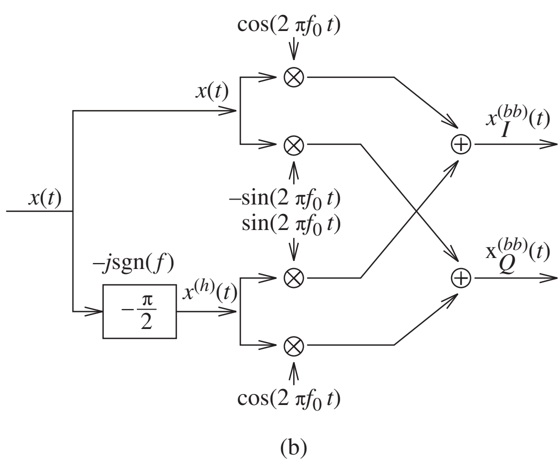

Figure 1.18 Relations to derive the baseband signal components. (a) Implementation using LPF and (b) Implementation using Hilbert filter.

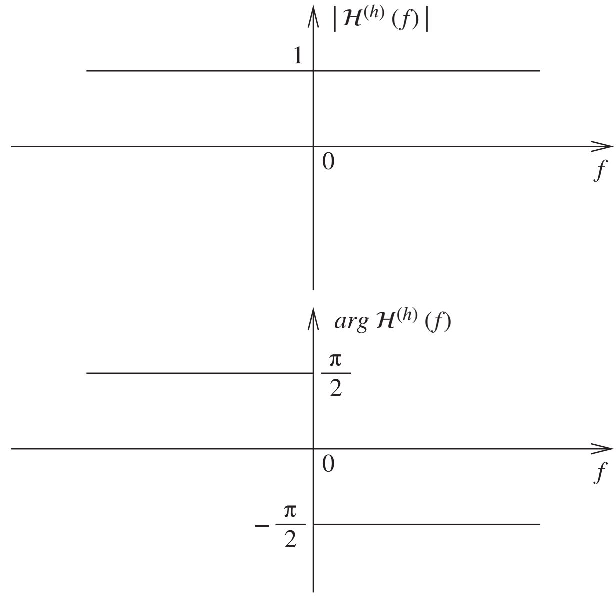

Figure 1.19 Magnitude and phase responses of the ideal Hilbert filter.

Comparing the frequency responses of the analytic filter (1.84) and of the Hilbert filter (1.97), we obtain the relation

$$\mathcal{H}^{(a)}(f) = 1 + j\mathcal{H}^{(h)}(f) \tag{1.101}$$

Then, letting

$$x^{(h)}(t) = x * h^{(h)}(t) \tag{1.102}$$

the analytic signal can be expressed as

$$x^{(a)}(t) = x(t) + jx^{(h)}(t) \tag{1.103}$$

Consequently, from (1.86), (1.94), and (1.95), we have

$$x_I^{(bb)}(t) = x(t)\cos(2\pi f_0 t) + x^{(h)}(t)\sin(2\pi f_0 t) \tag{1.104}$$

$$x_Q^{(bb)}(t) = x^{(h)}(t)\cos(2\pi f_0 t) - x(t)\sin(2\pi f_0 t) \tag{1.105}$$

as illustrated in Figure 1.18.[10]

Consequently, if x is the input signal, the output of the Hilbert filter (also denoted as Hilbert transform of x) is

$$x^{(h)}(t) = \frac{1}{\pi} \int_{-\infty}^{+\infty} \frac{x(\tau)}{t-\tau}\, d\tau \tag{1.99}$$

Moreover, noting that from (1.97) $(-j\,\text{sgn} f)(-j\,\text{sgn} f) = -1$, taking the Hilbert transform of the Hilbert transform of a signal, we get the initial signal with the sign changed. Then it results as

$$x(t) = -\frac{1}{\pi} \int_{-\infty}^{+\infty} \frac{x^{(h)}(\tau)}{t-\tau}\, d\tau \tag{1.100}$$

[10] We recall that the design of a filter, and in particular of a Hilbert filter, requires the introduction of a suitable delay. In other words, we are only able to produce an output with a delay t_D, $x^{(h)}(t-t_D)$. Consequently, in the block diagram of Figure 1.18, also x and the various sinusoidal waveforms must be delayed.

We note that in practical *systems*, transformations to obtain, e.g. the analytic signal, the complex envelope, or the Hilbert transform of a given signal, are implemented by filters. However, it is usually more convenient to perform signal analysis in the frequency domain by the Fourier transform. In the following two examples, we use frequency-domain techniques to obtain the complex envelope of a PB signal.

Example 1.4.1
Consider the sinusoidal signal

$$x(t) = A\cos(2\pi f_0 t + \varphi_0) \tag{1.106}$$

with

$$\mathcal{X}(f) = \frac{A}{2}e^{j\varphi_0}\delta(f - f_0) + \frac{A}{2}e^{-j\varphi_0}\delta(f + f_0) \tag{1.107}$$

The analytic signal is given by

$$\mathcal{X}^{(a)}(f) = Ae^{j\varphi_0}\delta(f - f_0) \quad \stackrel{\mathcal{F}^{-1}}{\longleftrightarrow} \quad x^{(a)}(t) = Ae^{j\varphi_0}e^{j2\pi f_0 t} \tag{1.108}$$

and

$$\mathcal{X}^{(bb)}(f) = Ae^{j\varphi_0}\delta(f) \quad \stackrel{\mathcal{F}^{-1}}{\longleftrightarrow} \quad x^{(bb)}(t) = Ae^{j\varphi_0} \tag{1.109}$$

We note that we have chosen as reference carrier frequency of the complex envelope the same carrier frequency as in (1.106).

Example 1.4.2
Let

$$x(t) = A\,\mathrm{sinc}(Bt)\cos(2\pi f_0 t) \tag{1.110}$$

with the Fourier transform given by

$$\mathcal{X}(f) = \frac{A}{2B}\left[\mathrm{rect}\left(\frac{f - f_0}{B}\right) + \mathrm{rect}\left(\frac{f + f_0}{B}\right)\right] \tag{1.111}$$

as illustrated in Figure 1.20. Then, using f_0 as reference carrier frequency,

$$\mathcal{X}^{(bb)}(f) = \frac{A}{B}\mathrm{rect}\left(\frac{f}{B}\right) \tag{1.112}$$

and

$$x^{(bb)}(t) = A\mathrm{sinc}(Bt) \tag{1.113}$$

Another *analytical technique* to get the expression of the signal after the various transformations is obtained by applying the following theorem.

Theorem 1.2
Let the product of two real signals be

$$x(t) = a(t)\ c(t) \tag{1.114}$$

where a is a BB signal with $\mathcal{B}_a = [0, B)$ and c is a PB signal with $\mathcal{B}_c = [f_0, +\infty)$. If $f_0 > B$, then the analytic signal of x is related to that of c by

$$x^{(a)}(t) = a(t)\ c^{(a)}(t) \tag{1.115}$$

□

Proof. We consider the general relation (1.91), valid for every real signal

$$c(t) = \frac{1}{2}\, c^{(a)}(t) + \frac{1}{2}\, c^{(a)*}(t) \tag{1.116}$$

Substituting (1.116) in (1.114) yields

$$x(t) = a(t)\frac{1}{2}c^{(a)}(t) + a(t)\frac{1}{2}c^{(a)*}(t) \tag{1.117}$$

In the frequency domain, the support of the first term in (1.117) is given by the interval $[f_0 - B, +\infty)$, while that of the second is equal to $(-\infty, -f_0 + B]$. Under the hypothesis that $f_0 \geq B$, the two terms in (1.117) have disjoint supports in the frequency domain and (1.115) is immediately obtained. □

Corollary 1.1
From (1.115), we obtain

$$x^{(h)}(t) = a(t)c^{(h)}(t) \tag{1.118}$$

and

$$x^{(bb)}(t) = a(t)c^{(bb)}(t) \tag{1.119}$$

In fact, from (1.103) we get

$$x^{(h)}(t) = Im\,[x^{(a)}(t)] \tag{1.120}$$

which substituted in (1.115) yields (1.118). Finally, (1.119) is obtained by substituting (1.86),

$$x^{(bb)}(t) = x^{(a)}(t)e^{-j2\pi f_0 t} \tag{1.121}$$

in (1.115). □

An interesting application of (1.120) is in the design of a Hilbert filter $h^{(h)}$ starting from a lowpass filter h. In fact, from (1.89) and (1.120), we get

$$h^{(h)}(t) = h(t)\sin(2\pi f_0 t) \tag{1.122}$$

Example 1.4.3
Let a modulated *double sideband* (DSB) signal be expressed as

$$x(t) = a(t)\cos(2\pi f_0 t + \varphi_0) \tag{1.123}$$

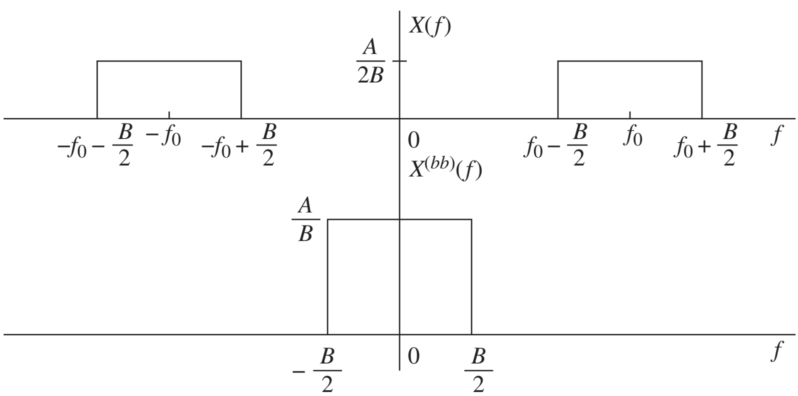

Figure 1.20 Frequency response of a PB signal and corresponding complex envelope.

Table 1.5: Some properties of the Hilbert transform.

property	*(real) signal*	*(real) Hilbert transform*
	$x(t)$	$x^{(h)}(t)$
duality	$x^{(h)}(t)$	$-x(t)$
time inverse	$x(-t)$	$-x^{(h)}(-t)$
even signal	$x(t) = x(-t)$	$x^{(h)}(t) = -x^{(h)}(-t)$, odd
odd signal	$x(t) = -x(-t)$	$x^{(h)}(t) = x^{(h)}(-t)$, even
product (see Theorem 1.2)	$a(t)\ c(t)$	$a(t)\ c^{(h)}(t)$
cosinusoidal signal	$\cos(2\pi f_0 t + \varphi_0)$	$\sin(2\pi f_0 t + \varphi_0)$
energy	$E_x = \int_{-\infty}^{+\infty} \|x(t)\|^2\ dt = \int_{-\infty}^{+\infty} \|x^{(h)}(t)\|^2 dt = E_{x^{(h)}}$	
orthogonality	$\int_{-\infty}^{+\infty} x(t)\ x^{(h)}(t)\ dt = 0$	

where a is a BB signal with bandwidth B. Then, if $f_0 > B$, from the above theorem we have the following relations:

$$x^{(a)}(t) = a(t)e^{j(2\pi f_0 t + \varphi_0)} \tag{1.124}$$

$$x^{(h)}(t) = a(t)\sin(2\pi f_0 t + \varphi_0) \tag{1.125}$$

$$x^{(bb)}(t) = a(t)e^{j\varphi_0} \tag{1.126}$$

We list in Table 1.5 some properties of the Hilbert transformation (1.102) that are easily obtained by using the Fourier transform and the properties of Table 1.1.

Baseband equivalent of a transformation

Given a transformation involving also passband signals, it is often useful to determine an equivalent relation between baseband complex representations of input and output signals. Three transformations are given in Figure 1.21, together with their baseband equivalent. Note that schemes in Figure 1.21a,b produce very different output signals, although both use a mixer with the same carrier.

We will prove the relation illustrated in Figure 1.21b. Assuming that h is the real-valued impulse response of an LPF and using (1.92),

$$\begin{aligned} y(t) &= \left\{ h * Re\,[x^{(bb)}(\tau)e^{j2\pi f_0 \tau} \left(\cos(2\pi f_0 \tau + \varphi_1)\right)] \right\}(t) \\ &= Re\left[\left(h * x^{(bb)} \frac{e^{-j\varphi_1}}{2} + h * x^{(bb)} \frac{e^{+j(2\pi 2 f_0 \tau + \varphi_1)}}{2} \right)(t)\right] \\ &= Re\left[\left(h * x^{(bb)} \frac{e^{-j\varphi_1}}{2} \right)(t)\right] \end{aligned} \tag{1.127}$$

where the last equality follows because the term with frequency components around $2f_0$ is filtered by the LPF.

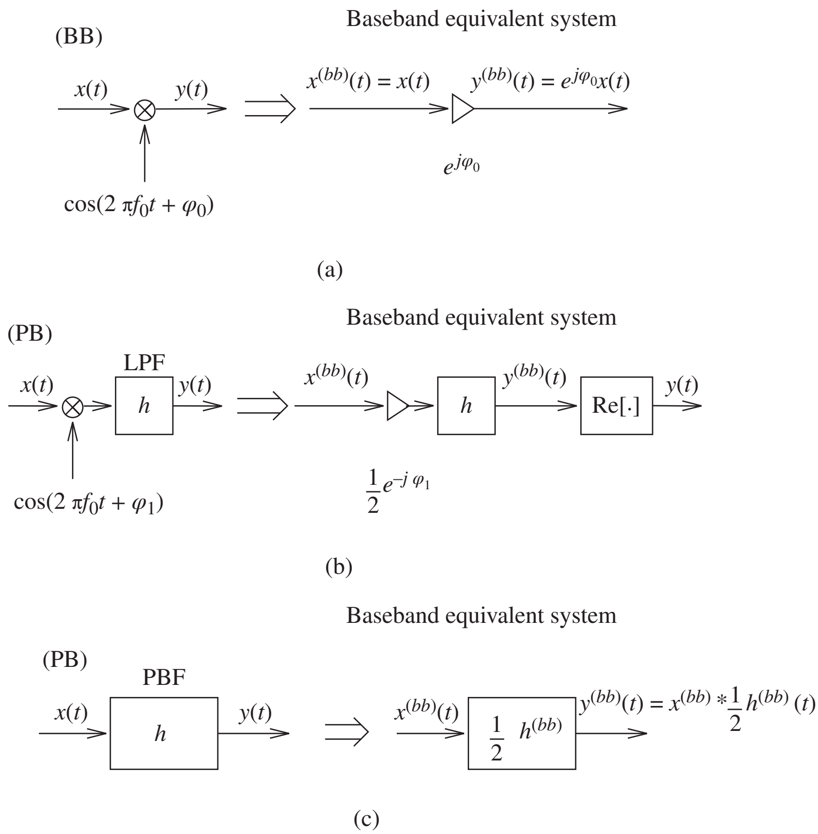

Figure 1.21 Passband transformations and their baseband equivalent. (a) Modulator, (b) demodulator, and (c) passband filtering.

We note, moreover, that the filter $h^{(bb)}$ in Figure 1.21 has in-phase component $h_I^{(bb)}$ and quadrature component $h_Q^{(bb)}$ that are related to $\mathcal{H}^{(a)}$ by (see (1.94) and (1.95))

$$\begin{aligned}\mathcal{H}_I^{(bb)}(f) &= \frac{1}{2}[\mathcal{H}^{(bb)}(f) + \mathcal{H}^{(bb)*}(-f)] \\ &= \frac{1}{2}[\mathcal{H}^{(a)}(f+f_0) + \mathcal{H}^{(a)*}(-f+f_0)]\end{aligned} \tag{1.128}$$

and

$$\begin{aligned}\mathcal{H}_Q^{(bb)}(f) &= \frac{1}{2j}[\mathcal{H}^{(bb)}(f) - \mathcal{H}^{(bb)*}(-f)] \\ &= \frac{1}{2j}[\mathcal{H}^{(a)}(f+f_0) - \mathcal{H}^{(a)*}(-f+f_0)]\end{aligned} \tag{1.129}$$

Consequently, if $\mathcal{H}^{(a)}$ has Hermitian symmetry around f_0, then

$$\mathcal{H}_I^{(bb)}(f) = \mathcal{H}_a^{(a)}(f+f_0)$$

and

$$\mathcal{H}_Q^{(bb)}(f) = 0$$

In other words, $h^{(bb)}(t) = h_I^{(bb)}(t)$ is real and the realization of the filter $\frac{1}{2}h^{(bb)}$ is simplified. In practice, this condition is verified by imposing that the filter $h^{(a)}$ has symmetrical frequency specifications around f_0.

Envelope and instantaneous phase and frequency

We will conclude this section with a few definitions. Given a PB signal x, with reference to the analytic signal we define

1. *Envelope*
$$M_x(t) = |x^{(a)}(t)| \tag{1.130}$$
2. *Instantaneous phase*
$$\varphi_x(t) = \arg x^{(a)}(t) \tag{1.131}$$
3. *Instantaneous frequency*
$$f_x(t) = \frac{1}{2\pi}\frac{d}{dt}\varphi_x(t) \tag{1.132}$$

In terms of the complex envelope signal $x^{(bb)}$, from (1.86) the equivalent relations follow:

$$M_x(t) = |x^{(bb)}(t)| \tag{1.133}$$
$$\varphi_x(t) = \arg x^{(bb)}(t) + 2\pi f_0 t \tag{1.134}$$
$$f_x(t) = \frac{1}{2\pi}\ \frac{d}{dt}[\arg x^{(bb)}(t)] + f_0 \tag{1.135}$$

Then, from the polar representation, $x^{(a)}(t) = M_x(t)\ e^{j\varphi_x(t)}$ and from (1.91), a PB signal x can be written as

$$x(t) = Re\,[x^{(a)}(t)] = M_x(t)\cos(\varphi_x(t)) \tag{1.136}$$

For example if $x(t) = A\cos(2\pi f_0 t + \varphi_0)$, it follows that

$$M_x(t) = A \tag{1.137}$$
$$\varphi_x(t) = 2\pi f_0 t + \varphi_0 \tag{1.138}$$
$$f_x(t) = f_0 \tag{1.139}$$

With reference to the above relations, three other definitions follow.

1. *Envelope deviation*
$$\Delta M_x(t) = |x^{(a)}(t)| - A = |x^{(bb)}(t)| - A \tag{1.140}$$
2. *Phase deviation*
$$\Delta\varphi_x(t) = \varphi_x(t) - (2\pi f_0 t + \varphi_0) = \arg x^{(bb)}(t) - \varphi_0 \tag{1.141}$$
3. *Frequency deviation*
$$\Delta f_x(t) = f_x(t) - f_0 = \frac{1}{2\pi}\frac{d}{dt}\Delta\varphi_x(t) \tag{1.142}$$

Then (1.136) becomes

$$x(t) = [A + \Delta M_x(t)]\cos(2\pi f_0 t + \varphi_0 + \Delta\varphi_x(t)) \tag{1.143}$$

1.5 Second-order analysis of random processes

We recall the functions related to the statistical description of random processes, especially those functions concerning second-order analysis.

1.5.1 Correlation

Let $x(t)$ and $y(t)$, $t \in \mathbb{R}$, be two continuous-time complex-valued random processes. We indicate the expectation operator with E.

1. *Mean value*
$$\mathtt{m}_x(t) = E[x(t)] \tag{1.144}$$
2. *Statistical power*
$$\mathtt{M}_x(t) = E[|x(t)|^2] \tag{1.145}$$
3. *Autocorrelation*
$$\mathtt{r}_x(t, t-\tau) = E[x(t)x^*(t-\tau)] \tag{1.146}$$
4. *Crosscorrelation*
$$\mathtt{r}_{xy}(t, t-\tau) = E[x(t)y^*(t-\tau)] \tag{1.147}$$
5. *Autocovariance*
$$\begin{aligned}\mathtt{c}_x(t, t-\tau) &= E[(x(t) - \mathtt{m}_x(t))(x(t-\tau) - \mathtt{m}_x(t-\tau))^*] \\ &= \mathtt{r}_x(t, t-\tau) - \mathtt{m}_x(t)\mathtt{m}_x^*(t-\tau)\end{aligned} \tag{1.148}$$
6. *Crosscovariance*
$$\begin{aligned}\mathtt{c}_{xy}(t, t-\tau) &= E[(x(t) - \mathtt{m}_x(t))(y(t-\tau) - \mathtt{m}_y(t-\tau))^*] \\ &= \mathtt{r}_{xy}(t, t-\tau) - \mathtt{m}_x(t)\mathtt{m}_y^*(t-\tau)\end{aligned} \tag{1.149}$$

Observation 1.2

- x and y are *orthogonal* if $\mathtt{r}_{xy}(t, t-\tau) = 0$, $\forall t, \tau$. In this case, we write $x \perp y$.[11]
- x and y are *uncorrelated* if $\mathtt{c}_{xy}(t, t-\tau) = 0$, $\forall t, \tau$.
- if at least one of the two random processes has zero mean, *orthogonality* is equivalent to *uncorrelation*.
- x is *wide-sense stationary* (WSS) if
  1. $\mathtt{m}_x(t) = \mathtt{m}_x$, $\forall t$,
  2. $\mathtt{r}_x(t, t-\tau) = \mathtt{r}_x(\tau)$, $\forall t$.

  In this case, $\mathtt{r}_x(0) = E[|x(t)|^2] = \mathtt{M}_x$ is the *statistical power*, whereas $\mathtt{c}_x(0) = \sigma_x^2 = \mathtt{M}_x - |\mathtt{m}_x|^2$ is the *variance* of x.

[11] We observe that the notion of *orthogonality between two random processes* is quite different from that of *orthogonality between two deterministic signals*. In fact, while in the deterministic case, it is sufficient that $\int_{-\infty}^{\infty} x(t)y^*(t)dt = 0$, in the random case, the crosscorrelation must be zero for all the delays and not only for the zero delay. In particular, we note that the *two random variables* v_1 and v_2 are orthogonal if $E[v_1 v_2^*] = 0$.

- x and y are *jointly wide-sense stationary* if
  1. $\mathtt{m}_x(t) = \mathtt{m}_x$, $\mathtt{m}_y(t) = \mathtt{m}_y$, $\forall t$,
  2. $\mathtt{r}_{xy}(t, t-\tau) = \mathtt{r}_{xy}(\tau)$, $\forall t$.

Properties of the autocorrelation function

1. $\mathtt{r}_x(-\tau) = \mathtt{r}_x^*(\tau)$, $\mathtt{r}_x(\tau)$ is a function with Hermitian symmetry.
2. $\mathtt{r}_x(0) \geq |\mathtt{r}_x(\tau)|$.
3. $\mathtt{r}_x(0)\mathtt{r}_y(0) \geq |\mathtt{r}_{xy}(\tau)|^2$.
4. $\mathtt{r}_{xy}(-\tau) = \mathtt{r}_{yx}^*(\tau)$.
5. $\mathtt{r}_{x^*}(\tau) = \mathtt{r}_x^*(\tau)$.

1.5.2 Power spectral density

Given the WSS random process $x(t)$, $t \in \mathbb{R}$, its *power spectral density* (PSD) is defined as the Fourier transform of its autocorrelation function

$$\mathcal{P}_x(f) = \mathcal{F}[\mathtt{r}_x(\tau)] = \int_{-\infty}^{+\infty} \mathtt{r}_x(\tau) e^{-j2\pi f\tau} d\tau \tag{1.150}$$

The inverse transformation is given by the following formula:

$$\mathtt{r}_x(\tau) = \int_{-\infty}^{+\infty} \mathcal{P}_x(f) e^{j2\pi f\tau} df \tag{1.151}$$

In particular from (1.151), we obtain the statistical power

$$\mathtt{M}_x = \mathtt{r}_x(0) = \int_{-\infty}^{+\infty} \mathcal{P}_x(f) df \tag{1.152}$$

Hence, the name PSD for the function $\mathcal{P}_x(f)$: it represents the distribution of the statistical power in the frequency domain.

The pair of equations (1.150) and (1.151) are obtained from the *Wiener–Khintchine theorem* [3].

Definition 1.8
The passband $\mathcal{B}$ of a random process x is defined with reference to its PSD function. □

Spectral lines in the PSD

In many applications, it is important to detect the presence of sinusoidal components in a random process. With this intent we give the following theorem.

Theorem 1.3
The PSD of a WSS process, $\mathcal{P}_x(f)$, can be uniquely decomposed into a component $\mathcal{P}_x^{(c)}(f)$ without delta functions and a discrete component consisting of delta functions (spectral lines) $\mathcal{P}_x^{(d)}(f)$, so that

$$\mathcal{P}_x(f) = \mathcal{P}_x^{(c)}(f) + \mathcal{P}_x^{(d)}(f) \tag{1.153}$$

where $\mathcal{P}_x^{(c)}(f)$ is an ordinary (piecewise linear) function and

$$\mathcal{P}_x^{(d)}(f) = \sum_{i \in \mathcal{I}} \mathtt{M}_i \delta(f - f_i) \tag{1.154}$$

where $\mathcal{I}$ identifies a discrete set of frequencies $\{f_i\}$, $i \in \mathcal{I}$. □

The inverse Fourier transform of (1.153) yields the relation

$$\mathtt{r}_x(\tau) = \mathtt{r}_x^{(c)}(\tau) + \mathtt{r}_x^{(d)}(\tau) \tag{1.155}$$

with

$$\mathtt{r}_x^{(d)}(\tau) = \sum_{i \in \mathcal{I}} \mathtt{M}_i e^{j2\pi f_i \tau} \tag{1.156}$$

The most interesting consideration is that the following random process decomposition corresponds to the decomposition (1.153) of the PSD:

$$x(t) = x^{(c)}(t) + x^{(d)}(t) \tag{1.157}$$

where $x^{(c)}$ and $x^{(d)}$ are *orthogonal* processes having PSD functions

$$\mathcal{P}_{x^{(c)}}(f) = \mathcal{P}_x^{(c)}(f) \quad \text{and} \quad \mathcal{P}_{x^{(d)}}(f) = \mathcal{P}_x^{(d)}(f) \tag{1.158}$$

Moreover, $x^{(d)}$ is given by

$$x^{(d)}(t) = \sum_{i \in \mathcal{I}} x_i e^{j2\pi f_i t} \tag{1.159}$$

where $\{x_i\}$ are orthogonal random variables (r.v.s.) having statistical power

$$E[|x_i|^2] = \mathtt{M}_i, \qquad i \in \mathcal{I} \tag{1.160}$$

where $\mathtt{M}_i$ is defined in (1.154).

Observation 1.3
The spectral lines of the PSD identify the periodic components in the process.

Definition 1.9
A WSS random process is said to be *asymptotically uncorrelated* if the following two properties hold:

$$(1) \quad \lim_{\tau \to \infty} \mathtt{r}_x(\tau) = |\mathtt{m}_x|^2 \tag{1.161}$$

$$(2) \quad \mathtt{c}_x(\tau) = \mathtt{r}_x(\tau) - |\mathtt{m}_x|^2 \quad \text{is absolutely integrable} \tag{1.162}$$

The property (1) shows that $x(t)$ and $x(t-\tau)$ become uncorrelated for $\tau \to \infty$. □

For such processes, one can prove that

$$\mathtt{r}_x^{(c)}(\tau) = \mathtt{c}_x(\tau) \quad \text{and} \quad \mathtt{r}_x^{(d)}(\tau) = |\mathtt{m}_x|^2 \tag{1.163}$$

Hence, $\mathcal{P}_x^{(d)}(f) = |\mathtt{m}_x|^2 \delta(f)$, and the process exhibits at most a spectral line at the origin.

Cross power spectral density

One can extend the definition of PSD to two jointly WSS random processes:

$$\mathcal{P}_{xy}(f) = \mathcal{F}[\mathtt{r}_{xy}(\tau)] \tag{1.164}$$

Since $\mathtt{r}_{xy}(-\tau) \neq \mathtt{r}_{xy}^*(\tau)$, $\mathcal{P}_{xy}(f)$ is in general a complex function.

Properties of the PSD

1. $\mathcal{P}_x(f)$ is a *real-valued function*. This follows from property 1 of the autocorrelation.
2. $\mathcal{P}_x(f)$ is generally *not an even function*. However, if the process x is real valued, then both $\mathtt{r}_x(\tau)$ and $\mathcal{P}_x(f)$ are even functions.
3. $\mathcal{P}_x(f)$ is a *non-negative function*.
4. $\mathcal{P}_{yx}(f) = \mathcal{P}^*_{xy}(f)$.
5. $\mathcal{P}_{x^*}(f) = \mathcal{P}_x(-f)$.

Moreover, the following inequality holds:

$$0 \le |\mathcal{P}_{xy}(f)|^2 \le \mathcal{P}_x(f)\mathcal{P}_y(f) \tag{1.165}$$

Definition 1.10 (White random process)
The zero-mean random process $x(t)$, $t \in \mathbb{R}$, is called *white* if

$$\mathtt{r}_x(\tau) = K\delta(\tau) \tag{1.166}$$

with K a positive real number. In this case, $\mathcal{P}_x(f)$ is a constant, i.e.

$$\mathcal{P}_x(f) = K \tag{1.167}$$

□

PSD through filtering

With reference to Figure 1.22, by taking the Fourier transform of the various crosscorrelations, the following relations are easily obtained:

$$\mathcal{P}_{yx}(f) = \mathcal{P}_x(f)\mathcal{H}(f) \tag{1.168}$$

$$\mathcal{P}_y(f) = \mathcal{P}_x(f)|\mathcal{H}(f)|^2 \tag{1.169}$$

$$\mathcal{P}_{yz}(f) = \mathcal{P}_x(f)\mathcal{H}(f)\mathcal{G}^*(f) \tag{1.170}$$

The relation (1.169) is of particular interest since it relates the PSDs of the output process of a filter to the PSD of the input process, through the frequency response of the filter. In the particular case in which y and z have disjoint passbands, i.e. $\mathcal{P}_y(f)\mathcal{P}_z(f) = 0$, then from (1.165) $\mathtt{r}_{yz}(\tau) = 0$, and $y \perp z$.

1.5.3 PSD of discrete-time random processes

Let $\{x(k)\}$ and $\{y(k)\}$ be two discrete-time random processes. Definitions and properties of Section 1.5.1 remain valid also for discrete-time processes: the only difference is that the correlation is now defined

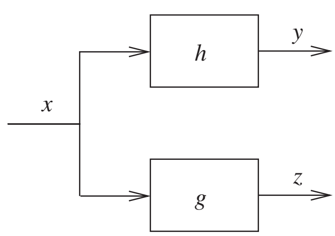

Figure 1.22 Reference scheme of PSD computations.

on discrete time and is called autocorrelation sequence (ACS). It is however interesting to review the properties of PSDs. Given a discrete-time WSS random process x, the PSD is obtained as

$$\mathcal{P}_x(f) = T_c \mathcal{F}[\mathtt{r}_x(n)] = T_c \sum_{n=-\infty}^{+\infty} \mathtt{r}_x(n) e^{-j2\pi f n T_c} \tag{1.171}$$

We note a further property: $\mathcal{P}_x(f)$ is a periodic function of period $1/T_c$. The inverse transformation yields:

$$\mathtt{r}_x(n) = \int_{-\frac{1}{2T_c}}^{\frac{1}{2T_c}} \mathcal{P}_x(f) e^{j2\pi f n T_c} df \tag{1.172}$$

In particular, the statistical power is given by

$$\mathtt{M}_x = \mathtt{r}_x(0) = \int_{-\frac{1}{2T_c}}^{\frac{1}{2T_c}} \mathcal{P}_x(f) df \tag{1.173}$$

Definition 1.11 (White random process)
A discrete-time random process $\{x(k)\}$ is *white* if

$$\mathtt{r}_x(n) = \sigma_x^2 \delta_n \tag{1.174}$$

In this case, the PSD is a constant:

$$\mathcal{P}_x(f) = \sigma_x^2 T_c \tag{1.175}$$

□

Definition 1.12
If the samples of the random process $\{x(k)\}$ are statistically independent and identically Distributed, we say that $\{x(k)\}$ has i.i.d. samples. □

Generating an i.i.d. sequence is not simple; however, it is easily provided by many random number generators [4]. However, generating, storing, and processing a finite length, i.i.d. sequence requires a complex processor and a lot of memory. Furthermore, the deterministic correlation properties of such a subsequence may not be very good. Hence, in Appendix 1.C we introduce a class of pseudonoise (PN) sequences, which are deterministic and periodic, with very good correlation properties. Moreover, the symbol alphabet can be just binary.

Spectral lines in the PSD

Also the PSD of a discrete time random process can be decomposed into ordinary components and spectral lines on a period of the PSD. In particular for a discrete-time WSS *asymptotically uncorrelated* random process, the relation (1.163) and the following are true

$$\mathcal{P}_x^{(c)}(f) = T_c \sum_{n=-\infty}^{+\infty} \mathtt{c}_x(n)\, e^{-j2\pi f n T_c} \tag{1.176}$$

$$\mathcal{P}_x^{(d)}(f) = |\mathtt{m}_x|^2 \sum_{\ell=-\infty}^{+\infty} \delta\left(f - \frac{\ell}{T_c}\right) \tag{1.177}$$

We note that, if the process has non-zero mean value, the PSD exhibits lines at multiples of $1/T_c$.

Example 1.5.1
We calculate the PSD of an i.i.d. sequence $\{x(k)\}$. From

$$\mathtt{r}_x(n) = \begin{cases} \mathtt{M}_x & n = 0 \\ |\mathtt{m}_x|^2 & n \neq 0 \end{cases} \tag{1.178}$$

it follows that

$$\mathtt{c}_x(n) = \begin{cases} \sigma_x^2 & n = 0 \\ 0 & n \neq 0 \end{cases} \tag{1.179}$$

Then

$$\mathtt{r}_x^{(c)}(n) = \sigma_x^2 \delta_n, \quad \mathtt{r}_x^{(d)}(n) = |\mathtt{m}_x|^2 \tag{1.180}$$

$$\mathcal{P}_x^{(c)}(f) = \sigma_x^2 T_c, \quad \mathcal{P}_x^{(d)}(f) = |\mathtt{m}_x|^2 \sum_{\ell=-\infty}^{+\infty} \delta\left(f - \frac{\ell}{T_c}\right) \tag{1.181}$$

PSD through filtering

Given the system illustrated in Figure 1.3, we want to find the relation between the PSDs of the input and output signals, assuming these processes are individually as well as jointly WSS. We introduce the z-transform of the correlation sequence:

$$P_x(z) = \sum_{n=-\infty}^{+\infty} \mathtt{r}_x(n) z^{-n} \tag{1.182}$$

From the comparison of (1.182) with (1.171), the PSD of x is related to $P_x(z)$ by

$$\mathcal{P}_x(f) = T_c P_x(e^{j2\pi f T_c}) \tag{1.183}$$

Using Table 1.3 in page 6, we obtain the relations between ACS and PSD listed in Table 1.6. Let the deterministic autocorrelation of h be defined as[12]

$$\mathtt{r}_h(n) = \sum_{k=-\infty}^{+\infty} h(k) h^*(k-n) = [h(m) * h^*(-m)](n) \tag{1.184}$$

whose z-transform is given by

$$P_h(z) = \sum_{n=-\infty}^{+\infty} \mathtt{r}_h(n)\, z^{-n} = H(z)\, H^*\left(\frac{1}{z^*}\right) \tag{1.185}$$

Table 1.6: Relations between ACS and PSD for discrete-time processes through a linear filter.

ACS	PSD
$\mathtt{r}_{yx}(n) = \mathtt{r}_x * h(n)$	$P_{yx}(z) = P_x(z)H(z)$
$\mathtt{r}_{xy}(n) = [\mathtt{r}_x(m) * h^*(-m)](n)$	$P_{xy}(z) = P_x(z)H^*(1/z^*)$
$\mathtt{r}_y(n) = \mathtt{r}_{xy} * h(n)$	$P_y(z) = P_{xy}(z)H(z)$
$= \mathtt{r}_x * \mathtt{r}_h(n)$	$= P_x(z)H(z)H^*(1/z^*)$

[12] We use the same symbol to indicate the correlation between random processes and the correlation between deterministic signals.

In case $P_h(z)$ is a rational function, from (1.185) one deduces that, if $P_h(z)$ has a pole (zero) of the type $e^{j\varphi}|a|$, it also has a corresponding pole (zero) of the type $e^{j\varphi}/|a|$. Consequently, the poles (and zeros) of $P_h(z)$ come in pairs of the type $e^{j\varphi}|a|$, $e^{j\varphi}/|a|$.

From the last relation in Table 1.6, we obtain the relation between the PSDs of input and output signals, i.e.

$$\mathcal{P}_y(f) = \mathcal{P}_x(f)\left|H(e^{j2\pi f T_c})\right|^2 \tag{1.186}$$

In the case of white noise input

$$P_y(z) = \sigma_x^2 H(z) H^*\left(\frac{1}{z^*}\right) \tag{1.187}$$

and

$$\mathcal{P}_y(f) = T_c \sigma_x^2 \left|H(e^{j2\pi f T_c})\right|^2 \tag{1.188}$$

In other words, $\mathcal{P}_y(f)$ has the same shape as the filter frequency response.

In the case of real filters

$$H^*\left(\frac{1}{z^*}\right) = H(z^{-1}) \tag{1.189}$$

Among the various applications of (1.188), it is worth mentioning the *process synthesis*, which deals with the generation of a random process having a pre-assigned PSD. Two methods are shown in Section 4.1.9.

Minimum-phase spectral factorization

In the previous section, we introduced the relation between an impulse response $\{h(k)\}$ and its ACS $\{\mathtt{r}_h(n)\}$ in terms of the z-transform. In many practical applications, it is interesting to determine the minimum-phase impulse response for a given autocorrelation function: with this intent we state the following theorem [5].

Theorem 1.4 (Spectral factorization for discrete-time processes)
Consider the process y with ACS $\{\mathtt{r}_y(n)\}$ having z-transform $P_y(z)$, which satisfies the Paley–Wiener condition for discrete-time systems, i.e.

$$\int_{1/T_c} \left|\ln P_y(e^{j2\pi f T_c})\right| df < \infty \tag{1.190}$$

where the integration is over an arbitrarily chosen interval $1/T_c$. Then the function $P_y(z)$ can be factorized as follows:

$$P_y(z) = f_0^2 \, \tilde{F}(z) \, \tilde{F}^*\left(\frac{1}{z^*}\right) \tag{1.191}$$

where

$$\tilde{F}(z) = 1 + \tilde{f}_1 z^{-1} + \tilde{f}_2 z^{-2} + \cdots \tag{1.192}$$

is monic, minimum phase, and associated with a causal sequence $\{1, \tilde{f}_1, \tilde{f}_2, \dots\}$. The factor f_0 in (1.191) is the geometric mean of $P_y(e^{j2\pi f T_c})$:

$$\ln f_0^2 = T_c \int_{1/T_c} \ln P_y(e^{j2\pi f T_c})\, df \tag{1.193}$$

The logarithms in (1.190) and (1.193) may have any common base.

The Paley–Wiener criterion implies that $P_y(z)$ may have only a discrete set of zeros on the unit circle, and that the spectral factorization (1.191) (with the constraint that $\tilde{F}(z)$ is causal, monic and minimum phase) is unique. For rational $P_y(z)$, the function $f_0\tilde{F}(z)$ is obtained by extracting the poles and zeros of $P_y(z)$ that lie inside the unit circle (see (1.453) and the considerations relative to (1.185)). Moreover, in (1.191) $f_0\tilde{F}^*(1/z^*)$ is the z-transform of an anticausal sequence $f_0\{\dots, \tilde{f}_2^*, \tilde{f}_1^*, 1\}$, associated with poles and zeros of $P_y(z)$ that lie outside the unit circle. □

1.5.4 PSD of passband processes

Definition 1.13
A WSS random process x is said to be PB (BB) if its PSD is of PB (BB) type. □

PSD of in-phase and quadrature components

Let x be a real PB WSS process. Our aim is to derive the PSD of the in-phase and quadrature components of the process. We assume that x does not have direct current (DC) components, i.e. a frequency component at $f = 0$, hence, its mean is zero and consequently also $x^{(a)}$ and $x^{(bb)}$ have zero mean.

We introduce the two (ideal) filters with frequency response

$$\mathcal{H}^{(+)}(f) = 1(f) \quad \text{and} \quad \mathcal{H}^{(-)}(f) = 1(-f) \tag{1.194}$$

Note that they have non-overlapping passbands. For the same input x, the output of the two filters is, respectively, $x^{(+)}$ and $x^{(-)}$. We find that

$$x(t) = x^{(+)}(t) + x^{(-)}(t) \tag{1.195}$$

with $x^{(-)}(t) = x^{(+)*}(t)$. The following relations hold

$$\mathcal{P}_{x^{(+)}}(f) = |\mathcal{H}^{(+)}(f)|^2 \mathcal{P}_x(f) = \mathcal{P}_x(f)1(f) \tag{1.196}$$

$$\mathcal{P}_{x^{(-)}}(f) = |\mathcal{H}^{(-)}(f)|^2 \mathcal{P}_x(f) = \mathcal{P}_x(f)1(-f) \tag{1.197}$$

and

$$\mathcal{P}_{x^{(+)}x^{(-)}}(f) = 0 \tag{1.198}$$

as $x^{(+)}$ and $x^{(-)}$ have non-overlapping passbands. Then $x^{(+)} \perp x^{(-)}$, and (1.195) yields

$$\mathcal{P}_x(f) = \mathcal{P}_{x^{(+)}}(f) + \mathcal{P}_{x^{(-)}}(f) \tag{1.199}$$

where $\mathcal{P}_{x^{(-)}}(f) = \mathcal{P}_{x^{(+)*}}(f) = \mathcal{P}_{x^{(+)}}(-f)$, using Property 5 of the PSD. The analytic signal $x^{(a)}$ is equal to $2x^{(+)}$, hence,

$$\mathtt{r}_{x^{(a)}}(\tau) = 4\mathtt{r}_{x^{(+)}}(\tau) \tag{1.200}$$

and

$$\mathcal{P}_{x^{(a)}}(f) = 4\mathcal{P}_{x^{(+)}}(f) \tag{1.201}$$

Moreover, being $x^{(a)*} = 2x^{(-)}$, it follows that $x^{(a)} \perp x^{(a)*}$ and

$$\mathtt{r}_{x^{(a)}x^{(a)*}}(\tau) = 0 \tag{1.202}$$

The complex envelope $x^{(bb)}$ is related to $x^{(a)}$ by (1.86) and

$$\mathtt{r}_{x^{(bb)}}(\tau) = \mathtt{r}_{x^{(a)}}(\tau)e^{-j2\pi f_0 \tau} \tag{1.203}$$

Hence,

$$\mathcal{P}_{x^{(bb)}}(f) = \mathcal{P}_{x^{(a)}}(f + f_0) = 4\mathcal{P}_{x^{(+)}}(f + f_0) \tag{1.204}$$

Moreover, from (1.202), it follows that $x^{(bb)} \perp x^{(bb)*}$.

Using (1.204), (1.199) can be written as

$$\mathcal{P}_x(f) = \frac{1}{4}[\mathcal{P}_{x^{(bb)}}(f-f_0) + \mathcal{P}_{x^{(bb)}}(-f-f_0)] \tag{1.205}$$

Finally, from

$$x_I^{(bb)}(t) = Re\,[x^{(bb)}(t)] = \frac{x^{(bb)}(t) + x^{(bb)*}(t)}{2} \tag{1.206}$$

and

$$x_Q^{(bb)}(t) = Im\,[x^{(bb)}(t)] = \frac{x^{(bb)}(t) - x^{(bb)*}(t)}{2j} \tag{1.207}$$

we obtain the following relations:

$$\mathtt{r}_{x_I^{(bb)}}(\tau) = \frac{1}{2}Re\,[\mathtt{r}_{x^{(bb)}}(\tau)] \tag{1.208}$$

$$\mathcal{P}_{x_I^{(bb)}}(f) = \frac{1}{4}[\mathcal{P}_{x^{(bb)}}(f) + \mathcal{P}_{x^{(bb)}}(-f)] \tag{1.209}$$

$$\mathtt{r}_{x_Q^{(bb)}}(\tau) = \mathtt{r}_{x_I^{(bb)}}(\tau) \tag{1.210}$$

$$\mathtt{r}_{x_Q^{(bb)}x_I^{(bb)}}(\tau) = \frac{1}{2}Im\,[\mathtt{r}_{x^{(bb)}}(\tau)] \tag{1.211}$$

$$\mathcal{P}_{x_Q^{(bb)}x_I^{(bb)}}(f) = \frac{1}{4j}[\mathcal{P}_{x^{(bb)}}(f) - \mathcal{P}_{x^{(bb)}}(-f)] \tag{1.212}$$

$$\mathtt{r}_{x_I^{(bb)}x_Q^{(bb)}}(\tau) = -\mathtt{r}_{x_Q^{(bb)}x_I^{(bb)}}(\tau) = -\mathtt{r}_{x_I^{(bb)}x_Q^{(bb)}}(-\tau) \tag{1.213}$$

The second equality in (1.213) follows from Property 4 of ACS.

From (1.213), we note that $\mathtt{r}_{x_I^{(bb)}x_Q^{(bb)}}(\tau)$ is an odd function. Moreover, from (1.212), we obtain $x_I^{(bb)} \perp x_Q^{(bb)}$ only if $\mathcal{P}_{x^{(bb)}}$ is an even function; in any case, the random variables $x_I^{(bb)}(t)$ and $x_Q^{(bb)}(t)$ are always orthogonal since $\mathtt{r}_{x_I^{(bb)}x_Q^{(bb)}}(0) = 0$. Referring to the block diagram in Figure 1.18b, as

$$\mathcal{P}_{x^{(h)}}(f) = \mathcal{P}_x(f) \quad \text{and} \quad \mathcal{P}_{x^{(h)}x}(f) = -j\,\text{sgn}(f)\,\mathcal{P}_x(f) \tag{1.214}$$

we obtain

$$\mathtt{r}_{x^{(h)}}(\tau) = \mathtt{r}_x(\tau) \quad \text{and} \quad \mathtt{r}_{x^{(h)}x}(\tau) = \mathtt{r}_x^{(h)}(\tau) \tag{1.215}$$

Then

$$\mathtt{r}_{x_I^{(bb)}}(\tau) = \mathtt{r}_{x_Q^{(bb)}}(\tau) = \mathtt{r}_x(\tau)\cos(2\pi f_0\tau) + \mathtt{r}_x^{(h)}(\tau)\sin(2\pi f_0\tau) \tag{1.216}$$

and

$$\mathtt{r}_{x_I^{(bb)}x_Q^{(bb)}}(\tau) = -\mathtt{r}_x^{(h)}(\tau)\cos(2\pi f_0\tau) + \mathtt{r}_x(\tau)\sin(2\pi f_0\tau) \tag{1.217}$$

In terms of statistical power, the following relations hold:

$$\mathtt{r}_{x^{(+)}}(0) = \mathtt{r}_{x^{(-)}}(0) = \frac{1}{2}\mathtt{r}_x(0) \tag{1.218}$$

$$\mathtt{r}_{x^{(bb)}}(0) = \mathtt{r}_{x^{(a)}}(0) = 4\mathtt{r}_{x^{(+)}}(0) = 2\mathtt{r}_x(0) \tag{1.219}$$

$$\mathtt{r}_{x_I^{(bb)}}(0) = \mathtt{r}_{x_Q^{(bb)}}(0) = \mathtt{r}_x(0) \tag{1.220}$$

$$\mathtt{r}_{x^{(h)}}(0) = \mathtt{r}_x(0) \tag{1.221}$$

Example 1.5.2

Let x be a WSS process with PSD

$$\mathcal{P}_x(f) = \frac{N_0}{2}\left[\text{rect}\left(\frac{f-f_0}{B}\right) + \text{rect}\left(\frac{f+f_0}{B}\right)\right] \tag{1.222}$$

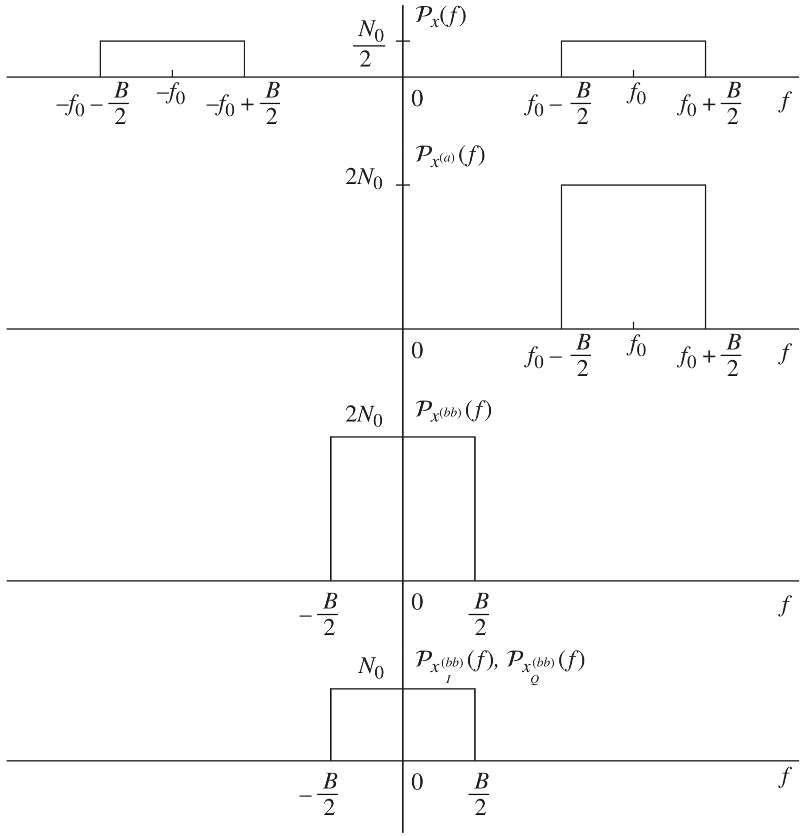

Figure 1.23 Spectral representation of a PB process and its BB components.

depicted in Figure 1.23. It is immediate to get

$$\mathcal{P}_{x^{(a)}}(f) = 2N_0 \text{rect}\left(\frac{f-f_0}{B}\right) \tag{1.223}$$

and

$$\mathcal{P}_{x^{(bb)}}(f) = 2N_0 \text{rect}\left(\frac{f}{B}\right) \tag{1.224}$$

Then

$$\mathcal{P}_{x_I^{(bb)}}(f) = \mathcal{P}_{x_Q^{(bb)}}(f) = \frac{1}{2}\mathcal{P}_{x^{(bb)}}(f) = N_0 \text{rect}\left(\frac{f}{B}\right) \tag{1.225}$$

Moreover, being $\mathcal{P}_{x_I^{(bb)} x_Q^{(bb)}}(f) = 0$, we have that $x_I^{(bb)} \perp x_Q^{(bb)}$.

Cyclostationary processes

We have seen that, if x is a real passband WSS process, then its complex envelope is WSS, and $x^{(bb)} \perp x^{(bb)*}$. The converse is also true: if $x^{(bb)}$ is a WSS process and $x^{(bb)} \perp x^{(bb)*}$, then

$$x(t) = Re\,[x^{(bb)}(t)\; e^{j2\pi f_0 t}] \tag{1.226}$$

is WSS with PSD given by (1.205). If $x^{(bb)}$ is WSS, however, with

$$\mathtt{r}_{x^{(bb)}x^{(bb)*}}(\tau) \neq 0 \tag{1.227}$$

observing (1.226) we find that the autocorrelation of x is a periodic function in t of period $1/f_0$:

$$\mathtt{r}_x(t, t-\tau) = \frac{1}{4}\left[\mathtt{r}_{x^{(bb)}}(\tau)e^{j2\pi f_0\tau} + \mathtt{r}^*_{x^{(bb)}}(\tau)e^{-j2\pi f_0\tau} + \mathtt{r}_{x^{(bb)}x^{(bb)*}}(\tau)e^{-j2\pi f_0\tau}e^{j4\pi f_0 t} + \mathtt{r}^*_{x^{(bb)}x^{(bb)*}}(\tau)e^{j2\pi f_0\tau}e^{-j4\pi f_0 t}\right] \tag{1.228}$$

In other words, x is a *cyclostationary* process of period $T_0 = 1/f_0$.[13]

In this case, it is convenient to introduce the *average correlation*

$$\overline{\mathtt{r}}_x(\tau) = \frac{1}{T_0}\int_0^{T_0} \mathtt{r}_x(t, t-\tau)dt \tag{1.229}$$

whose Fourier transform is the *average PSD*

$$\overline{\mathcal{P}}_x(f) = \mathcal{F}[\overline{\mathtt{r}}_x(\tau)] = \frac{1}{T_0}\int_0^{T_0} \mathcal{P}_x(f,t)dt \tag{1.230}$$

where

$$\mathcal{P}_x(f,t) = \mathcal{F}_\tau[\mathtt{r}_x(t, t-\tau)] \tag{1.231}$$

In (1.231), $\mathcal{F}_\tau$ denotes the Fourier transform with respect to the variable τ. In our case, it is

$$\overline{\mathcal{P}}_x(f) = \frac{1}{4}[\mathcal{P}_{x^{(bb)}}(f-f_0) + \mathcal{P}_{x^{(bb)}}(-f-f_0)] \tag{1.232}$$

as in the stationary case (1.205).

Example 1.5.3

Let x be a modulated DSB signal (see (1.123)), i.e.

$$x(t) = a(t)\cos(2\pi f_0 t + \varphi_0) \tag{1.233}$$

with a real random BB WSS process with bandwidth $B_a < f_0$ and autocorrelation $\mathtt{r}_a(\tau)$. From (1.126) it results $x^{(bb)}(t) = a(t)\ e^{j\varphi_0}$. Hence, we have

$$\mathtt{r}_{x^{(bb)}}(\tau) = \mathtt{r}_a(\tau), \qquad \mathtt{r}_{x^{(bb)}x^{(bb)*}}(\tau) = \mathtt{r}_a(\tau)\ e^{j2\varphi_0} \tag{1.234}$$

Because $\mathtt{r}_a(\tau)$ is not identically zero, observing (1.227) we find that x is cyclostationary with period $1/f_0$. From (1.232), the average PSD of x is given by

$$\overline{\mathcal{P}}_x(f) = \frac{1}{4}[\mathcal{P}_a(f-f_0) + \mathcal{P}_a(f+f_0)] \tag{1.235}$$

Therefore, x has a bandwidth equal to $2B_a$ and an average statistical power

$$\overline{\mathtt{M}}_x = \frac{1}{2}\ \mathtt{M}_a \tag{1.236}$$

We note that one finds the same result (1.235) assuming that φ_0 is a uniform r.v. in $[0, 2\pi)$; in this case x turns out to be WSS.

Example 1.5.4

Let x be a modulated *single sideband* (SSB) with an upper sideband, i.e.

$$\begin{aligned} x(t) &= Re\left[\frac{1}{2}\left(a(t) + ja^{(h)}(t)\right)e^{j(2\pi f_0 t + \varphi_0)}\right] \\ &= \frac{1}{2}\ a(t)\cos(2\pi f_0 t + \varphi_0) - \frac{1}{2}\ a^{(h)}(t)\sin(2\pi f_0 t + \varphi_0) \end{aligned} \tag{1.237}$$

[13] To be precise, x is cyclostationary in mean value with period $T_0 = 1/f_0$, while it is cyclostationary in correlation with period $T_0/2$.

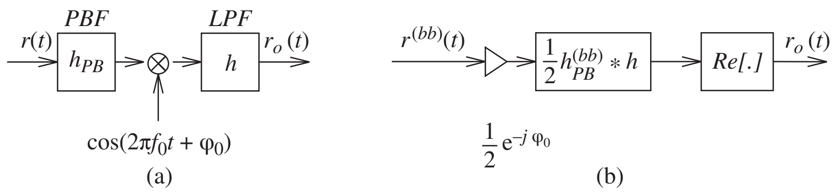

Figure 1.24 Coherent DSB demodulator and baseband-equivalent scheme. (a) Coherent DSB demodulator and (b) baseband-equivalent scheme.

where $a^{(h)}$ is the Hilbert transform of a, a real WSS random process with autocorrelation $\mathtt{r}_a(\tau)$ and bandwidth B_a.

We note that the modulating signal $(a(t) + ja^{(h)}(t))$ coincides with the analytic signal $a^{(a)}$ and its spectral support contains only positive frequencies.

Being

$$x^{(bb)}(t) = \frac{1}{2}(a(t) + ja^{(h)}(t))e^{j\varphi_0}$$

it results that $x^{(bb)}$ and $x^{(bb)*}$ have non-overlapping passbands and

$$\mathtt{r}_{x^{(bb)}x^{(bb)*}}(\tau) = 0 \tag{1.238}$$

The process (1.237) is then stationary with

$$\mathcal{P}_x(f) = \frac{1}{4}[\mathcal{P}_{a^{(+)}}(f - f_0) + \mathcal{P}_{a^{(+)}}(-f - f_0)] \tag{1.239}$$

where $a^{(+)}$ is defined in (1.195). In this case, x has bandwidth equal to B_a and statistical power given by

$$\mathtt{M}_x = \frac{1}{4}\,\mathtt{M}_a \tag{1.240}$$

Example 1.5.5 (DSB and SSB demodulators)
Let the signal r be the sum of a desired part x and additive white noise w with PSD equal to $\mathcal{P}_w(f) = N_0/2$,

$$r(t) = x(t) + w(t) \tag{1.241}$$

where the signal x is modulated DSB (1.233). To obtain the signal a from r, one can use the coherent demodulation scheme illustrated in Figure 1.24 (see Figure 1.21b), where h is an ideal lowpass filter, having a frequency response

$$\mathcal{H}(f) = \mathcal{H}_0 \operatorname{rect}\left(\frac{f}{2B_a}\right) \tag{1.242}$$

Let r_o be the output signal of the demodulator, given by the sum of the desired part x_o and noise w_o:

$$r_o(t) = x_o(t) + w_o(t) \tag{1.243}$$

We evaluate now the ratio between the powers of the signals in (1.243),

$$\Lambda_o = \frac{\mathtt{M}_{x_o}}{\mathtt{M}_{w_o}} \tag{1.244}$$

in terms of the reference signal-to-noise ratio

$$\Gamma = \frac{\mathtt{M}_x}{(N_0/2)\;2B_a} \tag{1.245}$$

Using the equivalent block scheme of Figure 1.24 and (1.126), we have

$$r^{(bb)}(t) = a(t)\, e^{j\varphi_0} + w^{(bb)}(t) \tag{1.246}$$

with $\mathcal{P}_{w^{(bb)}}(f) = 2N_0\, 1(f+f_0)$. Being

$$h * a(t) = \mathcal{H}_0\, a(t) \tag{1.247}$$

it results

$$\begin{aligned} x_o(t) &= Re\left[h * \frac{1}{2}\, e^{-j\varphi_1}\, a\, e^{j\varphi_0}\right](t) \\ &= \frac{\mathcal{H}_0}{2}\, a(t)\cos(\varphi_0 - \varphi_1) \end{aligned} \tag{1.248}$$

Hence, we get

$$\mathtt{M}_{x_o} = \frac{\mathcal{H}_0^2}{4}\, \mathtt{M}_a \cos^2(\varphi_0 - \varphi_1) \tag{1.249}$$

In the same baseband equivalent scheme, we consider the noise w_{eq} at the output of filter h; we find

$$\begin{aligned} \mathcal{P}_{w_{eq}}(f) &= \frac{1}{4}\, |\mathcal{H}(f)|^2\, 2N_0\, 1(f+f_0) \\ &= \frac{\mathcal{H}_0^2}{2}\, N_0\, \text{rect}\left(\frac{f}{2B_a}\right) \end{aligned} \tag{1.250}$$

Being now w WSS, $w^{(bb)}$ is uncorrelated with $w^{(bb)*}$ and thus w_{eq} with w_{eq}^*. Then, from

$$w_o(t) = w_{eq,I}(t) \tag{1.251}$$

and using (1.209) it follows

$$\mathcal{P}_{w_0}(f) = \frac{\mathcal{H}_0^2}{4}\, N_0\, \text{rect}\left(\frac{f}{2B_a}\right) \tag{1.252}$$

and

$$\mathtt{M}_{w_0} = \frac{\mathcal{H}_0^2}{4}\, N_0\, 2B_a \tag{1.253}$$

In conclusion, using (1.236), we have

$$\Lambda_o = \frac{(\mathcal{H}_0^2/4)\, \mathtt{M}_a \cos^2(\varphi_0 - \varphi_1)}{(\mathcal{H}_0^2/4)\, N_0\, 2B_a} = \Gamma \cos^2(\varphi_0 - \varphi_1) \tag{1.254}$$

For $\varphi_1 = \varphi_0$ (1.254) becomes

$$\Lambda_o = \Gamma \tag{1.255}$$

It is interesting to observe that, at the demodulator input, the ratio between the power of the desired signal and the power of the noise in the *passband of x* is given by

$$\Lambda_i = \frac{\mathtt{M}_x}{(N_0/2)\, 4B_a} = \frac{\Gamma}{2} \tag{1.256}$$

For $\varphi_1 = \varphi_0$ then

$$\Lambda_o = 2\Lambda_i \tag{1.257}$$

We will now analyse the case of a SSB signal x (see (1.237)), coherently demodulated, following the scheme of Figure 1.25, where h_{PB} is a filter used to eliminate the noise that otherwise, after the *mixer*, would have fallen within the passband of the desired signal. The ideal frequency response of h_{PB} is given by

$$\mathcal{H}_{PB}(f) = \text{rect}\left(\frac{f - f_0 - B_a/2}{B_a}\right) + \text{rect}\left(\frac{-f - f_0 - B_a/2}{B_a}\right) \tag{1.258}$$

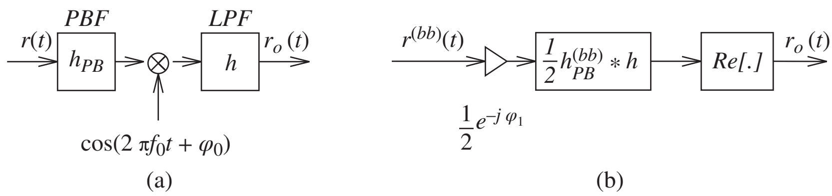

Figure 1.25 (a) Coherent SSB demodulator and (b) baseband-equivalent scheme.

Note that in this scheme, we have assumed the phase of the receiver carrier equal to that of the transmitter, to avoid distortion of the desired signal.

Being

$$\mathcal{H}_{PB}^{(bb)}(f) = 2 \,\mathrm{rect}\left(\frac{f - B_a/2}{B_a}\right) \tag{1.259}$$

the filter of the baseband-equivalent scheme is given by

$$h_{eq}(t) = \frac{1}{2}\, h_{PB}^{(bb)} * h(t) \tag{1.260}$$

with frequency response

$$\mathcal{H}_{eq}(f) = \mathcal{H}_0 \,\mathrm{rect}\left(\frac{f - B_a/2}{B_a}\right) \tag{1.261}$$

We now evaluate the desired component x_o. Using the fact $x^{(bb)} * h_{eq}(t) = \mathcal{H}_0\, x^{(bb)}(t)$, it results

$$\begin{aligned} x_o(t) &= Re\left[h_{eq} * \frac{1}{2}\, e^{-j\varphi_0}\, \frac{1}{2}(a + j\, a^{(h)})\, e^{j\varphi_0}\right](t) \\ &= \frac{\mathcal{H}_0}{4}\, Re\left[a(t) + j\, a^{(h)}(t)\right] = \frac{\mathcal{H}_0}{4}\, a(t) \end{aligned} \tag{1.262}$$

In the baseband-equivalent scheme, the noise w_{eq} at the output of h_{eq} has a PSD given by

$$\mathcal{P}_{w_{eq}}(f) = \frac{1}{4}\, |\mathcal{H}_{eq}(f)|^2\, 2N_0\, 1(f + f_0) = \frac{N_0}{2}\, \mathcal{H}_0^2 \,\mathrm{rect}\left(\frac{f - B_a/2}{B_a}\right) \tag{1.263}$$

From the relation $w_o = w_{eq,I}$ and using (1.209), which is valid because $w_{eq} \perp w_{eq}^*$, we have

$$\mathcal{P}_{w_o}(f) = \frac{1}{4}[\mathcal{P}_{w_{eq}}(f) + \mathcal{P}_{w_{eq}}(-f)] = \frac{\mathcal{H}_0^2}{8}\, N_0 \,\mathrm{rect}\left(\frac{f}{2B_a}\right) \tag{1.264}$$

and

$$\mathtt{M}_{w_o} = \frac{\mathcal{H}_0^2}{8}\, N_0\, 2B_a \tag{1.265}$$

Then we obtain

$$\Lambda_o = \frac{(\mathcal{H}_0^2/16)\, \mathtt{M}_a}{(\mathcal{H}_0^2/8)\, N_0\, 2B_a} \tag{1.266}$$

which using (1.240) and (1.245) can be written as

$$\Lambda_o = \Gamma \tag{1.267}$$

We note that the SSB system yields the same performance (for $\varphi_1 = \varphi_0$) of a DSB system, even though half of the bandwidth is required. Finally, it results

$$\Lambda_i = \frac{\mathtt{M}_x}{(N_0/2)\, 2B_a} = \Lambda_o \tag{1.268}$$

Observation 1.4
We note that also for the simple examples considered in this section, the desired signal is analysed via the various transformations, whereas the noise is analysed via the PSD. As a matter of fact, we are typically interested only in the statistical power of the noise at the system output. The demodulated signal x_o, on the other hand, must be expressed as the sum of a desired component proportional to a and an orthogonal component that represents the distortion, which is, typically, small and has the same effects as noise.

In the previous example, the considered systems do not introduce any distortion since x_o is proportional to a.

1.6 The autocorrelation matrix

Definition 1.14
Given the discrete-time wide-sense stationary random process $\{x(k)\}$, we introduce the random vector with N components

$$\boldsymbol{x}^T(k) = [x(k), x(k-1), \dots, x(k-N+1)] \tag{1.269}$$

The $N \times N$ autocorrelation matrix of $\boldsymbol{x}^*(k)$ is given by

$$\boldsymbol{R} = E[\boldsymbol{x}^*(k)\boldsymbol{x}^T(k)] = \begin{bmatrix} \mathtt{r}_x(0) & \mathtt{r}_x(-1) & \dots & \mathtt{r}_x(-N+1) \\ \mathtt{r}_x(1) & \mathtt{r}_x(0) & \dots & \mathtt{r}_x(-N+2) \\ \vdots & \vdots & \ddots & \dots \\ \mathtt{r}_x(N-1) & \mathtt{r}_x(N-2) & \dots & \mathtt{r}_x(0) \end{bmatrix}. \tag{1.270}$$

□

Properties

1. $\boldsymbol{R}$ is *Hermitian*: $\boldsymbol{R}^H = \boldsymbol{R}$. For real random processes $\boldsymbol{R}$ is *symmetric*: $\boldsymbol{R}^T = \boldsymbol{R}$.
2. $\boldsymbol{R}$ is a *Toeplitz matrix*, i.e. all elements along any diagonal are equal.
3. $\boldsymbol{R}$ is *positive semi-definite* and almost always *positive definite*. Indeed, taking an arbitrary vector $\boldsymbol{v}^T = [v_0, \dots, v_{N-1}]$, and letting $y_k = \boldsymbol{x}^T(k)\boldsymbol{v}$, we have

$$E[|y_k|^2] = E[\boldsymbol{v}^H\boldsymbol{x}^*(k)\boldsymbol{x}^T(k)\boldsymbol{v}] = \boldsymbol{v}^H\boldsymbol{R}\boldsymbol{v} = \sum_{i=0}^{N-1}\sum_{j=0}^{N-1} v_i^* \mathtt{r}_x(i-j) v_j \ge 0 \tag{1.271}$$

   If $\boldsymbol{v}^H\boldsymbol{R}\boldsymbol{v} > 0$, $\forall \boldsymbol{v} \neq \boldsymbol{0}$, then $\boldsymbol{R}$ is said to be *positive definite* and all its *principal minor* determinants are positive; in particular $\boldsymbol{R}$ is *non-singular*.

Eigenvalues

We indicate with $\det \boldsymbol{R}$ the determinant of a matrix $\boldsymbol{R}$. The eigenvalues of $\boldsymbol{R}$ are the solutions λ_i, $i = 1, \dots, N$, of the *characteristic equation* of order N

$$\det[\boldsymbol{R} - \lambda \boldsymbol{I}] = 0 \tag{1.272}$$

and the corresponding column eigenvectors $\boldsymbol{u}_i$, $i = 1, \dots, N$, satisfy the equation

$$\boldsymbol{R}\boldsymbol{u}_i = \lambda_i \boldsymbol{u}_i \tag{1.273}$$

Table 1.7: Correspondence between eigenvalues and eigenvectors of four matrices.

	$\boldsymbol{R}$	$\boldsymbol{R}^m$	$\boldsymbol{R}^{-1}$	$\boldsymbol{I}-\mu\boldsymbol{R}$
Eigenvalue	λ_i	λ_i^m	λ_i^{-1}	$(1-\mu\lambda_i)$
Eigenvector	$\boldsymbol{u}_i$	$\boldsymbol{u}_i$	$\boldsymbol{u}_i$	$\boldsymbol{u}_i$

Example 1.6.1
Let $\{w(k)\}$ be a white noise process. Its autocorrelation matrix $\boldsymbol{R}$ assumes the form

$$\boldsymbol{R} = \begin{bmatrix} \sigma_w^2 & 0 & \dots & 0 \\ 0 & \sigma_w^2 & \dots & 0 \\ \vdots & \vdots & \ddots & \vdots \\ 0 & 0 & \dots & \sigma_w^2 \end{bmatrix} \tag{1.274}$$

from which it follows that

$$\lambda_1 = \lambda_2 = \cdots = \lambda_N = \sigma_w^2 \tag{1.275}$$

and

$$\boldsymbol{u}_i \text{ can be any arbitrary vector} \qquad 1 \le i \le N \tag{1.276}$$

Example 1.6.2
We define a complex-valued sinusoid as

$$x(k) = e^{j(\omega k+\varphi)}, \qquad \omega = 2\pi f T_c \tag{1.277}$$

with φ a uniform r.v. in $[0, 2\pi)$. The autocorrelation matrix $\boldsymbol{R}$ is given by

$$\boldsymbol{R} = \begin{bmatrix} 1 & e^{-j\omega} & \dots & e^{-j(N-1)\omega} \\ e^{j\omega} & 1 & \dots & e^{-j(N-2)\omega} \\ \vdots & \vdots & \ddots & \vdots \\ e^{j(N-1)\omega} & e^{j(N-2)\omega} & \dots & 1 \end{bmatrix} \tag{1.278}$$

One can see that the rank of $\boldsymbol{R}$ is 1 and it will therefore have only one eigenvalue. The solution is given by

$$\lambda_1 = N \tag{1.279}$$

and the relative eigenvector is

$$\boldsymbol{u}_1^T = [1, e^{j\omega}, \dots, e^{j(N-1)\omega}] \tag{1.280}$$

Other properties

1. From $\boldsymbol{R}^m \boldsymbol{u} = \lambda^m \boldsymbol{u}$, we obtain the relations of Table 1.7.
2. If the eigenvalues are distinct, then the eigenvectors are linearly independent:

$$\sum_{i=1}^{N} c_i \boldsymbol{u}_i \neq \boldsymbol{0} \tag{1.281}$$

for all combinations of $\{c_i\}$, $i = 1, 2, \dots, N$, not all equal to zero. Therefore, in this case, the eigenvectors form a basis in $\mathbb{R}^N$.

3. The *trace* of a matrix $\boldsymbol{R}$ is defined as the sum of the elements of the main diagonal, and we indicate it with $\operatorname{tr}\boldsymbol{R}$. It holds

$$\operatorname{tr}\boldsymbol{R} = \sum_{i=1}^{N} \lambda_i \tag{1.282}$$

Eigenvalue analysis for Hermitian matrices

As previously seen, the autocorrelation matrix $\boldsymbol{R}$ is Hermitian, thus enjoys the following properties:

1. The eigenvalues of a Hermitian matrix are real.
   By left multiplying both sides of (1.273) by $\boldsymbol{u}_i^H$, it follows

$$\boldsymbol{u}_i^H \boldsymbol{R} \boldsymbol{u}_i = \lambda_i \boldsymbol{u}_i^H \boldsymbol{u}_i \tag{1.283}$$

   from which, by the definition of norm, we obtain

$$\lambda_i = \frac{\boldsymbol{u}_i^H \boldsymbol{R} \boldsymbol{u}_i}{\boldsymbol{u}_i^H \boldsymbol{u}_i} = \frac{\boldsymbol{u}_i^H \boldsymbol{R} \boldsymbol{u}_i}{\|\boldsymbol{u}_i\|^2} \tag{1.284}$$

   The ratio (1.284) is defined as *Rayleigh quotient*. As $\boldsymbol{R}$ is positive semi-definite, $\boldsymbol{u}_i^H \boldsymbol{R} \boldsymbol{u}_i \geq 0$, from which $\lambda_i \geq 0$.
2. If the eigenvalues of $\boldsymbol{R}$ are distinct, then the eigenvectors are orthogonal. In fact, from (1.273), we obtain:

$$\boldsymbol{u}_i^H \boldsymbol{R} \boldsymbol{u}_j = \lambda_j \boldsymbol{u}_i^H \boldsymbol{u}_j \tag{1.285}$$

$$\boldsymbol{u}_i^H \boldsymbol{R} \boldsymbol{u}_j = \lambda_i \boldsymbol{u}_i^H \boldsymbol{u}_j \tag{1.286}$$

   Subtracting the second equation from the first:

$$0 = (\lambda_j - \lambda_i) \boldsymbol{u}_i^H \boldsymbol{u}_j \tag{1.287}$$

   and since $\lambda_j - \lambda_i \neq 0$ by hypothesis, it follows $\boldsymbol{u}_i^H \boldsymbol{u}_j = 0$.
3. If the eigenvalues of $\boldsymbol{R}$ are distinct and their corresponding eigenvectors are normalized, i.e.

$$\|\boldsymbol{u}_i\|^2 = \boldsymbol{u}_i^H \boldsymbol{u}_i = \begin{cases} 1 & i = j \\ 0 & i \neq j \end{cases} \tag{1.288}$$

   then the matrix $\boldsymbol{U} = [\boldsymbol{u}_1, \boldsymbol{u}_2, \ldots, \boldsymbol{u}_N]$, whose columns are the eigenvectors of $\boldsymbol{R}$, is a unitary matrix, that is

$$\boldsymbol{U}^{-1} = \boldsymbol{U}^H \tag{1.289}$$

   This property is an immediate consequence of the orthogonality of the eigenvectors $\{\boldsymbol{u}_i\}$. Moreover, if we define the matrix

$$\boldsymbol{\Lambda} = \begin{bmatrix} \lambda_1 & 0 & \ldots & 0 \\ 0 & \lambda_2 & \ldots & 0 \\ \vdots & \vdots & \ddots & \vdots \\ 0 & 0 & \ldots & \lambda_N \end{bmatrix} \tag{1.290}$$

   we get

$$\boldsymbol{U}^H \boldsymbol{R} \boldsymbol{U} = \boldsymbol{\Lambda} \tag{1.291}$$

   From (1.291), we obtain the following important relations:

$$\boldsymbol{R} = \boldsymbol{U} \boldsymbol{\Lambda} \boldsymbol{U}^H = \sum_{i=1}^{N} \lambda_i \boldsymbol{u}_i \boldsymbol{u}_i^H \tag{1.292}$$

and

$$\boldsymbol{I} - \mu \boldsymbol{R} = \boldsymbol{U}(\boldsymbol{I} - \mu \boldsymbol{\Lambda})\boldsymbol{U}^H = \sum_{i=1}^{N} (1 - \mu \lambda_i) \boldsymbol{u}_i \boldsymbol{u}_i^H \tag{1.293}$$

4. The eigenvalues of a positive semi-definite autocorrelation matrix $\boldsymbol{R}$ and the PSD of x are related by the inequalities,

$$\min_f \{\mathcal{P}_x(f)\} \leq \lambda_i \leq \max_f \{\mathcal{P}_x(f)\}, \qquad i = 1, \ldots, N \tag{1.294}$$

In fact, let $U_i(f)$ be the Fourier transform of the sequence represented by the elements of $\boldsymbol{u}_i$, i.e.

$$U_i(f) = \sum_{n=1}^{N} u_{i,n} e^{-j2\pi f n T_c} \tag{1.295}$$

where $u_{i,n}$ is the n-th element of the eigenvector $\boldsymbol{u}_i$. Observing that

$$\boldsymbol{u}_i^H \boldsymbol{R} \boldsymbol{u}_i = \sum_{n=1}^{N} \sum_{m=1}^{N} u_{i,n}^* \mathtt{r}_x(n-m) u_{i,m} \tag{1.296}$$

and using (1.172) and (1.295), we have

$$\begin{aligned} \boldsymbol{u}_i^H \boldsymbol{R} u_i &= \int_{-\frac{1}{2T_c}}^{\frac{1}{2T_c}} \mathcal{P}_x(f) \sum_{n=1}^{N} u_{i,n}^* e^{j2\pi f n T_c} \sum_{m=1}^{N} u_{i,m} e^{-j2\pi f m T_c} df \\ &= \int_{-\frac{1}{2T_c}}^{\frac{1}{2T_c}} \mathcal{P}_x(f) \, |U_i(f)|^2 df \end{aligned} \tag{1.297}$$

Substituting the latter result in (1.284) one finds

$$\lambda_i = \frac{\displaystyle\int_{-\frac{1}{2T_c}}^{\frac{1}{2T_c}} \mathcal{P}_x(f) \, |U_i(f)|^2 df}{\displaystyle\int_{-\frac{1}{2T_c}}^{\frac{1}{2T_c}} |U_i(f)|^2 df} \tag{1.298}$$

from which (1.294) follows.

If we indicate with λ_{min} and λ_{max}, respectively, the minimum and maximum eigenvalue of $\boldsymbol{R}$, in view of the latter point, we can define the *eigenvalue spread* as:

$$\chi(\boldsymbol{R}) = \frac{\lambda_{max}}{\lambda_{min}} \leq \frac{\max_f \{\mathcal{P}_x(f)\}}{\min_f \{\mathcal{P}_x(f)\}} \tag{1.299}$$

From (1.299), we observe that $\chi(\boldsymbol{R})$ may assume large values in the case $\mathcal{P}_x(f)$ exhibits large variations. Moreover, $\chi(\boldsymbol{R})$ assumes the minimum value of 1 for a white process.

1.7 Examples of random processes

Before reviewing some important random processes, we recall the definition of Gaussian complex-valued random vector.

Example 1.7.1
A complex r.v. with a Gaussian distribution can be generated from two r.v.s. with uniform distribution (see Appendix 1.B for an illustration of the method).

Example 1.7.2
Let $\boldsymbol{x}^T = [x_1, \dots, x_N]$ be a real Gaussian random vector, each component has mean $\mathtt{m}_{x_i}$ and variance $\sigma^2_{x_i}$, denoted as $x_i \sim \mathcal{N}(\mathtt{m}_{x_i}, \sigma^2_{x_i})$. The joint probability density function (pdf) is

$$p_{\boldsymbol{x}}(\boldsymbol{\xi}) = [(2\pi)^N \det \boldsymbol{C}_N]^{-\frac{1}{2}} e^{-\frac{1}{2}(\boldsymbol{\xi}-\boldsymbol{m}_x)^T \boldsymbol{C}_N^{-1}(\boldsymbol{\xi}-\boldsymbol{m}_x)} \tag{1.300}$$

where $\boldsymbol{\xi}^T = [\xi_1, \dots, \xi_N]$, $\boldsymbol{m}_x = E[\boldsymbol{x}]$ is the vector of its components' mean values and $\boldsymbol{C}_N = E[(\boldsymbol{x} - \boldsymbol{m}_x)(\boldsymbol{x} - \boldsymbol{m}_x)^T]$ is its covariance matrix.

Example 1.7.3
Let $\boldsymbol{x}^T = [x_{1,I} + jx_{1,Q}, \dots, x_{N,I} + jx_{N,Q}]$ be a complex-valued Gaussian random vector. If the in-phase component $x_{i,I}$ and the quadrature component $x_{i,Q}$ are uncorrelated,

$$E[(x_{i,I} - \mathtt{m}_{x_{i,I}})(x_{i,Q} - \mathtt{m}_{x_{i,Q}})] = 0, \qquad i = 1, 2, \dots, N \tag{1.301}$$

Moreover, we have

$$\sigma^2_{x_{i,I}} = \sigma^2_{x_{i,Q}} = \frac{1}{2}\sigma^2_{x_i} \tag{1.302}$$

then the joint pdf is

$$p_{\boldsymbol{x}}(\boldsymbol{\xi}) = [\pi^N \det \boldsymbol{C}_N]^{-1} e^{-(\boldsymbol{\xi}-\boldsymbol{m}_x)^H \boldsymbol{C}_N^{-1}(\boldsymbol{\xi}-\boldsymbol{m}_x)} \tag{1.303}$$

with the vector of mean values and the covariance matrix given by

$$\boldsymbol{m}_x = E[\boldsymbol{x}] = E[\boldsymbol{x}_I] + jE[\boldsymbol{x}_Q] \tag{1.304}$$

$$\boldsymbol{C}_N = E[(\boldsymbol{x} - \boldsymbol{m}_x)(\boldsymbol{x} - \boldsymbol{m}_x)^H] \tag{1.305}$$

Vector $\boldsymbol{x}$ is called *circularly symmetric Gaussian* random vector. For the generic component, we write $x_i \sim \mathcal{CN}(\mathtt{m}_{x_i}, \sigma^2_{x_i})$ and

$$p_{x_i}(\xi_i) = \frac{1}{\sqrt{2\pi\sigma^2_{x_{i,I}}}} e^{-\frac{|\xi_{i,I} - \mathtt{m}_{x_{i,I}}|^2}{2\sigma^2_{x_{i,I}}}} \frac{1}{\sqrt{2\pi\sigma^2_{x_{i,Q}}}} e^{-\frac{|\xi_{i,Q} - \mathtt{m}_{x_{i,Q}}|^2}{2\sigma^2_{x_{i,Q}}}} \tag{1.306}$$

$$= \frac{1}{\pi\sigma^2_{x_i}} e^{-\frac{|\xi_i - \mathtt{m}_{x_i}|^2}{\sigma^2_{x_i}}} \tag{1.307}$$

with $\xi_i = \xi_{i,I} + j\xi_{i,Q}$ complex valued.

Example 1.7.4
Let $\boldsymbol{x}^T = [x_1, \dots, x_N] = [x_1(t_1), \dots, x_N(t_N)]$ be a complex-valued Gaussian (vector) process, with each element $x_i(t_i)$ having real and imaginary components that are uncorrelated Gaussian r.v.s. whose pdf is with zero mean and equal variance for all values of t_i. The vector $\boldsymbol{x}$ is called *circularly symmetric Gaussian random process*. The joint pdf in this case results

$$p_{\boldsymbol{x}}(\boldsymbol{\xi}) = [\pi^N \det \boldsymbol{C}]^{-1} e^{-\boldsymbol{\xi}^H \boldsymbol{C}^{-1} \boldsymbol{\xi}} \tag{1.308}$$

where $\boldsymbol{C}$ is the covariance matrix of $[x_1(t_1), x_2(t_2), \dots, x_N(t_N)]$.

Example 1.7.5
Let $x(t) = A\sin(2\pi ft + \varphi)$ be a real-valued sinusoidal signal with φ r.v. uniform in $[0, 2\pi)$, for which we will use the notation $\varphi \sim \mathcal{U}[0, 2\pi)$. The mean of x is

$$\begin{aligned} \mathtt{m}_x(t) &= E[x(t)] \\ &= \int_0^{2\pi} \frac{1}{2\pi} A\sin(2\pi ft + a)da \\ &= 0 \end{aligned} \tag{1.309}$$

and the autocorrelation function is given by

$$\mathtt{r}_x(\tau) = \int_0^{2\pi} \frac{1}{2\pi} A\sin(2\pi ft + a) A\sin[2\pi f(t-\tau) + a]da$$
$$= \frac{A^2}{2}\cos(2\pi f\tau) \tag{1.310}$$

Example 1.7.6
Consider the sum of N real-valued sinusoidal signals, i.e.

$$x(t) = \sum_{i=1}^{N} A_i \sin(2\pi f_i t + \varphi_i) \tag{1.311}$$

with $\varphi_i \sim \mathcal{U}[0, 2\pi)$ statistically independent, from Example 1.7.5 it is immediate to obtain the mean

$$\mathtt{m}_x(t) = \sum_{i=1}^{N} \mathtt{m}_{x_i}(t) = 0 \tag{1.312}$$

and the autocorrelation function

$$\mathtt{r}_x(\tau) = \sum_{i=1}^{N} \frac{A_i^2}{2}\cos(2\pi f_i\tau) \tag{1.313}$$

We note that, according to the Definition 1.9, page 31, the process (1.311) is not asymptotically uncorrelated.

Example 1.7.7
Consider the sum of N complex-valued sinusoidal signals, i.e.

$$x(t) = \sum_{i=1}^{N} A_i\ e^{j(2\pi f_i t + \varphi_i)} \tag{1.314}$$

with $\varphi_i \sim \mathcal{U}[0, 2\pi)$ statistically independent. Following a similar procedure to that used in Examples 1.7.5 and 1.7.6, we find

$$\mathtt{r}_x(\tau) = \sum_{i=1}^{N} |A_i|^2\ e^{j2\pi f_i\tau} \tag{1.315}$$

We note that the process (1.315) is not asymptotically uncorrelated.

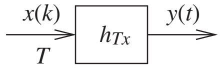

Figure 1.26 Modulator of a PAM system as interpolator filter.

Example 1.7.8
Let the discrete-time random process $y(k) = x(k) + w(k)$ be given by the sum of the random process x of Example 1.7.7 and white noise w with variance σ_w^2. Moreover, we assume x and w uncorrelated. In this case,

$$\mathtt{r}_y(n) = \sum_{i=1}^{N} |A_i|^2 \; e^{j2\pi f_i n T_c} + \sigma_w^2 \delta_n \tag{1.316}$$

Example 1.7.9
We consider a signal obtained by pulse-amplitude modulation (PAM), expressed as

$$y(t) = \sum_{k=-\infty}^{+\infty} x(k) \; h_{Tx}(t - kT) \tag{1.317}$$

The signal y is the output of the system shown in Figure 1.26, where h_{Tx} is a finite-energy pulse and $\{x(k)\}$ is a discrete-time (with T-spaced samples) WSS sequence, having PSD $\mathcal{P}_x(f)$. We note that $\mathcal{P}_x(f)$ is a periodic function of period $1/T$.

Let the deterministic autocorrelation of the signal h_{Tx} be

$$\mathtt{r}_{h_{Tx}}(\tau) = \int_{-\infty}^{+\infty} h_{Tx}(t) h_{Tx}^*(t - \tau) dt = [h_{Tx}(t) * h_{Tx}^*(-t)](\tau) \tag{1.318}$$

with Fourier transform $|\mathcal{H}_{Tx}(f)|^2$. In general, y is a cyclostationary process of period T. In fact, we have

1. *Mean*

$$\mathtt{m}_y(t) = \mathtt{m}_x \sum_{k=-\infty}^{+\infty} h_{Tx}(t - kT) \tag{1.319}$$

2. *Correlation*

$$\mathtt{r}_y(t, t - \tau) = \sum_{i=-\infty}^{+\infty} \mathtt{r}_x(i) \sum_{m=-\infty}^{+\infty} h_{Tx}(t - (i + m)\, T) h_{Tx}^*(t - \tau - mT) \tag{1.320}$$

If we introduce the average spectral analysis

$$\bar{\mathtt{m}}_y = \frac{1}{T} \int_0^T \mathtt{m}_y(t) \; dt = \mathtt{m}_x \mathcal{H}_{Tx}(0) \tag{1.321}$$

$$\bar{\mathtt{r}}_y(\tau) = \frac{1}{T} \int_0^T \mathtt{r}_y(t, t - \tau) dt = \frac{1}{T} \sum_{i=-\infty}^{+\infty} \mathtt{r}_x(i) \mathtt{r}_{h_{Tx}}(\tau - iT) \tag{1.322}$$

and

$$\overline{\mathcal{P}}_y(f) = \mathcal{F}[\bar{\mathtt{r}}_y(\tau)] = \left| \frac{1}{T} \mathcal{H}_{Tx}(f) \right|^2 \mathcal{P}_x(f) \tag{1.323}$$

we observe that the modulator of a PAM system may be regarded as an interpolator filter with frequency response $\mathcal{H}_{Tx}/T$.

3. *Average power for a white noise input* For a white noise input with power $\mathtt{M}_x$, from (1.322), the average statistical power of the output signal is given by

$$\overline{\mathtt{M}}_y = \mathtt{M}_x \frac{E_h}{T} \tag{1.324}$$

where $E_h = \int_{-\infty}^{+\infty} |h_{Tx}(t)|^2 \, dt$ is the energy of h_{Tx}.

4. *Moments of y for a circularly symmetric i.i.d. input*
Let $\{x(k)\}$ be a complex-valued random circularly symmetric sequence with zero mean (see (1.301) and (1.302)), i.e. letting

$$x_I(k) = Re[x(k)], \qquad x_Q(k) = Im[x(k)] \tag{1.325}$$

we have

$$E[x_I^2(k)] = E[x_Q^2(k)] = \frac{E[|x(k)|^2]}{2} \tag{1.326}$$

and

$$E[x_I(k)\, x_Q(k)] = 0 \tag{1.327}$$

These two relations can be merged into the single expression

$$E[x^2(k)] = E[x_I^2(k)] - E[x_Q^2(k)] + 2j\, E[x_I(k)\, x_Q(k)] = 0 \tag{1.328}$$

Filtering the i.i.d. input signal $\{x(k)\}$ by using the system depicted in Figure 1.26, and from the relation

$$\mathtt{r}_{yy^*}(t, t-\tau) = \sum_{i=-\infty}^{+\infty} \mathtt{r}_{xx^*}(i) \sum_{m=-\infty}^{+\infty} h_{Tx}(t-(i+m)T) h_{Tx}(t-\tau-mT) \tag{1.329}$$

we have

$$\mathtt{r}_{xx^*}(i) = E[x^2(k)]\delta(i) = 0 \tag{1.330}$$

and

$$\mathtt{r}_{yy^*}(t, t-\tau) = 0 \tag{1.331}$$

that is $y \perp y^*$. In particular, we have that y is circularly symmetric, i.e.

$$E[y^2(t)] = 0 \tag{1.332}$$

We note that the condition (1.331) can be obtained assuming the less stringent condition that $x \perp x^*$; on the other hand, this requires that the following two conditions are verified

$$\mathtt{r}_{x_I}(i) = \mathtt{r}_{x_Q}(i) \tag{1.333}$$

and

$$\mathtt{r}_{x_I x_Q}(i) = -\mathtt{r}_{x_I x_Q}(-i) \tag{1.334}$$

Observation 1.5
It can be shown that if the filter h_{Tx} has a bandwidth smaller than $1/(2T)$ and $\{x(k)\}$ is a WSS sequence, then $\{y(k)\}$ is WSS with PSD (1.323).

Example 1.7.10
Let us consider a PAM signal sampled with period $T_Q = T/Q_0$, where Q_0 is a positive integer number. Let

$$y_q = y(q\, T_Q), \qquad h_p = h_{Tx}(p\, T_Q) \tag{1.335}$$

from (1.317) it follows

$$y_q = \sum_{k=-\infty}^{+\infty} x(k)\, h_{q-kQ_0} \tag{1.336}$$

If $Q_0 \neq 1$, (1.336) describes the input–output relation of an interpolator filter (see (1.536)). We recall the statistical analysis given in Table 1.6, page 34. We denote with $\mathcal{H}(f)$ the Fourier transform (see (1.17)) and with $\mathtt{r}_h(n)$ the deterministic autocorrelation (see (1.184)) of the sequence $\{h_p\}$. We also assume that $\{x(k)\}$ is a WSS random sequence with mean $\mathtt{m}_x$ and autocorrelation $\mathtt{r}_x(n)$. In general, $\{y_q\}$ is a cyclostationary random sequence of period Q_0 with

1. *Mean*

$$\mathtt{m}_y(q) = \mathtt{m}_x \sum_{k=-\infty}^{+\infty} h_{q-kQ_0} \tag{1.337}$$

2. *Correlation*

$$\mathtt{r}_y(q, q-n) = \sum_{i=-\infty}^{+\infty} \mathtt{r}_x(i) \sum_{m=-\infty}^{+\infty} h_{q-(i+m)Q_0}\, h^*_{q-n-m\;Q_0} \tag{1.338}$$

By the average spectral analysis, we obtain

$$\overline{\mathtt{m}}_y = \frac{1}{Q_0} \sum_{q=0}^{Q_0-1} \mathtt{m}_y(q) = \mathtt{m}_x\, \frac{\mathcal{H}(0)}{Q_0} \tag{1.339}$$

where

$$\mathcal{H}(0) = \sum_{p=-\infty}^{+\infty} h_p \tag{1.340}$$

and

$$\overline{\mathtt{r}}_y(n) = \frac{1}{Q_0} \sum_{q=0}^{Q_0-1} \mathtt{r}_y(q, q-n) = \frac{1}{Q_0} \sum_{i=-\infty}^{+\infty} \mathtt{r}_x(i)\, \mathtt{r}_h(n - iQ_0) \tag{1.341}$$

Consequently, the average PSD is given by

$$\overline{\mathcal{P}}_y(f) = T_Q\, \mathcal{F}[\overline{\mathtt{r}}_y(n)] = \left| \frac{1}{Q_0}\, \mathcal{H}(f) \right|^2 \mathcal{P}_x(f) \tag{1.342}$$

If $\{x(k)\}$ is white noise with power $\mathtt{M}_x$, from (1.341) it results

$$\overline{\mathtt{r}}_y(n) = \mathtt{M}_x\, \frac{\mathtt{r}_h(n)}{Q_0} \tag{1.343}$$

In particular, the average power of the filter output signal is given by

$$\overline{\mathtt{M}}_y = \mathtt{M}_x\, \frac{E_h}{Q_0} \tag{1.344}$$

where $E_h = \sum_{p=-\infty}^{+\infty} |h_p|^2$ is the energy of $\{h_p\}$. We point out that the condition $\overline{\mathtt{M}}_y = \mathtt{M}_x$ is satisfied if the energy of the filter impulse response is equal to the interpolation factor Q_0.

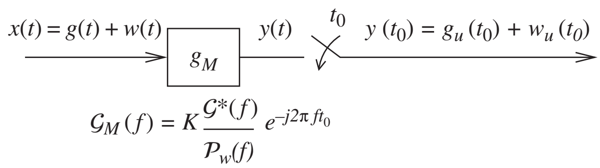

Figure 1.27 Reference scheme for the matched filter.

1.8 Matched filter

Referring to Figure 1.27, we consider a finite-energy signal pulse g in the presence of additive noise w having zero mean and PSD $\mathcal{P}_w$. The signal

$$x(t) = g(t) + w(t) \tag{1.345}$$

is filtered with a filter having impulse response g_M. We indicate with g_u and w_u, respectively, the desired signal and the noise component at the output:

$$g_u(t) = g_M * g(t) \tag{1.346}$$

$$w_u(t) = g_M * w(t) \tag{1.347}$$

The output is

$$y(t) = g_u(t) + w_u(t) \tag{1.348}$$

We now suppose that y is observed at a given instant t_0. The problem is to determine g_M so that the ratio between the square amplitude of $g_u(t_0)$ and the power of the noise component $w_u(t_0)$ is maximum, i.e.

$$g_M \; : \; \max_{g_M} \frac{|g_u(t_0)|^2}{E[|w_u(t_0)|^2]} \tag{1.349}$$

The optimum filter has frequency response

$$\mathcal{G}_M(f) = K \frac{\mathcal{G}^*(f)}{\mathcal{P}_w(f)} e^{-j2\pi f t_0} \tag{1.350}$$

where K is a constant. In other words, the best filter selects the frequency components of the desired input signal and weights them with weights that are inversely proportional to the noise level.

Proof. $g_u(t_0)$ coincides with the inverse Fourier transform of $\mathcal{G}_M(f)\mathcal{G}(f)$ evaluated in $t = t_0$, while the power of $w_u(t_0)$ is equal to

$$\mathtt{r}_{w_u}(0) = \int_{-\infty}^{+\infty} \mathcal{P}_w(f) |\mathcal{G}_M(f)|^2 df \tag{1.351}$$

Then we have

$$\begin{aligned} \frac{|g_u(t_0)|^2}{\mathtt{r}_{w_u}(0)} &= \frac{\left| \int_{-\infty}^{+\infty} \mathcal{G}_M(f) \mathcal{G}(f) e^{j2\pi f t_0} df \right|^2}{\int_{-\infty}^{+\infty} \mathcal{P}_w(f) |\mathcal{G}_M(f)|^2 df} \\ &= \frac{\left| \int_{-\infty}^{+\infty} \mathcal{G}_M(f) \sqrt{\mathcal{P}_w(f)} \frac{\mathcal{G}(f)}{\sqrt{\mathcal{P}_w(f)}} e^{j2\pi f t_0} df \right|^2}{\int_{-\infty}^{+\infty} \mathcal{P}_w(f) |\mathcal{G}_M(f)|^2 df} \end{aligned} \tag{1.352}$$

where the integrand at the numerator was divided and multiplied by $\sqrt{\mathcal{P}_w(f)}$. Implicitly, it is assumed that $\mathcal{P}_w(f) \neq 0$. Applying the Schwarz inequality[14] to the functions

$$\mathcal{G}_M(f)\sqrt{\mathcal{P}_w(f)} \tag{1.355}$$

and

$$\frac{\mathcal{G}^*(f)}{\sqrt{\mathcal{P}_w(f)}}\, e^{-j2\pi f t_0} \tag{1.356}$$

it turns out

$$\frac{|g_u(t_0)|^2}{\mathtt{r}_{w_u}(0)} \leq \int_{-\infty}^{+\infty} \left| \frac{\mathcal{G}(f)}{\sqrt{\mathcal{P}_w(f)}} e^{j2\pi f t_0} \right|^2 df = \int_{-\infty}^{+\infty} \left| \frac{\mathcal{G}(f)}{\sqrt{\mathcal{P}_w(f)}} \right|^2 df \tag{1.357}$$

Therefore, the maximum value is equal to the right-hand side of (1.357) and is achieved for

$$\mathcal{G}_M(f)\sqrt{\mathcal{P}_w(f)} = K \frac{\mathcal{G}^*(f)}{\sqrt{\mathcal{P}_w(f)}}\, e^{-j2\pi f t_0} \tag{1.358}$$

where K is a constant. From (1.358), the solution (1.350) follows immediately. □

White noise case

If w is white, then $\mathcal{P}_w(f) = \mathcal{P}_w$ is a constant and the optimum solution (1.350) becomes

$$\mathcal{G}_M(f) = K\mathcal{G}^*(f)e^{-j2\pi f t_0} \tag{1.359}$$

Correspondingly, the filter has impulse response

$$g_M(t) = Kg^*(t_0 - t) \tag{1.360}$$

from which the name of *matched filter* (MF), i.e. matched to the input signal pulse. The desired signal pulse at the filter output has the frequency response

$$\mathcal{G}_u(f) = K|\mathcal{G}(f)|^2 e^{-j2\pi f t_0} \tag{1.361}$$

From the definition of the autocorrelation function of pulse g,

$$\mathtt{r}_g(\tau) = \int_{-\infty}^{+\infty} g(a)g^*(a-\tau)da \tag{1.362}$$

then, as depicted in Figure 1.28,

$$g_u(t) = K\mathtt{r}_g(t - t_0) \tag{1.363}$$

i.e. the pulse at the filter output coincides with the autocorrelation function of the pulse g. If E_g is the energy of g, using the relation $E_g = \mathtt{r}_g(0)$ the maximum of the functional (1.349) becomes

$$\frac{|g_u(t_0)|^2}{\mathtt{r}_{w_u}(0)} = \frac{|K|^2 \mathtt{r}_g^2(0)}{\mathcal{P}_w |K|^2 \mathtt{r}_g(0)} = \frac{E_g}{\mathcal{P}_w} \tag{1.364}$$

---

[14] Given two signals x and y it holds

$$\left| \int_{-\infty}^{\infty} x(t)y^*(t)dt \right|^2 \leq \int_{-\infty}^{\infty} |x(t)|^2 dt \int_{-\infty}^{\infty} |y(t)|^2 dt \tag{1.353}$$

where equality holds if and only if

$$y(t) = Kx(t) \tag{1.354}$$

with K a complex constant.

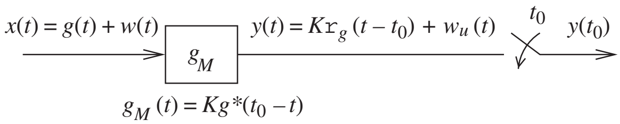

Figure 1.28 Matched filter for an input pulse in the presence of white noise.

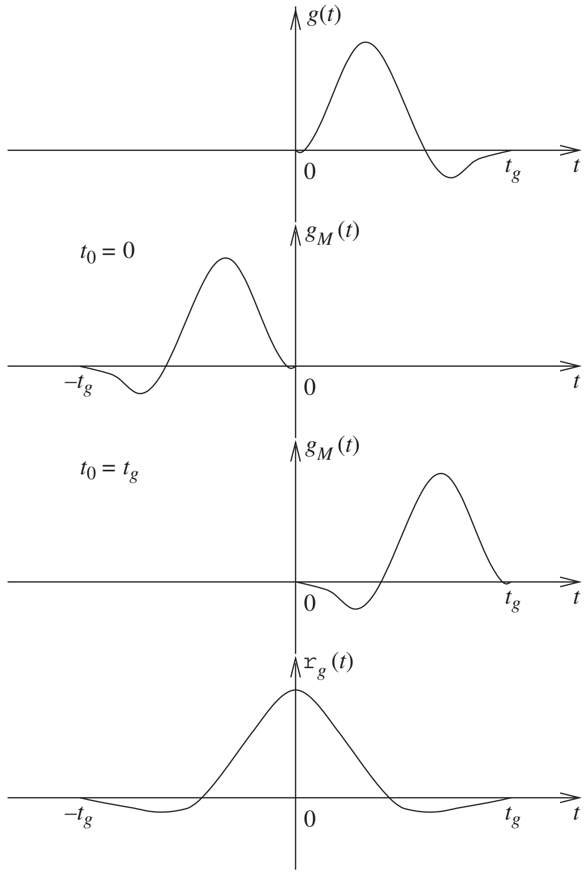

Figure 1.29 Various pulse shapes related to a matched filter.

In Figure 1.29, the different pulse shapes are illustrated for a signal pulse g with limited duration t_g. Note that in this case, the matched filter has also limited duration, and it is causal if $t_0 \geq t_g$.

Example 1.8.1 (MF for a rectangular pulse)
Let

$$g(t) = \mathtt{w}_T(t) = \text{rect}\left(\frac{t - T/2}{T}\right) \tag{1.365}$$

with

$$\mathtt{r}_g(\tau) = T\left(1 - \frac{|\tau|}{T}\right)\text{rect}\left(\frac{\tau}{2T}\right) \tag{1.366}$$

For $t_0 = T$, the matched filter is proportional to g

$$g_M(t) = K\mathtt{w}_T(t) \tag{1.367}$$

and the output pulse in the absence of noise is equal to

$$g_u(t) = KT\left(1 - \left|\frac{t-T}{T}\right|\right)\mathrm{rect}\left(\frac{t-T}{2T}\right) \tag{1.368}$$

1.9 Ergodic random processes

The functions that have been introduced in the previous sections for the analysis of random processes give a valid statistical description of an ensemble of realizations of a random process. We investigate now the possibility of moving from ensemble averaging to time averaging, that is we consider the problem of estimating a statistical descriptor of a random process from the observation of a single realization. Let x be a discrete-time WSS random process having mean $\mathtt{m}_x$. If in the limit it holds[15]

$$\lim_{K\to\infty}\frac{1}{K}\sum_{k=0}^{K-1} x(k) = E[x(k)] = \mathtt{m}_x \tag{1.369}$$

then x is said to be *ergodic in the mean*. In other words, for when the above limit holds, the time-average of samples tends to the statistical mean as the number of samples increases. We note that the existence of the limit (1.369) implies the condition

$$\lim_{K\to\infty} E\left[\left|\frac{1}{K}\sum_{k=0}^{K-1} x(k) - \mathtt{m}_x\right|^2\right] = 0 \tag{1.370}$$

or equivalently

$$\lim_{K\to\infty}\frac{1}{K}\sum_{n=-(K-1)}^{K-1}\left[1 - \frac{|n|}{K}\right]\mathtt{c}_x(n) = 0 \tag{1.371}$$

From (1.371), we see that for a random process to be ergodic in the mean, some conditions on the second-order statistics must be verified. Analogously to definition (1.369), we say that x is *ergodic in correlation* if in the limits it holds:

$$\lim_{K\to\infty}\frac{1}{K}\sum_{k=0}^{K-1} x(k)x^*(k-n) = E[x(k)x^*(k-n)] = \mathtt{r}_x(n) \tag{1.372}$$

Also for processes that are ergodic in correlation, one could get a condition of ergodicity similar to that expressed by the limit (1.371). Let $y(k) = x(k)x^*(k-n)$. Observing (1.372) and (1.369), we find that the ergodicity in correlation of the process x is equivalent to the ergodicity in the mean of the process y. Therefore, it is easy to deduce that the condition (1.371) for y translates into a condition on the statistical moments of the fourth order for x.

In practice, we *will assume all stationary processes to be ergodic*; ergodicity is however difficult to prove for non-Gaussian random processes. We will not consider particular processes that are not ergodic such as $x(k) = A$, where A is a random variable, or $x(k)$ equal to the sum of sinusoidal signals (see (1.311)).

[15] The *limit* is meant in the mean square sense, that is the variance of the r.v. $\left(\frac{1}{K}\sum_{k=0}^{K-1} x(k) - \mathtt{m}_x\right)$ vanishes for $K \to \infty$.

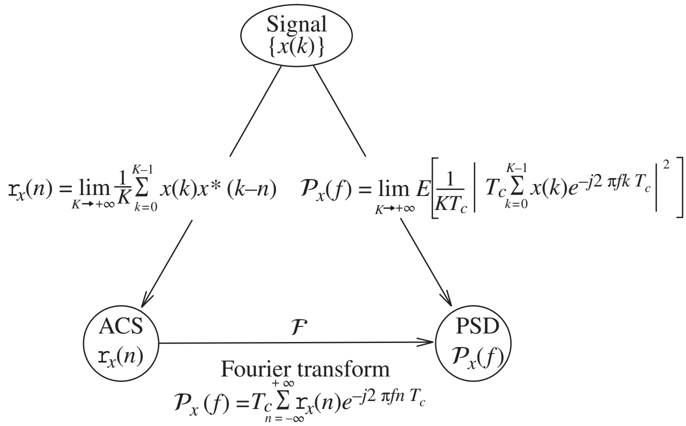

Figure 1.30 Relation between ergodic processes and their statistical description.

The property of ergodicity assumes a fundamental importance if we observe that from a single Realization, it is possible to obtain an estimate of the autocorrelation function, and from this, the PSD. Alternatively, one could prove that under the hypothesis[16]

$$\sum_{n=-\infty}^{+\infty} |n|\ \mathtt{r}_x(n) < \infty \tag{1.373}$$

the following limit holds:

$$\lim_{K\to\infty} E\left[\frac{1}{KT_c}\left|T_c\sum_{k=0}^{K-1} x(k)\ e^{-j2\pi fkT_c}\right|^2\right] = \mathcal{P}_x(f) \tag{1.374}$$

Then, exploiting the ergodicity of a WSS random process, one obtains the relations among the process itself, its autocorrelation function, and PSD shown in Figure 1.30. We note how the direct computation of the PSD, given by (1.374), makes use of a statistical ensemble of the Fourier transform of the process x, while the indirect method via ACS makes use of a single realization.

If we let

$$\tilde{\mathcal{X}}_{KT_c}(f) = T_c\ \mathcal{F}[x(k)\ \mathtt{w}_K(k)] \tag{1.375}$$

where $\mathtt{w}_K$ is the rectangular window of length K (see (1.401)) and $T_d = KT_c$, (1.374) becomes

$$\mathcal{P}_x(f) = \lim_{T_d\to\infty} \frac{E[|\tilde{\mathcal{X}}_{T_d}(f)|^2]}{T_d} \tag{1.376}$$

The relation (1.376) holds also for continuous-time ergodic random processes, where $\tilde{\mathcal{X}}_{T_d}(f)$ denotes the Fourier transform of the windowed realization of the process, with a rectangular window of duration T_d.

[16] We note that for random processes with non-zero mean and/or sinusoidal components this property is not verified. Therefore, it is usually recommended that the deterministic components of the process be removed before the spectral estimation is performed.

1.9.1 Mean value estimators

Given the random process $\{x(k)\}$, we wish to estimate the mean value of a related process $\{y(k)\}$: for example to estimate the statistical power of x we set $y(k) = |x(k)|^2$, while for the estimation of the correlation of x with lag n, we set $y(k) = x(k)x^*(k-n)$. Based on a realization of $\{y(k)\}$, from (1.369) an estimate of the mean value of y is given by the expression

$$\hat{\mathtt{m}}_y = \frac{1}{K}\sum_{k=0}^{K-1} y(k) \tag{1.377}$$

In fact, (1.377) attempts to determine the average component of the signal $\{y(k)\}$. As illustrated in Figure 1.31a, in general, we can think of extracting the average component of $\{y(k)\}$ using an LPF filter h having unit gain, i.e. $\mathcal{H}(0) = 1$, and suitable bandwidth B. Let K be the length of the impulse response with support from $k = 0$ to $k = K - 1$. Note that for a unit step input signal, the transient part of the output signal will last $K - 1$ time instants. Therefore, we assume

$$\hat{\mathtt{m}}_y = z(k) = h * y(k) \qquad \text{for } k \geq K-1 \tag{1.378}$$

We now compute the mean and variance of the estimate. From (1.378), the mean value is given by

$$E[\hat{\mathtt{m}}_y] = \mathtt{m}_y\mathcal{H}(0) = \mathtt{m}_y \tag{1.379}$$

as $\mathcal{H}(0) = 1$. Using the expression in Table 1.6 of the correlation of a filter output signal given the input, the variance of the estimate is given by

$$\mathrm{var}[\hat{\mathtt{m}}_y] = \sigma_y^2 = \sum_{n=-\infty}^{+\infty} \mathtt{r}_h(-n)\mathtt{c}_y(n) \tag{1.380}$$

Assuming

$$S = \sum_{n=-\infty}^{+\infty} |\mathtt{c}_y(n)| = \sigma_y^2 \sum_{n=-\infty}^{+\infty} \frac{|\mathtt{c}_y(n)|}{\sigma_y^2} < \infty \tag{1.381}$$

and being $|\mathtt{r}_h(n)| \leq \mathtt{r}_h(0)$, the variance in (1.380) is *bounded* by

$$\mathrm{var}[\hat{\mathtt{m}}_y] \leq E_h S \tag{1.382}$$

where $E_h = \mathtt{r}_h(0)$.

For an ideal lowpass filter,

$$\mathcal{H}(f) = \mathrm{rect}\left(\frac{f}{2B}\right), \qquad |f| < \frac{1}{2T_c} \tag{1.383}$$

assuming as filter length K that of the principal lobe of $\{h(k)\}$, and neglecting a delay factor, it results as $E_h = 2B$ and $K \simeq 1/B$. Introducing the criterion that for a good estimate, it must be

$$\mathrm{var}\,[\hat{\mathtt{m}}_y] \leq \varepsilon \tag{1.384}$$

with $\varepsilon \ll |\mathtt{m}_y|^2$, from (1.382) it follows

$$B \leq \frac{\varepsilon}{2S} \tag{1.385}$$

and

$$K \geq \frac{2S}{\varepsilon} \tag{1.386}$$

In other words, from (1.381) and (1.386), for a fixed ε, the length K of the filter impulse response must be larger, or equivalently the bandwidth B must be smaller, to obtain estimates for those processes $\{y(k)\}$ that exhibit larger variance and/or larger correlation among samples. Because of their simple implementation, two commonly used filters are the rectangular window and the exponential filter, whose impulse responses are shown in Figure 1.31.

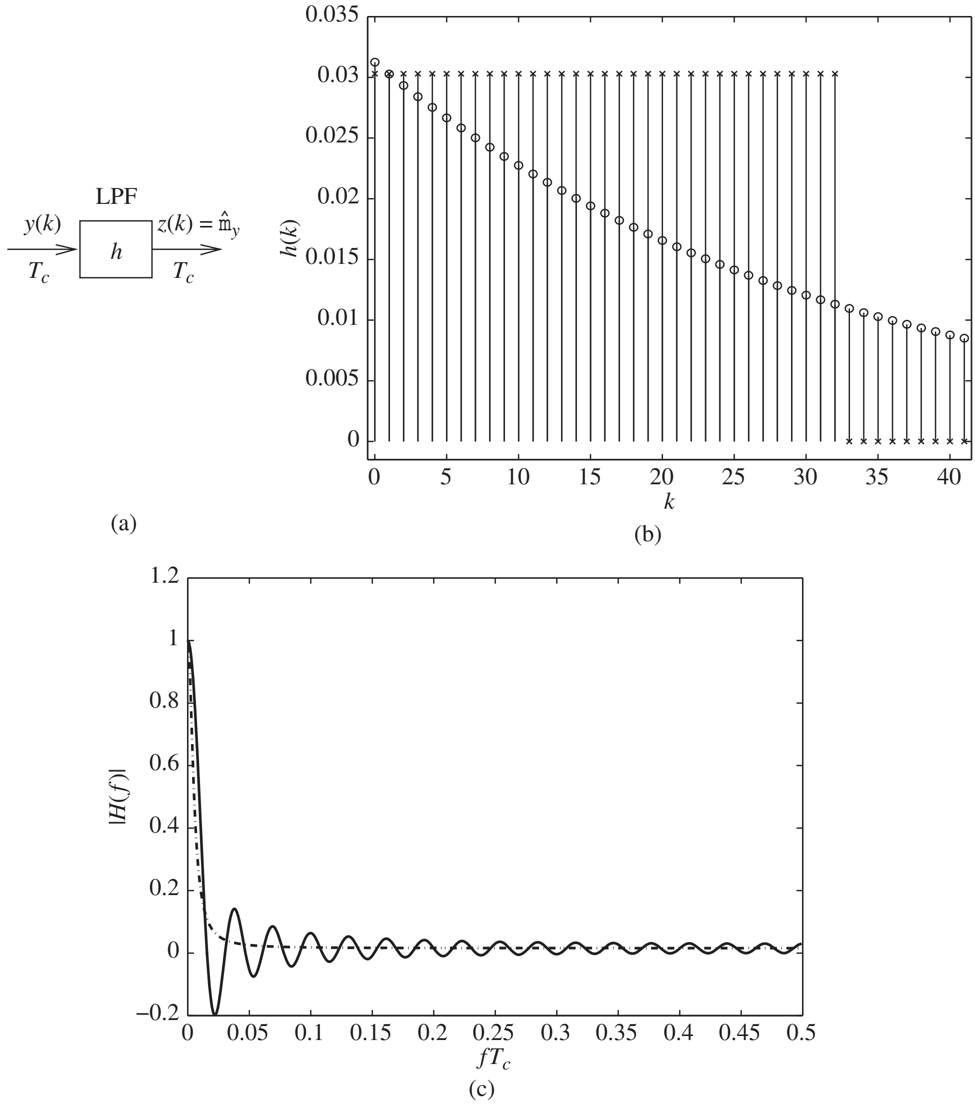

Figure 1.31 (a) Time average as output of a narrow band lowpass filter. (b) Typical impulse responses: exponential filter with parameter $a = 1 - 2^{-5}$ and rectangular window with $K = 33$. (c) Corresponding frequency responses.

Rectangular window

For a rectangular window,

$$h(k) = \begin{cases} \dfrac{1}{K} & k = 0, 1, \dots, K-1 \\ 0 & \text{elsewhere} \end{cases} \tag{1.387}$$

the frequency response is given by (see (1.24))

$$\mathcal{H}(f) = e^{-j2\pi f\left(\frac{K-1}{2}\right)T_c}\ \mathrm{sinc}_K(fKT_c) \tag{1.388}$$

We have $E_h = 1/K$ and, adopting as bandwidth the frequency of the first zero of $|\mathcal{H}(f)|$, $B = 1/(KT_c)$. The filter output is given by

$$z(k) = \sum_{n=0}^{K-1} \frac{1}{K} y(k-n) \tag{1.389}$$

that can be expressed as

$$z(k) = z(k-1) + \frac{y(k) - y(k-K)}{K} \tag{1.390}$$

Exponential filter

For an exponential filter

$$h(k) = \begin{cases} (1-a)a^k & k \geq 0 \\ 0 & \text{elsewhere} \end{cases} \tag{1.391}$$

with $|a| < 1$, the frequency response is given by

$$\mathcal{H}(f) = \frac{1-a}{1 - ae^{-j2\pi f T_c}} \tag{1.392}$$

Moreover, $E_h = (1-a)/(1+a)$ and, adopting as length of h the time constant of the filter, i.e. the interval it takes for the amplitude of the impulse response to decrease of a factor e,

$$K - 1 = \frac{1}{\ln 1/a} \simeq \frac{1}{1-a} \tag{1.393}$$

where the approximation holds for $a \simeq 1$. The 3 dB filter bandwidth is equal to

$$B = \frac{1-a}{2\pi} \frac{1}{T_c} \qquad \text{for } a > 0.9 \tag{1.394}$$

The filter output has a simple expression given by the recursive equation

$$z(k) = az(k-1) + (1-a)\, y(k) \tag{1.395}$$

We note that choosing a as

$$a = 1 - 2^{-l} \tag{1.396}$$

then (1.395) becomes

$$z(k) = z(k-1) + 2^{-l}(y(k) - z(k-1)) \tag{1.397}$$

whose computation requires only two additions and one *shift* of l bits. Moreover, from (1.393), the filter time constant is given by

$$K - 1 = 2^l \tag{1.398}$$

General window

In addition to the two filters described above, a general window can be defined as

$$h(k) = A\mathtt{w}(k) \tag{1.399}$$

with $\{\mathtt{w}(k)\}$ window[17] of length K. Factor A in (1.399) is introduced to normalize the area of h to 1. We note that, for random processes with slowly time-varying statistics, (1.390) and (1.397) give an expression to update the estimates.

[17] We define the *continuous-time rectangular window* with duration T_d as

$$\mathtt{w}_{T_d}(t) = \text{rect}\left(\frac{t - T_d/2}{T_d}\right) = \begin{cases} 1 & 0 < t < T_d \\ 0 & \text{elsewhere} \end{cases} \tag{1.400}$$

Commonly used *discrete-time windows* are:

1.9.2 Correlation estimators

Let $\{x(k)\}$, $k = 0, 1, \dots, K-1$, be a realization of a random process with K samples. We examine two estimates.

Unbiased estimate

The unbiased estimate

$$\hat{\mathtt{r}}_x(n) = \frac{1}{K-n} \sum_{k=n}^{K-1} x(k)x^*(k-n) \qquad n = 0, 1, \dots, K-1 \tag{1.405}$$

has mean

$$E[\hat{\mathtt{r}}_x(n)] = \frac{1}{K-n} \sum_{k=n}^{K-1} E[x(k)x^*(k-n)] = \mathtt{r}_x(n) \tag{1.406}$$

If the process is Gaussian, one can show that the variance of the estimate is approximately given by

$$\mathrm{var}[\hat{\mathtt{r}}_x(n)] \simeq \frac{K}{(K-n)^2} \sum_{m=-\infty}^{+\infty} [\mathtt{r}_x^2(m) + \mathtt{r}_x(m+n)\mathtt{r}_x(m-n)] \tag{1.407}$$

from which it follows

$$\mathrm{var}\,[\hat{\mathtt{r}}_x(n)] \xrightarrow[K\to\infty]{} 0 \tag{1.408}$$

The above limit holds for $n \ll K$. Note that the variance of the estimate increases with the correlation lag n.

Biased estimate

The biased estimate

$$\check{\mathtt{r}}_x(n) = \frac{1}{K} \sum_{k=n}^{K-1} x(k)x^*(k-n) = \left(1 - \frac{|n|}{K}\right) \hat{\mathtt{r}}_x(n) \tag{1.409}$$

---

1. *Rectangular window*

$$\mathtt{w}(k) = \mathtt{w}_D(k) = \begin{cases} 1 & k = 0, 1, \dots, D-1 \\ 0 & \text{elsewhere} \end{cases} \tag{1.401}$$

where D denotes the length of the rectangular window expressed in number of samples.

2. *Raised cosine or Hamming window*

$$\mathtt{w}(k) = \begin{cases} 0.54 + 0.46\cos\left(2\pi \dfrac{k - \frac{D-1}{2}}{D-1}\right) & k = 0, 1, \dots, D-1 \\ 0 & \text{elsewhere} \end{cases} \tag{1.402}$$

3. *Hann window*

$$\mathtt{w}(k) = \begin{cases} 0.50 + 0.50\cos\left(2\pi \dfrac{k - \frac{D-1}{2}}{D-1}\right) & k = 0, 1, \dots, D-1 \\ 0 & \text{elsewhere} \end{cases} \tag{1.403}$$

4. *Triangular or Bartlett window*

$$\mathtt{w}(k) = \begin{cases} 1 - 2\left|\dfrac{k - \frac{D-1}{2}}{D-1}\right| & k = 0, 1, \dots, D-1 \\ 0 & \text{elsewhere} \end{cases} \tag{1.404}$$

has mean satisfying the following relations:

$$E[\check{\mathtt{r}}_x(n)] = \left(1 - \frac{|n|}{K}\right) \mathtt{r}_x(n) \xrightarrow[K\to\infty]{} \mathtt{r}_x(n) \tag{1.410}$$

Unlike the unbiased estimate, the mean of the biased estimate is not equal to the autocorrelation function, but approaches it as K increases. Note that the biased estimate differs from the autocorrelation function by one additive constant, denoted as *bias*:

$$\mu_{bias} = E[\check{\mathtt{r}}_x(n)] - \mathtt{r}_x(n) \tag{1.411}$$

For a Gaussian process, the variance of the biased estimate is

$$\mathrm{var}[\check{\mathtt{r}}_x(n)] = \left(\frac{K-|n|}{K}\right)^2 \mathrm{var}[\hat{\mathtt{r}}_x(n)] \simeq \frac{1}{K} \sum_{m=-\infty}^{+\infty} [\mathtt{r}_x^2(m) + \mathtt{r}_x(m+n)\mathtt{r}_x(m-n)] \tag{1.412}$$

In general, the biased estimate of the ACS exhibits a mean-square error[18] larger than the unbiased, especially for large values of n. It should also be noted that the estimate does not necessarily yield sequences that satisfy the properties of autocorrelation functions: for example the following property may not be verified:

$$\hat{\mathtt{r}}_x(0) \geq |\hat{\mathtt{r}}_x(n)|, \qquad n \neq 0 \tag{1.414}$$

1.9.3 Power spectral density estimators

After examining ACS estimators, we review some spectral density estimation methods.

Periodogram or instantaneous spectrum

Let $\tilde{\mathcal{X}}(f) = T_c\mathcal{X}(f)$, where $\mathcal{X}(f)$ is the Fourier transform of $\{x(k)\}$, $k = 0, \dots, K-1$; an estimate of the statistical power of $\{x(k)\}$ is given by

$$\hat{\mathtt{M}}_x = \frac{1}{K}\sum_{k=0}^{K-1} |x(k)|^2 = \frac{1}{KT_c}\int_{-\frac{1}{2T_c}}^{\frac{1}{2T_c}} |\tilde{\mathcal{X}}(f)|^2 \, df \tag{1.415}$$

using the properties of the Fourier transform (Parseval theorem). Based on (1.415), a PSD estimator called *periodogram* is given by

$$\mathcal{P}_{PER}(f) = \frac{1}{KT_c}|\tilde{\mathcal{X}}(f)|^2 \tag{1.416}$$

We can write (1.416) as

$$\mathcal{P}_{PER}(f) = T_c \sum_{n=-(K-1)}^{K-1} \check{\mathtt{r}}_x(n)\, e^{-j2\pi f n T_c} \tag{1.417}$$

[18] For example, for the estimator (1.405) the mean-square error is defined as

$$E\left[|\hat{\mathtt{r}}_x(n) - \mathtt{r}_x(n)|^2\right] = \mathrm{var}[\hat{\mathtt{r}}_x(n)] + |\mu_{bias}|^2 \tag{1.413}$$

and, consequently,

$$\begin{aligned} E[\mathcal{P}_{PER}(f)] &= T_c \sum_{n=-(K-1)}^{K-1} E[\check{\mathtt{r}}_x(n)] e^{-j2\pi f n T_c} \\ &= T_c \sum_{n=-(K-1)}^{K-1} \left(1 - \frac{|n|}{K}\right) \mathtt{r}_x(n) e^{-j2\pi f n T_c} \\ &= T_c \mathcal{W}_B * \mathcal{P}_x(f) \end{aligned} \tag{1.418}$$

where $\mathcal{W}_B(f)$ is the Fourier transform of the *symmetric Bartlett window*

$$\mathtt{w}_B(n) = \begin{cases} 1 - \dfrac{|n|}{K} & |n| \le K-1 \\ 0 & |n| > K-1 \end{cases} \tag{1.419}$$

and

$$\mathcal{W}_B(f) = K\,[\mathrm{sinc}_K(fkT_c)]^2 \tag{1.420}$$

We note the periodogram estimate is affected by *bias* for finite K. Moreover, it also exhibits a large variance, as $\mathcal{P}_{PER}(f)$ is computed using the samples of $\check{\mathtt{r}}_x(n)$ even for lags up to $K-1$, whose variance is very large.

Welch periodogram

This method is based on applying (1.374) for finite K. Given a sequence of K samples, different subsequences of consecutive D samples are extracted. Subsequences may partially overlap. Let $x^{(s)}$ be the s-th subsequence, characterized by S samples in common with the preceding subsequence $x^{(s-1)}$ and with the following one $x^{(s+1)}$. In general, $0 \le S \le D/2$, with the choice $S = 0$ yielding subsequences with no overlap and therefore with less correlation. The number of subsequences N_s is[19]

$$N_s = \left\lfloor \frac{K-D}{D-S} + 1 \right\rfloor \tag{1.421}$$

Let $\mathtt{w}$ be a window (see footnote 17 on page 59) of D samples: then

$$x^{(s)}(k) = \mathtt{w}(k)\, x(k + s(D-S)), \qquad k = 0, 1, \ldots, D-1 \;\; s = 0, 1, \ldots, N_s - 1 \tag{1.422}$$

For each s, compute the Fourier transform

$$\tilde{\mathcal{X}}^{(s)}(f) = T_c \sum_{k=0}^{D-1} x^{(s)}(k) e^{-j2\pi f k T_c} \tag{1.423}$$

and obtain

$$\mathcal{P}_{PER}^{(s)}(f) = \frac{1}{D T_c \mathtt{M}_\mathtt{w}} |\tilde{\mathcal{X}}^{(s)}(f)|^2 \tag{1.424}$$

where

$$\mathtt{M}_\mathtt{w} = \frac{1}{D} \sum_{k=0}^{D-1} \mathtt{w}^2(k) \tag{1.425}$$

is the normalized energy of the window. As a last step, for each frequency, average the periodograms:

$$\mathcal{P}_{WE}(f) = \frac{1}{N_s} \sum_{s=0}^{N_s-1} \mathcal{P}_{PER}^{(s)}(f) \tag{1.426}$$

[19] The symbol $\lfloor a \rfloor$ denotes the function *floor*, that is the largest integer smaller than or equal to a. The symbol $\lceil a \rceil$ denotes the function *ceiling*, that is the smallest integer larger than or equal to a.

The mean of the estimate is given by

$$E[\mathcal{P}_{WE}(f)] = T_c[|\mathcal{W}|^2 * \mathcal{P}_x](f) \tag{1.427}$$

where

$$\mathcal{W}(f) = \sum_{k=0}^{D-1} \mathtt{w}(k)e^{-j2\pi fkT_c} \tag{1.428}$$

Assuming the process Gaussian and the different subsequences statistically independent, we get[20]

$$\mathrm{var}[\mathcal{P}_{WE}(f)] \propto \frac{1}{N_s}\mathcal{P}_x^2(f) \tag{1.429}$$

Note that the partial overlap introduces correlation between subsequences. From (1.429), we see that the variance of the estimate is reduced by increasing the number of subsequences. In general, D must be large enough so that the *generic subsequence represents the process*[21] and also N_s must be large to obtain a reliable estimate (see (1.429)); therefore, the application of the Welch method requires many samples.

Blackman and Tukey correlogram

For an *unbiased* estimate of the ACS, $\{\hat{\mathtt{r}}_x(n)\}$, $n = -L, \ldots, L$, consider the Fourier transform

$$\mathcal{P}_{BT}(f) = T_c \sum_{n=-L}^{L} \mathtt{w}(n)\hat{\mathtt{r}}_x(n)\; e^{-j2\pi fnT_c} \tag{1.430}$$

where $\mathtt{w}$ is a window[22] of length $2L + 1$, with $\mathtt{w}(0) = 1$. If K is the number of samples of the realization sequence, we require that $L \leq K/5$ to reduce the variance of the estimate. Then if the Bartlett window (1.420) is chosen, one finds that $\mathcal{P}_{BT}(f) \geq 0$.

In terms of the mean value of the estimate, we find

$$E[\mathcal{P}_{BT}(f)] = T_c(\mathcal{W} * \mathcal{P}_x)(f) \tag{1.431}$$

For a Gaussian process, if the Bartlett window is chosen, the variance of the estimate is given by

$$\mathrm{var}[\mathcal{P}_{BT}(f)] = \frac{1}{K}\mathcal{P}_x^2(f)E_{\mathtt{w}} = \frac{2}{3}\frac{L}{K}\mathcal{P}_x^2(f) \tag{1.432}$$

Windowing and window closing

The windowing operation of time sequence in the periodogram, and of the ACS in the correlogram, has a strong effect on the performance of the estimate. In fact, any truncation of a sequence is equivalent to a windowing operation, carried out via the rect function. The choice of the window type in the frequency domain depends on the compromise between a narrow central lobe (to reduce *smearing*) and a fast decay of secondary lobes (to reduce *leakage*). *Smearing* yields a lower spectral resolution, that is the capability to distinguish two spectral lines that are close. On the other hand, *leakage* can mask spectral components that are further apart and have different amplitudes.

The choice of the window length is based on the compromise between spectral resolution and the variance of the estimate. An example has already been seen in the correlogram, where the condition $L \leq K/5$ must be satisfied. Another example is the Welch periodogram. For a given observation of K samples, it is

[20] Notation $a \propto b$ means that a is proportional to b.

[21] For example, if x is a sinusoidal process, DT_c must at least be greater than 5 or 10 periods of x.

[22] The windows used in (1.430) are the same introduced in footnote 17: the only difference is that they are now centered around zero instead of $(D-1)/2$. To simplify the notation, we will use the same symbol in both cases.

initially better to choose a small number of samples over which to perform the DFT, and therefore a large number of windows (subsequences) over which to average the estimate. The estimate is then repeated by increasing the number of samples per window, thus decreasing the number of windows. In this way, we get estimates with not only a higher resolution but also characterized by an increasing variance. The procedure is terminated once it is found that the increase in variance is no longer compensated by an increase in the spectral resolution. The aforementioned method is called *window closing*.

Example 1.9.1
Consider a realization of $K = 10\,000$ samples of the signal:

$$y(kT_c) = \frac{1}{A_h} \sum_{n=-16}^{16} h(nT_c)w((k-n)T_c) + A_1 \cos(2\pi f_1 kT_c + \varphi_1) + A_2 \cos(2\pi f_2 kT_c + \varphi_2) \tag{1.433}$$

where $\varphi_1, \varphi_2 \sim \mathcal{U}[0, 2\pi)$, $w(nT_c)$ is a white random process with zero mean and variance $\sigma_w^2 = 5$, $T_c = 0.2$, $A_1 = 1/20$, $f_1 = 1.5$, $A_2 = 1/40$, $f_2 = 1.75$, and

$$A_h = \sum_{-16}^{16} h(kT_c) \tag{1.434}$$

Moreover

$$h(kT_c) = \frac{\sin\left(\pi(1-\rho)\dfrac{kT_c}{T}\right) + 4\rho\dfrac{kT_c}{T}\cos\left(\pi(1+\rho)\dfrac{kT_c}{T}\right)}{\pi\left[1-\left(4\rho\dfrac{kT_c}{T}\right)^2\right]\dfrac{kT_c}{T}} \mathrm{rect}\left(\frac{kT_c}{8T+T_c}\right) \tag{1.435}$$

with $T = 4T_c$ and $\rho = 0.32$.

Actually y is the sum of two sinusoidal signals and filtered white noise through h. Consequently, observing (1.188) and (1.313),

$$\begin{aligned}\mathcal{P}_y(f) = \sigma_w^2\, T_c\, \frac{|\mathcal{H}(f)|^2}{A_h^2} &+ \frac{A_1^2}{4}(\delta(f-f_1) + \delta(f+f_1)) \\ &+ \frac{A_2^2}{4}(\delta(f-f_2) + \delta(f+f_2))\end{aligned} \tag{1.436}$$

where $\mathcal{H}(f)$ is the Fourier transform of $\{h(kT_c)\}$.

The shape of the PSD in (1.436) is shown in Figures 1.32–1.34 as a solid line. A Dirac impulse is represented by an isosceles triangle having a base equal to twice the desired frequency resolution F_q. Consequently, a Dirac impulse, for example of area $A_1^2/4$ will have a height equal to $A_1^2/(4F_q)$, thus, maintaining the equivalence in statistical power between different representations.

We now compare several spectral estimates, obtained using the previously described methods; in particular, we will emphasize the effect on the resolution of the type of window used and the number of samples for each window.

We state beforehand the following important result. Windowing a complex sinusoidal signal $\{e^{j2\pi f_1 kT_c}\}$ with $\{\mathtt{w}(k)\}$ produces a signal having Fourier transform equal to $\mathcal{W}(f-f_1)$, where $\mathcal{W}(f)$ is the Fourier transform of w. Therefore, in the frequency domain, the spectral line of a sinusoidal signal becomes a signal with shape $\mathcal{W}(f)$ centred around f_1.

In general, from (1.424), the periodogram of a real sinusoidal signal with amplitude A_1 and frequency f_1 is

$$\mathcal{P}_{PER}(f) = \frac{T_c}{D\mathtt{M}_\mathtt{w}}\left(\frac{A_1}{2}\right)^2 |\mathcal{W}(f-f_1) + \mathcal{W}(f+f_1)|^2 \tag{1.437}$$

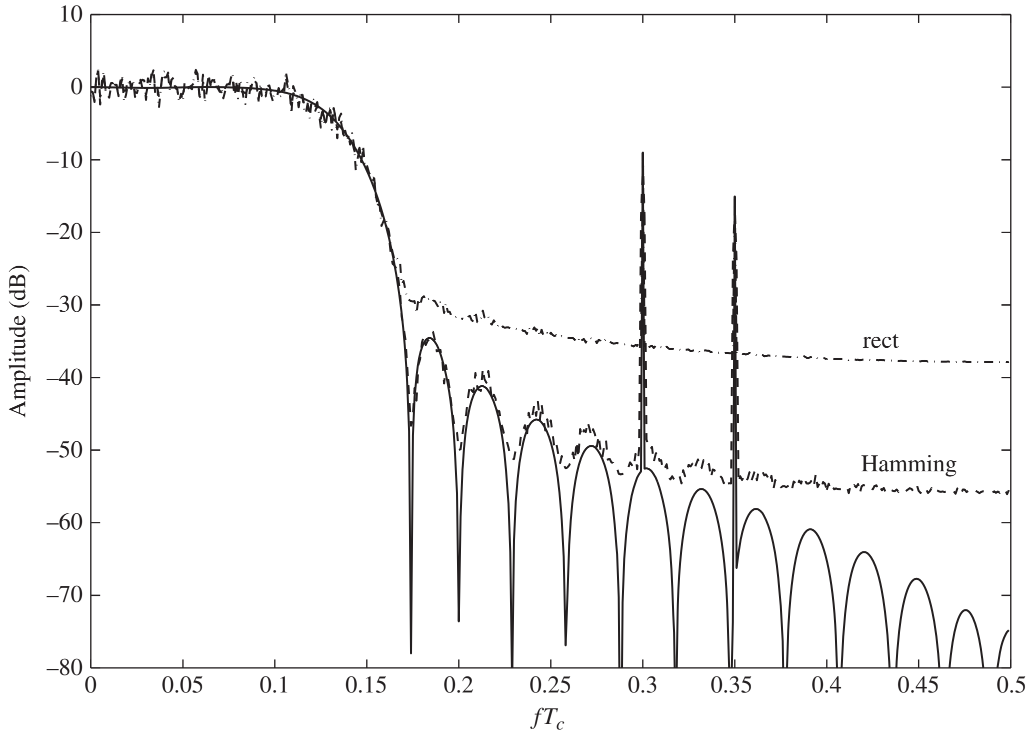

Figure 1.32 Comparison between spectral estimates obtained with Welch periodogram method, using the Hamming or the rectangular window, and the analytical PSD given by (1.436).

Figure 1.32 shows, in addition to the analytical PSD (1.436), the estimate obtained by the Welch periodogram method using the Hamming or the rectangular windows. Parameters used in (1.423) and (1.426) are: $D = 1000$, $N_s = 19$, and 50% overlap between windows. We observe that the use of the Hamming window yields an improvement of the estimate due to less *leakage*. Likewise Figure 1.33 shows how the Hamming window also improves the estimate carried out with the correlogram; in particular, the estimates of Figure 1.33 were obtained using in (1.430) $L = 500$. Lastly, Figure 1.34 shows how the resolution and the variance of the estimate obtained by the Welch periodogram vary with the parameters D and N_s, using the Hamming window. Note that by increasing D, and hence decreasing N_s, both resolution and variance of the estimate increase.

1.10 Parametric models of random processes

ARMA

Let us consider the realization of a random process x according to the *auto-regressive moving average* (ARMA) model illustrated in Figure 1.35. In other words, the process x, also called observed sequence, is the output of an IIR filter having as input white noise with variance σ_w^2, and is given by the recursive

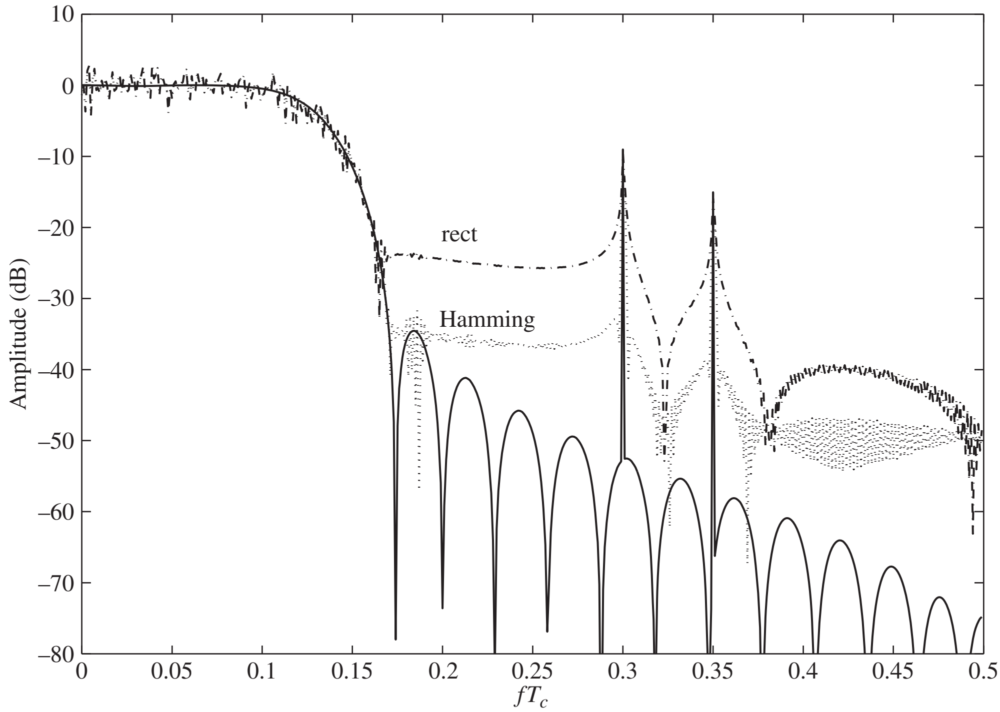

Figure 1.33 Comparison between spectral estimates obtained with the correlogram using the Hamming or the rectangular window, and the analytical PSD given by (1.436).

equation[23]

$$x(k) = -\sum_{n=1}^{p} \mathtt{a}_n x(k-n) + \sum_{n=0}^{q} \mathtt{b}_n w(k-n) \tag{1.438}$$

and the model is denoted as $ARMA(p, q)$.

Rewriting (1.438) in terms of the filter impulse response h_{ARMA}, we find in general

$$x(k) = \sum_{n=0}^{+\infty} h_{ARMA}(n) w(k-n) \tag{1.439}$$

which indicates that the filter used to realize the ARMA model is causal. From (1.63), one finds that the filter transfer function is given by

$$H_{ARMA}(z) = \frac{B(z)}{A(z)} \quad \text{where} \quad \begin{cases} B(z) = \sum_{n=0}^{q} \mathtt{b}_n z^{-n} \\ A(z) = \sum_{n=0}^{p} \mathtt{a}_n z^{-n} \ \text{ assuming } \mathtt{a}_0 = 1 \end{cases} \tag{1.440}$$

Using (1.188), the PSD of the process x is given by

$$\mathcal{P}_x(f) = T_c \sigma_w^2 \left| \frac{\mathcal{B}(f)}{\mathcal{A}(f)} \right|^2 \quad \text{where} \quad \begin{cases} \mathcal{B}(f) = B(e^{j2\pi f T_c}) \\ \mathcal{A}(f) = A(e^{j2\pi f T_c}) \end{cases} \tag{1.441}$$

[23] In a simulation of the process, the first samples $x(k)$ generated by (1.438) should be neglected because they depend on the initial conditions. Specifically, if N_{ARMA} is the *length* of the filter impulse response h_{ARMA}, the minimum number of samples to be ignored is $N_{ARMA} - 1$, equal to the filter transient.